INL/EXT-20-58029
Revision 0

AGC-3 Irradiated Material Properties Analysis

April 2020

William E. Windes
David T. Rohrbaugh
W. David Swank

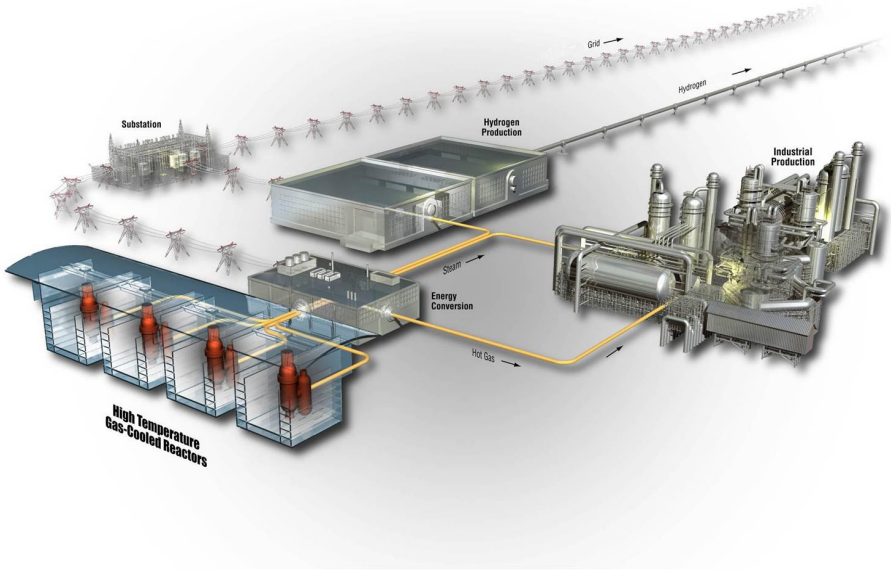

Changing the World's Energy Future

Idaho National Laboratory

INL is a U.S. Department of Energy National Laboratory operated by Battelle Energy Alliance, LLC

INL/EXT-20-58029
Revision 0

AGC-3 Irradiated Material Properties Analysis

William E. Windes
David T. Rohrbaugh
W. David Swank

April 2020

Idaho National Laboratory
INL ART Program
Idaho Falls, Idaho 83415

http://www.inl.gov

Prepared for the
U.S. Department of Energy
Office of Nuclear Energy
Under DOE Idaho Operations Office
Contract DE-AC07-05ID14517

INL ART Program

AGC-3 Irradiated Material Properties Analysis

INL/EXT-20-58029
Revision 0

April 2020

Approved by:

William E. Windes Author/INL ART Graphite R&D Technical Lead	04-29-2020 Date
Timothy D. Burchell ORNL Graphite Technical Peer Reviewer	04-29-2020 Date
Gerhard Strydom INL ART Director	04-29-2020 Date
Michelle Sharp INL Quality Assurance	04-29-2020 Date

SUMMARY

This report documents the analysis of the irradiated material property data from the Advanced Graphite Creep (AGC)-3 graphite specimens. This is the third in a series of six irradiation test trains planned as part of the AGC experiment to fully characterize the neutron irradiation effects and radiation creep behavior of current nuclear graphite grades. The AGC-3 capsule was irradiated in the Idaho National Laboratory Advanced Test Reactor at a nominal temperature of 800°C, beginning with irradiation Cycle 152B on November 28, 2012, and ending with Cycle 155B on April 12, 2014, with a total received dose range of 0.9 to 3.7 dpa. Larger creep and control specimens located more centrally in the capsule received a dose of 1.0 to 3.7 dpa.

AGC-3 was designed to provide irradiation conditions similar to AGC-1 and AGC-2 capsules (similar graphite grades tested, specimen dimensions, mechanical loading conditions) but at a different nominal irradiation temperature of 800°C. AGC-3 was irradiated for a short duration to provide material property values at lower dose levels. AGC-4 will have a longer duration and provide material property values at higher dose levels. After irradiation, material property and dimensional strain measurements were conducted on all AGC-3 specimens (from 11 nuclear graphite grades) using the same equipment and approved standards as were conducted before irradiation. The specimen loading configuration for all graphite grades within AGC-3 followed a similar pattern as earlier AGC capsules to provide easy future comparison of all irradiated material property data.

Significant modifications were made to the AGC-3 capsule design to improve the uniformity of the specimen temperature. These changes significantly improved the axial temperature variations as encountered within AGC-1. While the AGC-1 irradiation temperature ranged from 409 to 761°C (average 644°C, 78°C standard deviation), the AGC-3 temperature range was significantly reduced to 748–937°C (average 821°C, 30°C standard deviation).

The material property data covered in this report include specimen density, resistivity, Young's modulus (both by sonic resonance method and sonic velocity method), shear modulus, coefficient of thermal expansion, and thermal diffusivity. Behavior trends from the data are discussed with respect to the experimental variables of irradiation dose, temperature, stress, and graphite grade affecting these property changes.

CONTENTS

FIGURES

TABLES

ABBREVIATIONS and ACRONYMS

AG	against grain
AGC	Advanced Graphite Creep
ATR	Advanced Test Reactor
ART	Advanced Reactor Technologies
CTE	Coefficient of Thermal Expansion
DOE	Department of Energy
HDG	High Dose Graphite
HOPG	highly ordered pyrolitic graphite
HTR	high temperature reactor
INL	Idaho National Laboratory
PIE	post-irradiation examination
QA	quality assurance
WG	with grain

AGC-3 Irradiated Material Properties Analysis

1. INTRODUCTION

The Advanced Reactor Technologies (ART) Graphite Research and Development Program is conducting an extensive graphite irradiation experiment to provide data for licensing of a high-temperature reactor (HTR) design. In past applications, graphite has been used effectively as a structural and moderator material in both research and commercial high-temperature gas-cooled reactor designs.[1, 2] Nuclear graphite H-451, used previously in the United States for nuclear reactor graphite components, is no longer available and new nuclear graphite grades have been developed that are considered suitable candidates for new HTR reactor designs. A complete properties database must be developed for these current grades of graphite to support the design and licensing of HTR core components within a commercial reactor. Quantitative data on in-service irradiated material performance are required for the physical, mechanical, and thermal properties of each graphite grade, with a specific emphasis on data accounting for the life-limiting effects of irradiation creep on key physical properties of the HTR candidate graphite grades. Further details on the research and development activities and associated rationale required to qualify nuclear-grade graphite for use within the HTR are documented in the graphite technology research and development plan.[3, 4]

The Advanced Graphite Creep (AGC) experiment is currently underway to determine the in-service behavior of these new graphite grades for HTR applications. This test series will examine the properties and behaviors of nuclear-grade graphite over a large spectrum of temperatures, irradiation fluence, and applied stress levels that are expected to induce irradiation creep strains within an HTR graphite component. Irradiation data are provided through the AGC test series, which comprises six planned capsules irradiated in the Advanced Test Reactor (ATR) in a large flux trap at Idaho National Laboratory (INL). The AGC irradiation conditions are similar to the anticipated environment within a high-temperature core design. Each irradiation capsule is composed of more than 400 graphite specimens that are characterized before and after irradiation to determine the irradiation-induced changes in material properties and the rate of life-limiting irradiation creep for each graphite grade.

The creep-rate calculations and analysis for the AGC-3 graphite specimens is documented in INL-EXT-19-54725, *AGC-3 Irradiation Creep Strain Data Analysis*.[5] This current report addresses the post-irradiation examination (PIE) analysis of the irradiation-induced material property changes within the AGC-3 graphite specimens. The data and information produced in this document and the referenced documents within were generated under the approved quality assurance (QA) programs for the respective organizations, including INL and Oak Ridge National Laboratory in compliance with the appropriate NQA-1 requirements. It is anticipated that all data will be robust enough to stand up to a review by the Nuclear Regulatory Commission as support for a graphite reactor design selection.

2. ADVANCED GRAPHITE CREEP EXPERIMENT

The AGC test series is designed to obtain irradiation data necessary to determine the safe operating envelope of graphite core components for an HTR by measuring the irradiated material property changes and the behavior of several new nuclear graphite grades over a large range of temperatures, neutron fluence, and mechanical compressive loads. The experiment consists of three interrelated stages: pre-irradiation characterization of the graphite specimens, the irradiation test series (designated as six separate irradiation test train capsules), and PIE and analysis of the graphite specimens after irradiation. Separate reports for each distinct stage are prepared after each individual activity is completed.

Each AGC test train (capsule) begins with a characterization plan describing the thermal, physical, and mechanical measurement techniques that will be used to characterize the graphite samples irradiated in each AGC capsule. After describing the testing methodology, the pre-irradiation material properties for

each specimen are detailed in the pre-irradiation examination report. The pre-irradiation examination report details the total number of graphite grades and individual specimens, the specimen loading configuration designed to expose all specimens to the entire range of irradiation conditions, and the pre-irradiation material property testing data and results. The as-run irradiation report details the irradiation history of each capsule while in the reactor, noting any changes from the technical and functional specifications for each specific test series capsule and identifying the possible improvements to the next test series capsule design. The disassembly report details specimen recovery from the irradiation capsule, noting any damage to the specimens and providing an inventory of recovered specimens for PIE testing. The PIE data report details the changes in specimen dimensional measurements as well as irradiated material properties upon exposure to neutron irradiation. Finally, the irradiation-induced analysis reports analyze the irradiation results reported within the data package reports, utilizing the irradiation conditions recorded within the as-run irradiation report. The PIE analysis report(s) can be presented as two separate reports with irradiation creep analysis reported separately from the material property changes. However, both PIE analyses interpret the irradiation behavior of the graphite grades to assist in determining a credible, safe operating envelope for graphite core components in an HTR design and licensing application.

This report is an AGC PIE analysis report on irradiation-induced material property changes within the third AGC capsule (AGC-3). A previous AGC PIE analysis report on the irradiation-induced creep was published previously as "AGC-3 Irradiation Creep Strain Data Analysis."[5] Data from the "AGC-3 Specimen Post-Irradiation Data Package Report" was used to analyze the electrical resistivity, elastic moduli, thermal expansion and thermal diffusivity for each graphite grade..[6]

2.1 Design Parameters of AGC Experiment

The AGC test series is designed to measure changes in key thermal, physical, and mechanical material properties over the anticipated range of HTR operating conditions..[7] By comparing the material properties of each specimen before and after irradiation, the experiment generates quantitative material property change data and irradiation creep data that will be used to predict the in-service behavior and operating performance of the current nuclear graphite grades for HTR designs. Specific emphasis is placed on data that pertain to the life-limiting effects of irradiation creep on graphite components and the effects creep may have on key irradiated material properties of several candidate graphite grades for use in an HTR design.

The critical component of the experiment is the irradiation test series, which irradiates the graphite specimens after pre-irradiation examination characterization has been completed. The AGC test series is composed of six planned irradiation test trains that are irradiated in ATR in a large flux trap, as described in the "Graphite Technology Development Plan."[3] The test series exposes test specimens of select nuclear graphite grades to temperatures and the initial range of irradiation dose that are expected within an HTR design. Specifically, graphite specimens will be exposed to a fast neutron dose ranging from 1 to 7 dpa and nominal temperatures of 600, 800, and 1,100°C, as shown in Figure 1. The first and second AGC capsules, AGC-1 and AGC-2, were designed to be irradiated within the ATR's south flux trap. All other AGC capsules will be irradiated within ATR's east flux trap..[8] It should be noted that in 2018 a major change to the AGC experiment occurred where the highest temperature capsules (AGC-5 and AGC-6) were repurposed to re-irradiate select specimens from the previous capsules (AGC-1 through AGC-4). Details from this change are discussed in Section 3.2, Future Changes to AGC Experiment.

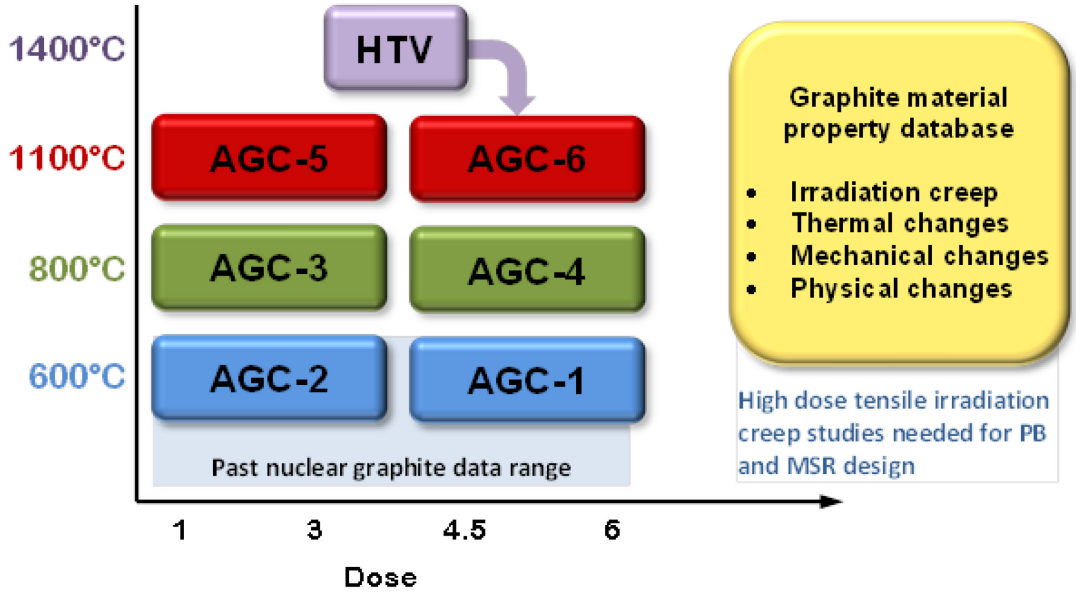

Figure 1. Irradiation dose and temperature parameters for the AGC experiment (HTV = high-temperature vessel, MSR = molten salt reactor, PB = pebble bed).

In addition to determining the irradiation-induced changes to the material properties of selected nuclear graphite grades, the AGC experiment dedicates a significant amount of scope to determining rates of irradiation-induced creep for different nuclear graphite grades. The traditional method for measuring irradiation-induced creep is to apply a significant mechanical load (inducing a mechanical stress within the graphite) to half the specimens during irradiation while leaving the remaining half of the specimens unloaded (unstressed). Mechanically loaded (stressed) specimens are traditionally designated as the creep specimens, and the unloaded (unstressed) specimens are designated as the control specimens. The resulting difference in dimensional change between the loaded and unloaded specimens (assuming that temperature and dose levels are the same) provides the amount of irradiation-induced creep strain for the graphite specimens. From this strain level, a creep rate for each graphite grade can be calculated as a function of dose if both specimens were irradiated at the same constant temperature and dose level. Thus, each capsule is designed to be irradiated at a constant temperature, allowing only the dose and applied mechanical load to vary within the test train of each test-series capsule. With all graphite specimens at a constant temperature, only the applied stress level and dose will affect the calculated creep rate of each graphite grade within a test series capsule.

The AGC experiment is designed to measure the constant creep strain behavior (secondary creep) of the various grades. The experiment assumes that the induced creep strain for all specimens is within the secondary creep regime; therefore, it behaves linearly with respect to received neutron dose.[3,7,8]

While the effects from applied mechanical stresses and neutron dose can be determined within each irradiation capsule, the temperature dependency of any irradiation-induced material property changes within the graphite grades is achieved by comparing the measured values of the specimens between irradiation capsules. Because each test train is irradiated at a constant temperature (600, 800, or 1,100°C), the temperature-induced/enhanced material property changes must be determined by comparing specimens in different capsules exposed to similar doses and applied mechanical load levels. All AGC capsules are designed to have the same specimen stacking patterns. Thus, if specimens of identical graphite grades are located in similar positions within each capsule, a similar dose and load level will be imposed on a consistent grade of graphite. Maintaining consistent specimen positions for each grade

within the six different capsules will allow the determination of temperature-induced changes for irradiation creep and material properties across the AGC experiment.

2.2 AGC Graphite Grades and Specimen Dimensions

The AGC experiment is designed to ascertain the irradiation behavior of currently available nuclear graphite grades within the anticipated operating parameters of an HTR design. By exposing a variety of nuclear graphite grades representing the range of fabrication parameters (grain size, fabrication processes, and raw source material) to the expected operating conditions for an HTR design (600°C–1,100°C and 0.5–7 dpa dose), a comprehensive understanding of the irradiation response and behavior of graphite components in general can be achieved. This will limit the need for additional research in the future if the current graphite grades are altered (i.e., new raw material sources are used) or new grades are utilized in future reactors.

The AGC experiment utilizes a variety of current graphite grades to envelope the major fabrication parameters believed to be responsible for the irradiation behavior of nuclear graphite.[3,4] This range of fabrication parameters is represented by AGC major grades, which were deemed to be production-ready grades that could be used in current or future HTR designs. Major graphite grades are one type of sample within the AGC irradiation capsule. In addition, four other sample types are designated within the AGC experiment. The five AGC sample types are categorized as follows: [7, 9]

1. Major Grades (Irradiation Creep and Control Specimens)

   These graphite grades are current reactor candidates for the core structures of an HTR design as well as historical (reference) grades. Due to their fabrication maturity and consistency, HTR core components are most likely to be formed from these major grades and are expected to receive reasonably large neutron doses in their lifetime. Only major grade specimens were used to determine the critical irradiation-induced creep strain rate.

2. Minor grades (6-mm-tall, button-shaped piggyback specimens).

   These grades are HTR-relevant grades that are not yet production ready or are most likely to be used in low neutron dose regions of the core (e.g., the permanent structure of the prismatic block HTR design).

3. Alternate grades (6-mm-tall, button-shaped piggyback specimens).

   These are grades that current HTR vendors have identified as being of interest as alternate graphite grades for certain components within the reactor.

4. Experimental grades (6-mm-tall, button-shaped piggyback specimens).

   Experimental graphite grades are included in AGC to assess the viability of new graphite grades whose manufacturing processes and raw materials are such that they may offer superior irradiation stability. Additionally, other carbonaceous materials such as fuel compact matrix materials, carbon-carbon composites, silicon-carbide composites, or other experimental materials that could offer superior performance within the extreme environment of an HTR core are included.

5. Single crystal graphite (piggyback specimens).

   Samples of highly ordered pyrolytic graphite (HOPG) are included in AGC to assess the fundamental irradiation response of single crystal graphite. These specimens offer a specific dimensional change behavior of graphite, which is particularly significant to the behavior of polycrystalline (polygranular) graphite grades.

To provide all necessary material property tests in the AGC experiment, each test series capsule contains two primary specimens: (1) “creep” specimens, providing irradiation creep-rate value as well as mechanical properties; and (2) button-shaped “piggyback” specimens, providing thermal material property changes to the graphite. Creep specimens are fabricated only from major grade graphite types. Piggyback specimens are fabricated from major, minor, and experimental-grade graphite types. The piggyback specimens are not mechanically loaded and are subjected only to neutron irradiation at high operating temperatures to assess the effects of a reactor environment on the specific graphite grade.[9, 10, 11]

All specimens are 12.4 mm in diameter, with the larger creep specimens having a nominal length of 25.4 mm, and the button-shaped piggyback specimens having a nominal length of 6.3 mm. Small graphite containers that are 12.4 mm in diameter by 6 mm long contain the thin wafer HOPG specimens. The large creep specimens provide a means to acquire dimensional and volume change, elastic modulus, thermal expansion, and electrical resistivity measurements. However, these creep specimens are not suitable for thermal diffusivity measurements because of their length. The small button-shaped piggyback specimens permitted only dimensional measurements, density, and thermal diffusivity testing to be performed. Together, both types of specimens provide the changes in material properties for stressed and unstressed graphite grades.

2.3 General AGC Test Train Design

All AGC test trains and irradiation capsules have the same general physical configuration to provide consistent dose and applied mechanical stresses on specimens of similar graphite grades. While there are key machining and structural differences between capsules to change the irradiation temperature for the different capsules, the majority of the AGC design is identical for all capsules. A schematic of the general AGC test train and location of graphite specimens within the test train is shown in Figure 2.

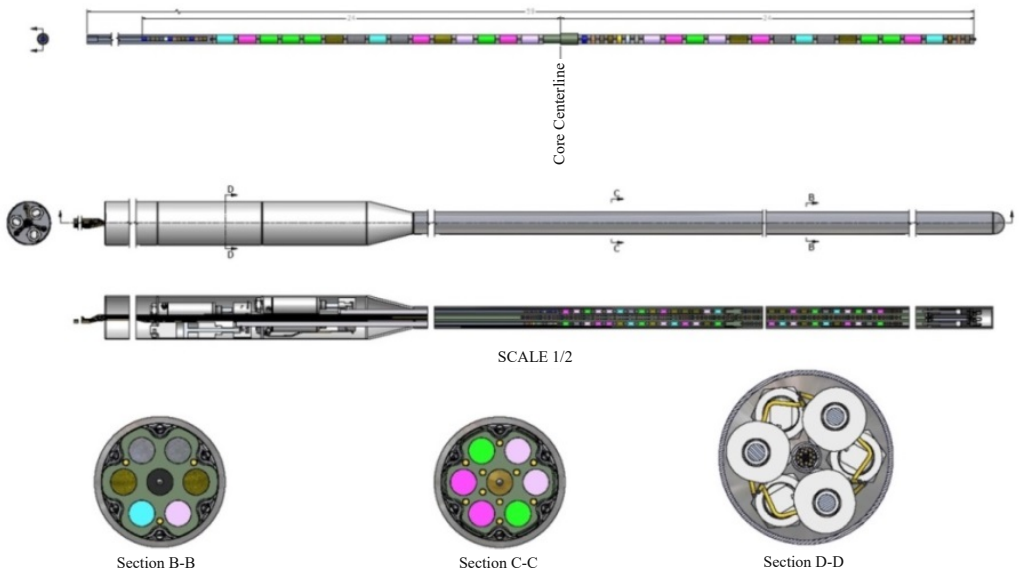

Figure 2. The general AGC creep capsule layout with Section B-B illustrating stack positions of unstressed specimens, Section C-C illustrating stack positions of stressed specimens, and Section D-D illustrating pneumatic ram positions within the top head of the test train.

All irradiation capsules have six channels located in the outer perimeter of the graphite specimen holder body and a center channel. All channels are 12.9 mm (0.51 in.) in diameter and are designed to hold all types of AGC specimens. The upper (top) half the outer channels has mechanical loads applied to

the specimens. However, the lower (bottom) half for these channels has no mechanical load applied to the specimens in these locations. Due to the neutron flux profile in ATR, matched pairs with similar neutron fluence and temperatures are achieved by pre-ordering the specimen axial locations. Specimens in the upper half of the channels were stressed by the applied mechanical load while their matched-pair received a similar dose in an unstressed state. Three stress levels—13.8 MPa, 17.2 MPa, and 20.7 MPa (2.0 ksi, 2.5 ksi, and 3.0 ksi) nominal—are applied in all AGC capsules to provide a known stress on the graphite specimens during irradiation. These mechanical stress levels are high enough to produce irradiation-induced creep strain with the graphite specimens.

Temperature values within all AGC capsules are calculated based on thermocouple readings at select positions within the capsule. Specimen temperature is calculated with a finite element model that has been calibrated to predict the known thermocouple readings in the capsule. Dose levels are calculated using Monte Carlo N-Particle Transport Code models and operating conditions in the ATR core and are corroborated from flux wire data.

3. Establishing Specimen Dose and Applied Load

To achieve the desired irradiation dose levels and applied mechanical loads to the specific specimens, an exact specimen loading order is critical. Because irradiation creep is usually determined by the difference in dimensional change occurring within matched-pair specimens that have an applied load and those that do not, it is crucial to understand where every specimen is located within an AGC capsule.

Specimens within the upper half of the capsule have a mechanical load applied to them via a pneumatic ram system. Specimens within the lower half remain unloaded and thus have no applied stress. A careful specimen loading order within the irradiation capsule is required to ensure similar dose levels and temperature distribution for specimens in the upper and lower stacks. Other considerations include the size of each creep specimen, the need for periodically placed flux wires, and the space requirements in the top of the stacks for the pneumatic push rods. The core flux mid-plane, in relation to the capsule arrangement, was established so that the reactor neutron flux field could be correlated to the physical elevations and positions in the capsule to yield accurate irradiation dose levels, Figure 3..[12]

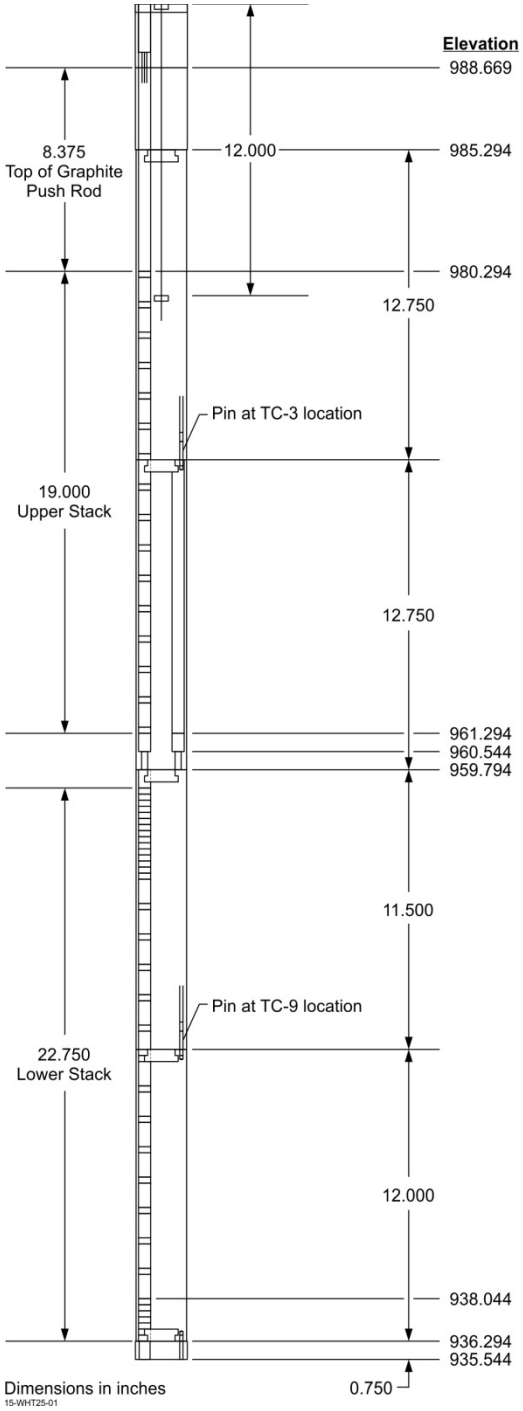

Figure 3. Elevation sketch of the AGC capsule.

Irradiation dose values, as a function of distance from the reactor core centerline, are calculated from the total calculated fluence using standard conversion factors for carbon in a fast neutron irradiation field (E >0.1 MeV)..[13]A neutron flux gradient across the capsule thickness requires the capsule to be rotated 180 degrees at the irradiation midpoint. This rotation results in a uniform neutron-fluence profile for all stacks, regardless of their position within the capsule.

As described in previous reports,[13] the ATR neutron flux profile is not completely symmetrical along the vertical axis. Thus, to produce matched-pair specimens that have similar dose profiles both above and below the core mid-plane, an offset position from the mid-plane is required. An offset distance of 31.75 mm (1.25 in.) from the core mid-plane for the bottom creep specimens produces the closest dose matches between specimens. While it was impossible to exactly match the dose levels for both the upper and lower specimens, the dose levels for each specimen pair were fairly close, ranging from 0 to 2%.[13]

3.1 Physical Positions of Creep Specimens in the Stacks

Once the specimen-position offset is established for the bottom half of the specimens, the number of total creep specimens for each grade of graphite is determined. It should be noted that the specimen stacking order for subsequent AGC irradiation capsules was changed from that initially established for the AGC-1 test train. In the initial AGC capsule design, AGC-1 utilized 6.35-mm-long NBG-25 graphite spacers between all creep specimens to separate them from each other. It was determined that this was not necessary, and the 6.35-mm-long NBG-25 graphite spacers were eliminated for all subsequent AGC test trains. The decision to eliminate spacers increased the total number of creep specimens in the AGC-3 capsule to 222 total specimens.

As mentioned above, the six outer stacks in the capsule allow the specimens in two of the channel stacks to be loaded at 13.8 MPa, while the other two pairs of channels are loaded at 17.2 and 20.7 MPa, respectively. Because two stacks are at similar applied stress levels, the specimen loading order can be shifted between the two stacks, allowing the same grade of graphite to be mechanically loaded over a broader neutron dose range, as illustrated in Figure 4. Assuming that both stacks will have the same applied stress level, receive similar dose levels per position, and have a constant temperature allows this shifting of the specimens and, consequently, a more uniform, smoother dose profile for each graphite grade.

A final consideration when establishing the specimen loading positions is the grain orientation of the specimens. All AGC capsules attempt to account for the grain orientation relative to irradiation behavior. For extruded graphite grades, the against-grain (AG) and WG directions are obviously perpendicular and parallel to the extrusion direction, respectively. Iso-molded grades are assumed to have little-to-no grain direction and there is no consideration for their orientation. However, in the case of the vibration-molded graphite grades (i.e., NBG-17 and -18), there are actually two WG directions and one AG direction as a consequence of the fabrication process. The total number of WG and AG specimens is dependent on the particular AGC capsule pair (i.e., AGC-1 and AGC-2 have the same number of specimens with similar orientation).

Once these considerations are accounted for, the dose-level profiles are determined for each graphite grade within each channel stack. It should be noted that due to the elimination of the majority of the NBG-25 spacers from the AGC-1 design, the dose-level profiles for each graphite grade have been altered for the succeeding AGC capsules.[8, 14, 15, 16, 17] However, the changes are modest, allowing nearly direct comparison between all subsequent AGC capsules.

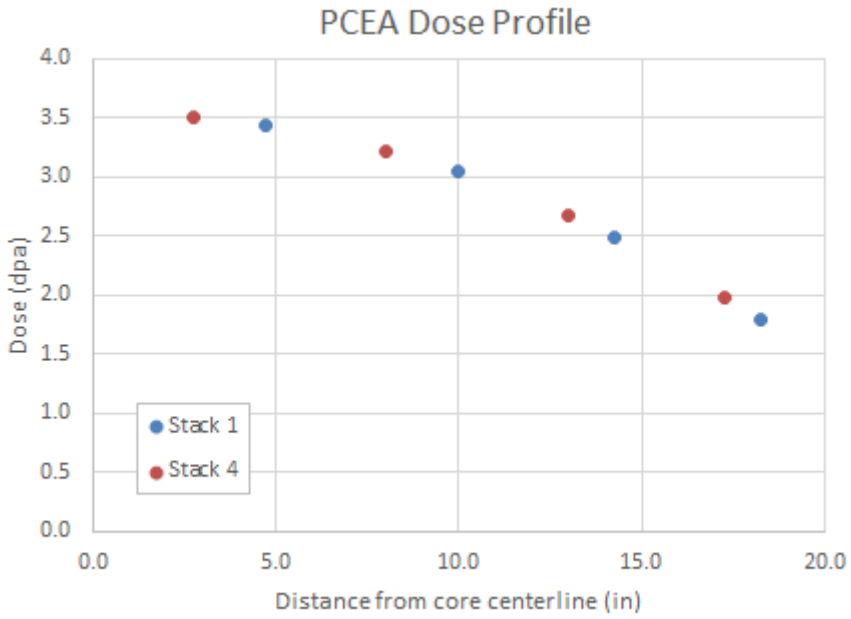

Figure 4. A typical dose profile for creep graphite specimens utilizing similar applied stress levels in matched stacks.

3.2 Future Changes to AGC Experiment

It should be noted that in 2018, the Department of Energy (DOE) ART approved of a major design change to the AGC experiment. It was determined that the AGC experiment should extend the neutron dose range from 0–7 dpa to a more pertinent 0–15 dpa dose that is of more use to current HTR designs. This new neutron dose increase will extend the current nuclear grades past turnaround dose levels and into the non-linear tertiary-creep regime. To achieve this higher maximum dose level, it was decided to repurpose the last two irradiation capsules, AGC-5 and AGC-6, which were to be irradiated at Very High Temperature Reactor conditions of 1100°C. Under the new direction (2018), AGC-5 and AGC-6 capsules will be used to irradiate previously exposed specimens from AGC-2, AGC-3, and AGC-4 once they have undergone PIE, Figure 5. AGC-5 will be renamed as High Dose Graphite (HDG)-1 and will re-irradiate AGC-2 specimens at irradiation temperatures of 600°C. AGC-6 will be renamed as HDG-2 and will re-irradiate selected specimens from AGC-3 and AGC-4 at irradiation temperatures of 800°C. No graphite specimens will be irradiated at temperatures of 1100°C. Once irradiation is complete in HDG-1 and HDG-2, all specimens will undergo a second PIE testing to determine the effects of this higher dose level on material properties.

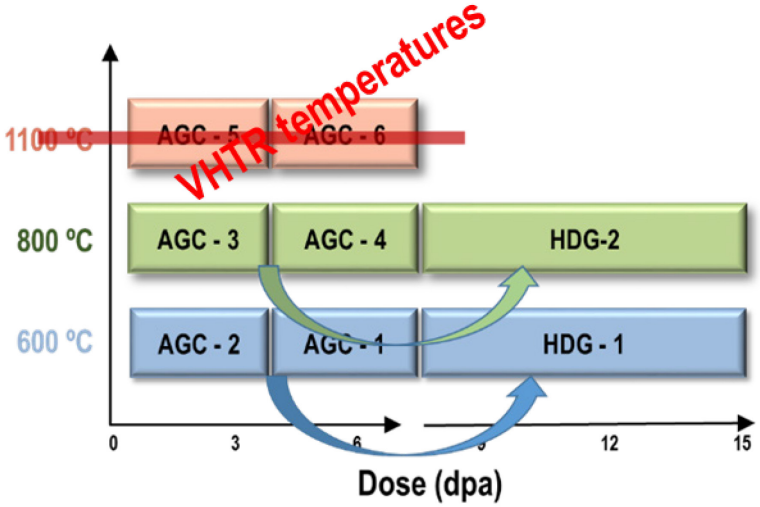

Figure 5. New AGC Experiment irradiation schedule illustrating the elimination of very high-temperature irradiations (1100°C) and the extension of the dose range to 15 dpa.

This major change will not affect AGC-3 or AGC-4 irradiations and PIE. Thus, no changes to the capsule design, specimen testing, or PIE analysis on the initial 0–7 dpa, 600°C and 800°C irradiations will occur. Any changes in support for the HDG irradiations will be detailed in future HDG-1 and HDG-2 reports.

4. AGC-3 TEST TRAIN CAPSULE

The AGC-3 capsule was to be irradiated in the ATR at a nominal temperature of 800°C, beginning with irradiation Cycle 152B on November 28, 2012. The AGC-3 irradiation capsule is the companion capsule for AGC-4. Both of these capsules are to be irradiated at 800°C but have different dose ranges of ~1.0 to 3.5 and ~3.5–7.0 dpa, respectively.

The overall design of AGC-3 was kept as close to the AGC-2 capsule as possible.[18] however, some were, some significant modifications made to the AGC-3 capsule. First, a major design change to the capsule was made to allow finer control of the internal capsule temperature. A new advanced temperature-control system allowed greater control of the temperature conducting gas mixture (the He-Ar gas ratio) within five distinct axial regions of the capsule, rather than just one gas composition over the entire capsule length.[17] By altering the gas composition within these five different regions, a much finer control of the temperature throughout the length of the capsule was achieved.

Other design changes included the complete removal of major grades IG-430 and H-451 from AGC-3 capsule. Also, all of the minor grade piggyback specimens were removed and replaced with either major grade or experimental-grade piggyback specimens. All AGC-3 design documents and drawings pertinent to the AGC-3 graphite specimens have been reported in the previous AGC-3 graphite pre-irradiation data analysis report, INL/EXT-13-30297.[9]

4.1 AGC-3 Graphite Grades

The major grades of the nuclear graphite tested in AGC-3 are similar to those tested in AGC-2. The difference is that H-451 and IG-430 were removed from the AGC-3 capsule and replaced with Grade 2114. The major grades for AGC-3 are now NBG-17, NBG-18, PCEA, IG-110, and 2114. Minor, alternate, and experimental grades of graphite are presented below:[9]

1. Major grades: NBG-17, NBG-18, PCEA, IG-110, and 2114
2. Minor grades: None
3. Alternate grades: PCIB and GrafTech
4. Experimental grades: SGL, SGL-SiC, and MLRF
5. Single crystal graphite: HOPG.

A more complete description of the graphite specimens included in AGC-3 is given in Table 1.[4] Specimen ID letters were given to each graphite grade in place of their name designations to shorten the specimen identification number for each specimen. This allowed the specimen to have a short ID number, which was necessary for the laser engraving of each specimen. For grades NBG-17, NBG-18, IG-110, and PCEA (i.e., codes A, B, D, E, and T), both WG and AG specimen orientations are included in the capsule.

Table 1. Major, minor, alternate, and experimental graphite grades within the AGC-3 capsule.

Graphite Grade	Forming Method	Intended Purpose	AGC Code Letter
NBG-17	Vibrational molded	AREVA Next Generation Nuclear Plant design	A
NBG-18	Vibrational molded	Pebble Bed modular reactor (not currently being pursued)	B
PCEA	Extruded	AREVA Next Generation Nuclear Plant design	D
IG-110	Isostatically pressed	HTR– Pebble-Bed module (Japan and China)	E
2114	Isostatically pressed	Candidate graphite	T
HOPG	Vapor deposited	Fundamental studies	CAN101-CAN117
GrafTech	Isostatically pressed	Alternate/experiment candidate grades TS and PCIB-MG	200,324,325,328
PCIB	Isostatically pressed	Alternate candidate	P
SGL	Vibrational molded	SiC coating experiments	S1-S20
SGL-SiC	Vibrational molded	SiC coating experiments	A-H
MLRF	Vibrational molded	SiC coating experiments	CAN121-CAN129

4.2 AGC-3 Specimen Stack Positions

The final loading configuration for the outer channel/stacks was determined for each graphite grade to optimize the number of specimens for each grade, to create a smooth dose profile for the creep and piggyback specimens, and to ensure the proper position of creep specimens to create a symmetric dose profile above and below the core centerline.[19, 20, 21]

A further decision was made to increase the creep specimen number population for the newer graphite grades because little-to-no irradiation data are available on these grades. Specifically, more specimens of graphite grades NBG-18 and PCEA were chosen to be irradiated instead of the IG-110 and NBG-17 graphite grades.[22] NBG-18 and PCEA were determined to have 16 specimens per applied stress level for a total of 48 specimens within AGC-3. The super-fine-grained Grade 2114 (the modern replacement for the old grade 2020) was newly added to AGC-3 and is represented by 16 specimens at the lower applied stress levels with 15 specimens at the highest stress level, for a total of 47 specimens. NBG-17 was represented by only 12 specimens per applied stress level, for a total of 36 specimens, and IG-110 was represented by 14 specimens, totaling 42 specimens within AGC-3. Table 2 lists the total number of specimens irradiated per major graphite grade.

Table 2. Total number of irradiated-creep specimens in the AGC-3 test series capsule.

Graphite Grade	Number of Creep Specimens
PCEA	48
NBG-18	46
IG-110	42
NBG-17	36
2114	47
Total Creep	219

In AGC-3, approximately 75% of creep specimens for PCEA and IG-110 were oriented in the WG direction and 25% of the specimens were AG. However, in the case of the vibration-molded graphite grades (i.e., NBG-17 and -18), which possess two WG directions and one AG direction, it was logical to split the WG and AG specimens evenly (i.e., 50/50 ratio) rather than following the 75/25 ratio established for the extruded specimens. The Grade 2114 specimens were only extracted from the billet in one grain orientation.

The orientation of the specimen is designated by the second digit in the sample identification number. Specimen identification numbers possessing a “W” in the second digit are specimens in the WG orientation (e.g., DW101). Specimen identification numbers possessing an “A” in the second digit are specimens machined from an AG orientation (e.g., DA402). As discussed in the previous AGC-3 Creep Strain Analysis report,[5] vibrationally molded grades are designated with an “L” or “P” for the two WG orientations (e.g., BP402 for an NBG-18 grade specimen).

The final loading configuration is documented in INL-EXT-19-54725, *AGC-3 Irradiation Creep Strain Data Analysis*.[5] This includes loading order of control, creep, and piggyback specimens, lower stack offsets, and flux wire locations. Following irradiation in the ATR at INL, the AGC-3 capsule was disassembled.[23] All specimens recovered from disassembly were visually inspected at the INL Carbon Characterization Laboratory before being stored in the irradiated graphite storage vault. It should be noted that NBG-18 specimens BP3302 and BL3103, and 2114 specimen TW3405 were lost (missing) during

AGC-3 disassembly activities.[23] After accounting for all recovered specimens from the AGC-3 capsule, PIE and testing were performed for each specimen at the INL Carbon Characterization Laboratory.

5. AGC-3 AS-RUN IRRADIATION CONDITIONS

AGC-3 was designed to provide irradiation conditions similar to the 600°C graphite irradiations (i.e., AGC-1 and AGC-2) with similar graphite grades, the same applied mechanical stresses, and similar He-Ar gas environment, but irradiated at 800°C. AGC-3 is also the lower dose 800°C capsule (0-3.5 dpa), requiring a shorter irradiation time within ATR. AGC-4 is designated as the higher dose 800°C capsule (3.5–7.0 dpa), requiring an irradiation period in ATR twice as long. An additional objective was to implement capsule design improvements learned from AGC-1 and AGC-2 to reduce the large specimen temperature range experienced in AGC-1.

AGC-3 was irradiated in the south flux trap of ATR between November 28, 2012, and April 12, 2014, over four reactor cycles: Cycles 152B, 154B, 155A, and 155B (the AGC-3 capsule was not in ATR for Cycles 153A/B and 154A). AGC-3 received 4374 MW days or approximately 209.5 effective full power days of irradiation..[24] The average estimated irradiation temperature for all samples in the AGC-3 test train was 820°C, with a standard deviation of 30°C and a total range of 748–918°C. While the temperature range was much better than the prototype AGC-1 irradiation capsule, the AGC-3 irradiation temperature range exceeded the design (800 ±50°C)..[25]

From the effective full power days of irradiation, the average radiation dose of all specimens in AGC-3 was 2.8 dpa, with a standard deviation of 0.8 dpa and a total range of 0.9–3.7 dpa. This includes the piggyback specimens in the extreme top and bottom positions of the irradiation capsule. The final specimen dose levels ranged from 0.9–3.7 dpa with the specimens at the mid-plane elevation receiving the highest accumulated dose levels. It should be noted that the majority of the piggyback specimens were located within the unloaded central stack of the AGC-3 capsule. However, a small fraction of the piggybacks was used in the outer stacks primarily near the bottom of the capsule to ensure the creep specimens were centrally located within the reactor core mid-plane. Since these select piggyback specimens were near the bottom end of the capsule, they received much lower dose levels than the creep specimens.

Irradiation creep is defined as the difference in dimensional change between stressed (creep) and unstressed (control) samples irradiated at similar dose and temperature levels. To induce irradiation creep strain within the AGC-3 creep specimens, one-half of the specimens were subjected to mechanical stresses while the remainder of the specimens had no applied stresses. As described in "AGC-3 Specimen Load Calculations by Stack," (ECAR-3932, INL/MIS-19-52628),.[26] because of a gas leak in the specimen loading system, stressed samples were subjected to only two stresses: 13.8 MPa for specimens in Stacks 1, 2, 4, and 5 and 20.7 MPa in Stacks 3 and 6. ECAR-3932 gives details on how the specimen stresses were calculated for each stack of specimens. This report also explains the uncertainty on the load data.

The temperature of the AGC-3 capsule ranged from 748–937°C (an average of 821°C, 30°C standard deviation). Temperature values within all AGC capsules are calculated based upon thermocouple readings at select positions within the capsule. Specimen temperature is calculated with a finite element model that has been calibrated to predict the known thermocouple readings in the capsule. The temperature calculations as well as a detailed uncertainty analysis of the temperature model used to derive the specimen temperatures are given in ECAR-3386.[25]

6. MATERIAL PROPERTY DATA

Pre-irradiation material property data for all major graphite grades are reported in INL's INL/EXT-13-30297, Rev 0, *AGC-3 Graphite Pre-irradiation Data Analysis Report*.[9, 27] The data analysis report also details dimensional sizes of the specimens in the capsule; creep, control, and piggyback specimens. The post-irradiation material property data are provided in the INL report INL/EXT 17-43823, *AGC-3 Specimen Post-Irradiation Examination Data Package Report*.[6] Table 3 below shows the breakdown of specimens in the AGC-3 capsule by graphite grade, grain orientation, and specimen type.

Table 3. Number of with-grain, against-grain, creep, and piggyback specimens for the major graphite grades in the AGC-3 capsule.

	Creep/Control Specimens		**Piggyback Specimens**	
	With Grain	**Against Grain**	**With Grain**	**Against Grain**
NBG-17	18	18	21	9
NBG-18	23	23	11	9
PCEA	36	12	11	18
IG-110	30	12	17	12
2114	47	0	24	0

Dimensional measurements were made on all specimens (creep, control, and piggyback). In addition, the density, resistivity, Young's modulus (both by sonic resonance method and sonic velocity method), shear modulus, and thermal expansion was measured on the larger creep and control specimens. Only density and thermal diffusivity measurements were made on the smaller piggyback specimens.

Dimensional change was calculated and recorded for the AGC-3 creep analysis and reported in the AGC-3 creep analysis report.[5] All measurements were made according to an appropriate ASTM standard. Table 4 below lists the ASTM standards that were used when making the graphite material properties measurements. Further details of how these measurement standards are applied to the graphite specimens can be found in PLN-4888, "AGC-3 Graphite Specimen Post-irradiation Characterization Plan."[28] This plan describes the measurement techniques, equipment, and standards used to gather the data analyzed in this report.

Table 4. ASTM standards used for AGC-3 property measurements.

Measurement	**ASTM Standard**	**Material Property**
Standard Test Method for Bulk Density by Physical Measurements of Manufactured Carbon and Graphite Articles	ASTM C559-16	Bulk density
Standard Test Method for Moduli of Elasticity and Fundamental Frequencies of Carbon and Graphite Materials by Sonic	ASTM C747-16	Young's modulus (flexural mode)
Standard Test Method for Sonic Velocity in Manufactured Carbon and Graphite Materials for Use in Obtaining an Approximate Young's Modulus	ASTM C769-98(2005)	Young's and Shear modulus

Measurement	ASTM Standard	Material Property
Standard Test Method for Electrical Resistivity of Manufactured Carbon and Graphite Articles at Room Temperature	ASTM C611-98 (2016)	Electrical resistivity
Standard Test Method for Thermal Diffusivity by the Flash Method	ASTM E1461-13	Thermal diffusivity
Standard Test Method for Linear Thermal Expansion of Solid Materials with a Push-Rod Dilatometer	ASTM E228-17	Coefficient of thermal expansion

Note:*All ASTM standards are reapproved every 5 years. During this review, the technical content of the standard is confirmed to still be valid. In some cases, this process of reapproval will cause rise to a more in-depth revision. When a new revision takes place the publication year is changed. Over the long duration of the full ART AGC irradiation experiment matrix the ASTM standards followed will be reapproved and revised. These standards are reviewed for technical equivalency prior to each publication of an AGC characterization plan. This makes it possible to compare and analyze data across the full experiment matrix. When a revision is technically equivalent to its predecessor, the new version is used and referenced throughout the full test (e.g., characterization plan, pre-irradiation analysis and post-irradiation analysis). If the revision is not technically equivalent, the previous version will continue to be followed and referenced.*

When interpreting the material property measurements and property changes, the measured data was analyzed against the five variables within the experiment. These variables are specimen dose, irradiation temperature, applied stress, grain orientation, and the graphite grade/type. The irradiation temperature for all AGC-3 is relatively constant ranging between 748 and 937°C over the irradiation dose range 0.9 and 3.7 dpa, due to the flux profile of the reactor. Figure 6 illustrates this relationship in the AGC-3 capsule.

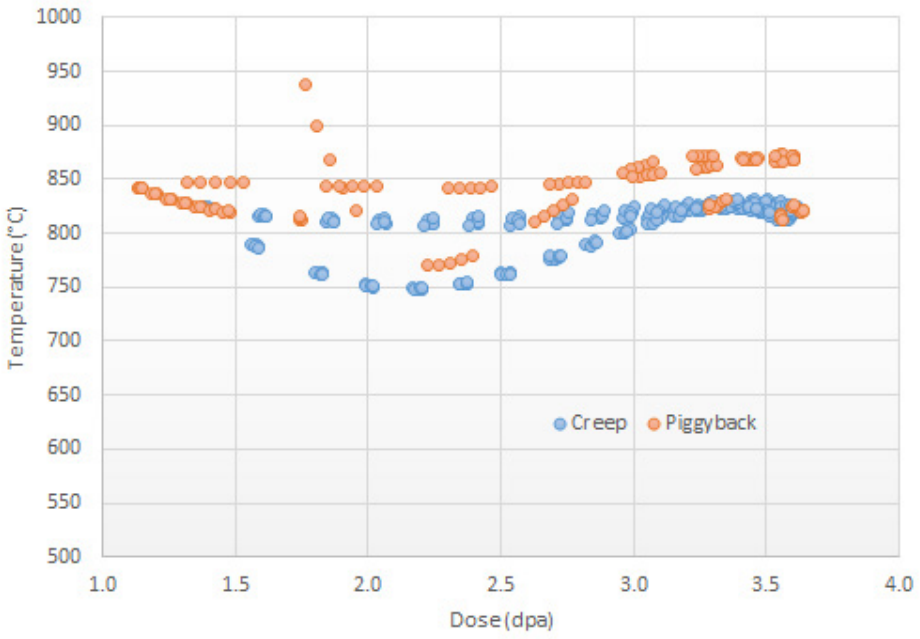

Figure 6. AGC-3 specimen irradiation temperature versus dose.

Finally, the irradiated material property data are presented as a percentage change from the unirradiated material property values. This approach to presenting the irradiation data serves two primary purposes: (1) the quantitative irradiation-induced changes are easily illustrated and (2) the AGC experiment was originally designed to provide the irradiation-induced *change* in each material property rather than the absolute irradiation value. The mean irradiation-induced changes for each the material properties will then be added to the more statistically accurate as-fabricated (Baseline) material property mean values to arrive at the absolute irradiation value for each property. This methodology was undertaken due to the simple fact that the sample population for the irradiated specimens is limited (only a few hundred irradiated specimens for each capsule) while the Baseline data population was designed to be significantly larger, and thus more statistically accurate. All data presented in this analysis will be the calculated relative difference between the pre-irradiation and post-irradiation material property values for each specimen.

The relative changes between the unirradiated and irradiated material were evaluated using a percent difference formula shown below:

$$\%Difference = \left(\frac{X_{post} - X_{pre}}{X_{pre}}\right) \times 100 \quad (1)$$

Where X represents a specific material property.

6.1 Density

Studies from the ART Baseline program have demonstrated that density has a strong correlation to most graphite material property values. Even small variations within a single graphite grade can lead to significant changes in property values. Therefore, any irradiation-induced density change is important to the analysis of the graphite behavior. Dimensional and mass measurements are performed to ASTM Standard C559-90 (Reapproved 2010). This standard describes in detail the procedure for making dimensional and mass measurements for calculating bulk density of manufactured carbon and graphite articles. The bulk density of the specimen is calculated as follows:

$$D = {}^{M}/_{V} \quad (2)$$

where:

D = bulk density, g/cm3

M = mass, g

V = volume, cm^3

(Note: the SI units for density are kg/m^3. We commonly use g/cm^3 in our data)

Density measurements were made on all AGC-3 graphite specimens before and after irradiation. Density changes in the AGC-3 specimens ranged from -0.16 to 4.43% as a function of dose (Figure 7). As anticipated, the density change appears to be linear with respect to the received dose for all specimens over the full range of irradiation temperatures and specimen stress in correlation with the linear irradiated dimensional change and creep behavior anticipated for these lower received dose levels. A linear regression of the data between the dose range of ~1.1 dpa to ~3.6 dpa shows that significant changes do not occur until around 1 dpa, regardless of graphite grade or test conditions.

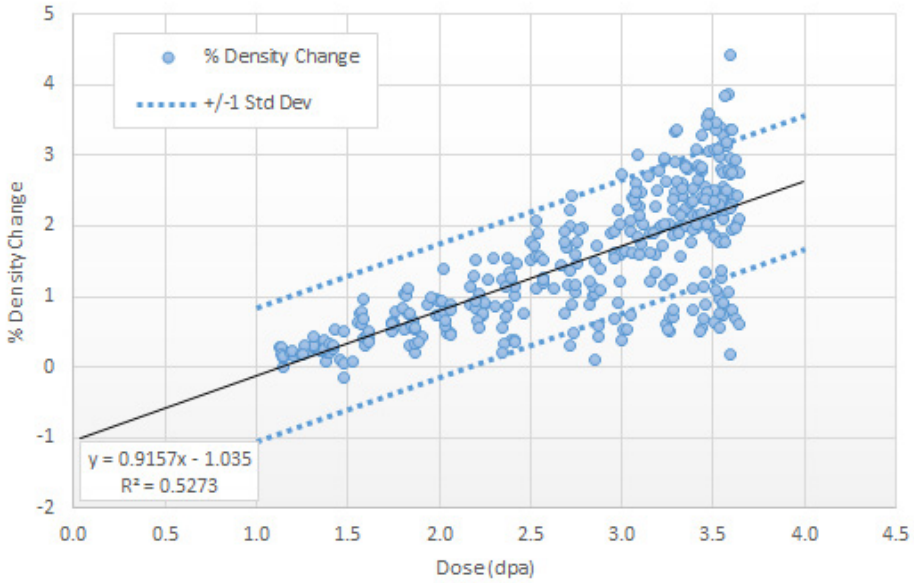

Figure 7. Percentage change of density for all AGC-3 graphite specimens.

The next figure demonstrates the irradiation-induced density changes resulting from irradiation only (no mechanical loaded specimens are considered). Figure 8 illustrates the density change for all unstressed AGC-3 graphite grades with increasing received dose (control and piggyback specimens). As expected, due to irradiation-induced dimensional change, the density for all graphite grades increases simply as a result of exposure to a neutron dose. The extent of change is less than that shown in Figure 7 because the additional dimensional change resulting from mechanical loading is not considered. With the exception of Grade 2114, the regression slopes for all grades are similar demonstrating a similar density change response. However, there are some differences in what dose the initial change in density occurs.

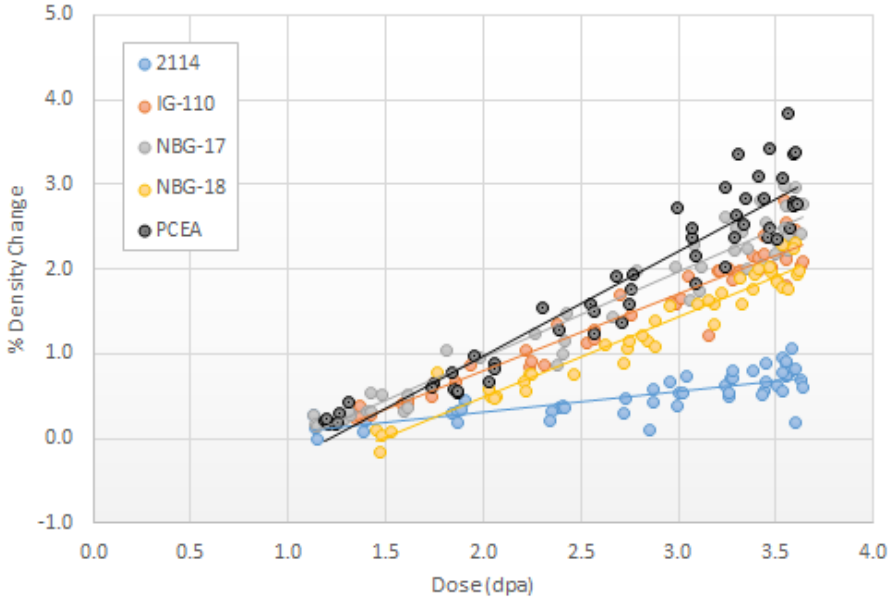

Figure 8. Percent density change versus dose by graphite grade for control specimens only (no applied mechanical loads).

The effect of the applied mechanical stress on the average percent change in specimen density for the five major grades of graphite is shown in Figure 9 (variation in irradiation dose is not considered). Control specimens are not stressed in the experiment; therefore, the specimens are represented by the "0 MPa" grouping on the left-hand side of the plot. Two levels of applied stress are shown as 13.8 MPa and 20.7 MPa. The number of specimens tested for each grade of graphite at the various stress conditions are shown inside each bar. The ±1 standard deviation of the mean is represented by the error bars. These standard deviations are relatively large due to the averaging of data from all grain orientations, specimen irradiation temperatures, and all received doses. However, it can be observed that the density change generally increases as the applied stress increases. For specimens with the highest stress levels, grade PCEA had the highest average percent change in density at 2.7%, while Grade 2114 had the least at 0.5%.

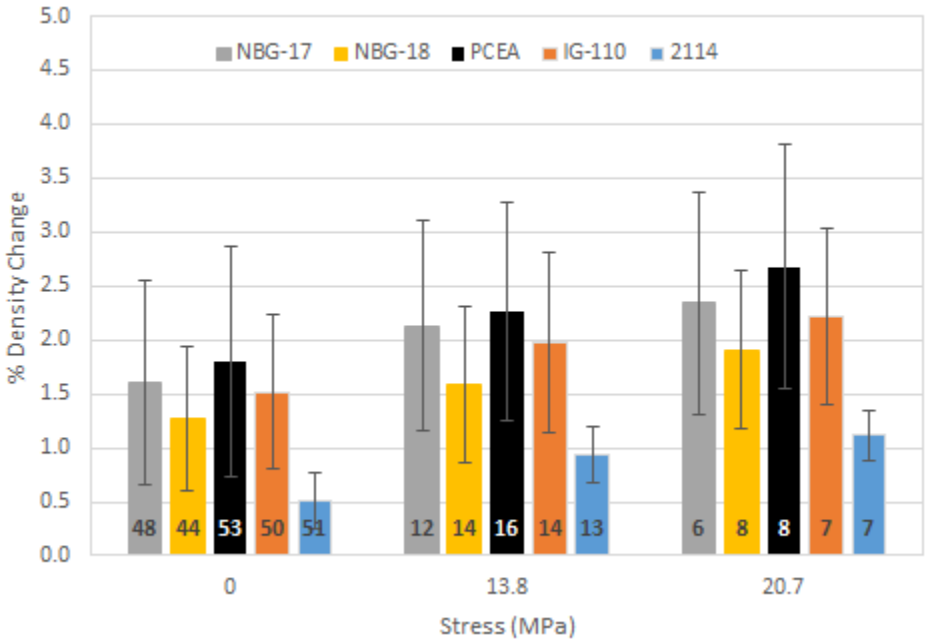

Figure 9. Average percent density change by graphite grade and applied load. The error bars represent +/- 1 standard deviation from the mean and the numbers in the bars represent the sample size.

Figure 10 shows the percent density change as a function of the measured permanent strain in the axial direction, which is the loaded direction for the creep specimens. All stressed (creep) specimens are depicted by the large symbols and the unstressed (control) specimens are shown by the smaller symbols. It is interesting to note that the creep strain observed for stressed creep specimens was significantly larger (when considering all graphite grades nearly three times) than the strain unstressed control specimens for similar density changes. This indicates significant microstructural differences between stressed and unstressed samples where the same irradiation-induced densification occurs, but with larger differences in the axial strain values along the loaded direction.

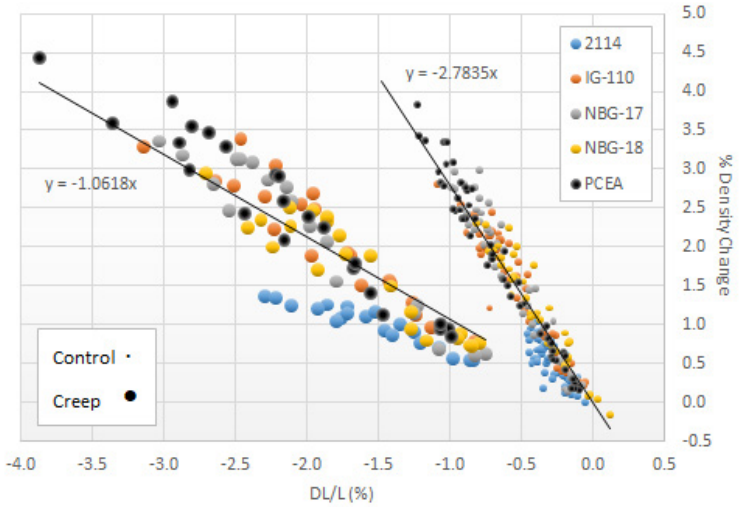

Figure 10. Percent density change versus specimen strain by graphite grade for creep, control, and unstressed piggyback specimens.

Figure 11 demonstrates the effects of combining irradiation dose and applied load on the density changes with stressed and unstressed specimens. An attempt is made to discriminate between density change for applied mechanical stresses and received dose by plotting the data with stressed and unstressed data points as a function of received dose. As noted previously, the stressed specimens show a greater density change than unstressed specimens for similar dose levels indicating differences within the microstructure. The separation between the stressed and unstressed data points appears to be greatest for graphite Grade 2114. This level of separation is not as noticeable in the other graphite grades and as seen previously, the rate of change with dose for the Grade 2114 specimens is noticeably less than the other graphite grades.

Figure 12 shows the same data as Figure 11 but is grouped by the graphite grades fabrication process. Each of the trendlines in the plot have different slopes, with the extruded and vibra-molded graphites showing the most similarity.

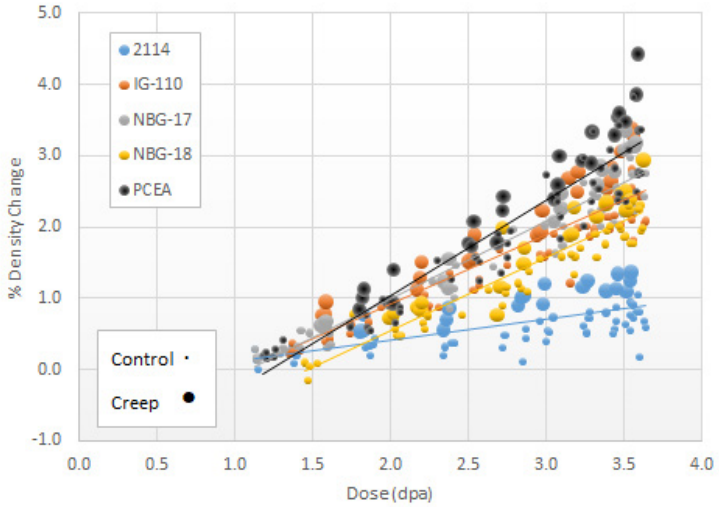

Figure 11. Percent density change versus dose by graphite grade for control and creep specimens.

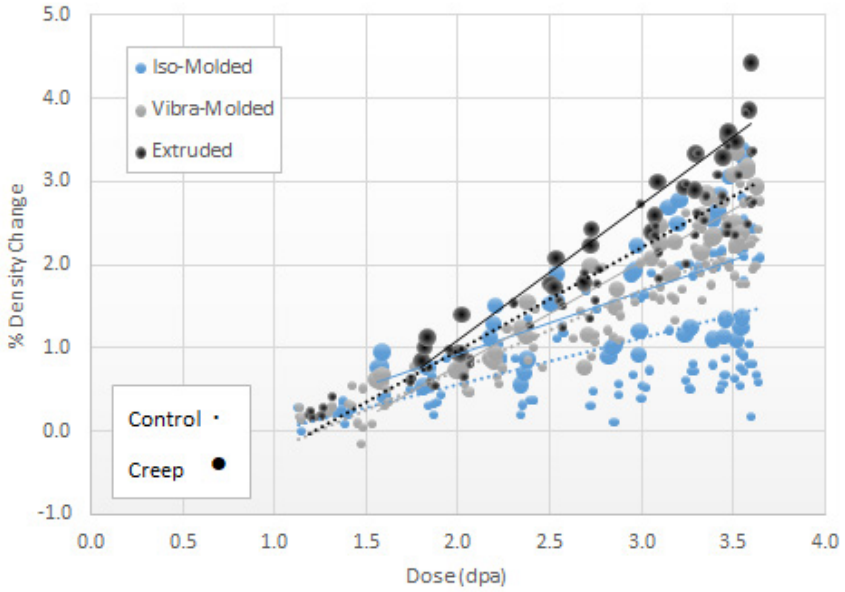

Figure 12. Percent density change versus dose by fabrication process for creep and control specimens.

While dose, applied stress, and graphite grade are considered major factors in density changes, the grain orientation of the specimen can affect the response as well. Four graphite grades are included in the specimen population, which possess distinct grain orientation directions. Figure 13 and Figure 14 show the effects of grain orientation on density changes for grades PCEA, NBG-17, NBG-18, and IG-110 (Grade 2114 only has one direction) in both a stressed and unstressed condition. Neither figure shows a clear correlation observed with grain direction. Note that the error bars (± 1 standard deviation) are relatively large due to the inclusion of multiple variables.

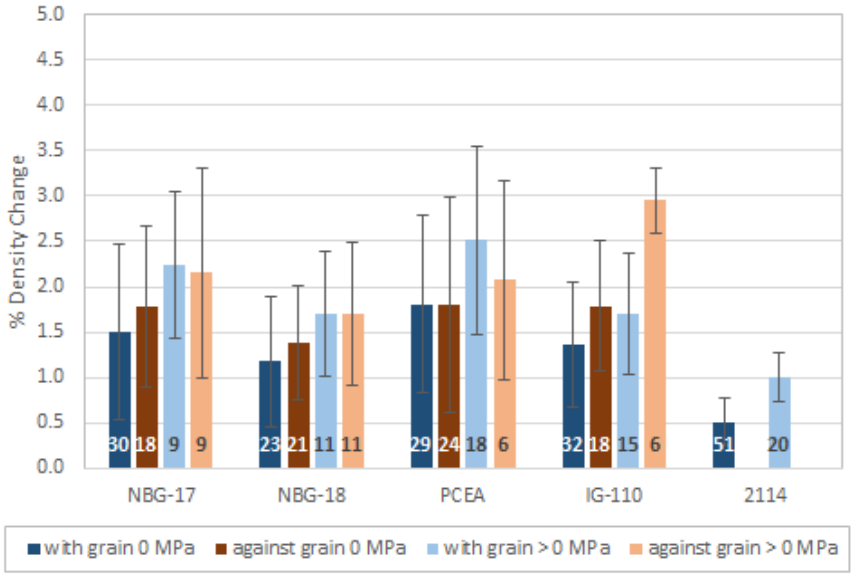

Figure 13. Average percent density change by grain orientation and graphite grade, for control and creep specimens. The error bars represent +/- 1 standard deviation from the mean and the numbers in the bars represent the sample size.

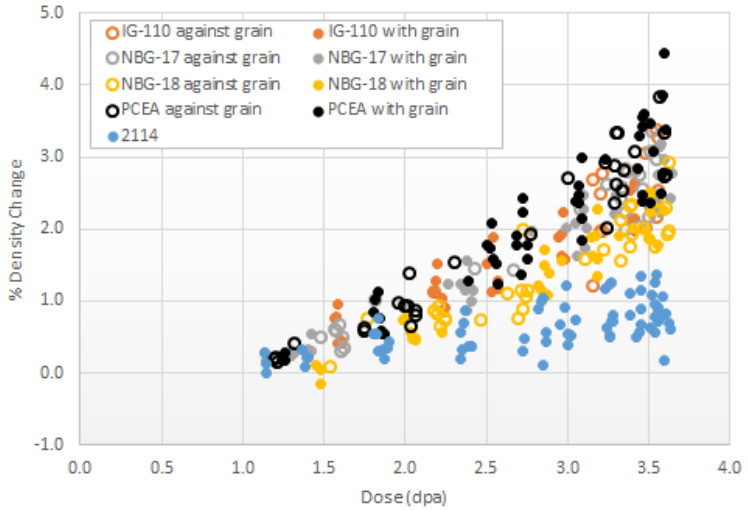

Figure 14. Percent density change versus dose by grade and specimen grain orientation.

Although the AGC-3 capsule was designed for a nominal irradiation temperature of 800°C, the actual irradiation temperatures for each specimen ranged between 748 and 937°C (average 821°C, 30°C standard deviation). The percent change in density for both the stressed and unstressed specimens of the five grades of graphite is plotted separately as a function of dose for two temperature ranges: >821°C and <821°C (Figure 15). By plotting the data in this way, the effect of dose is isolated for two temperature ranges. All grades of graphite show no real separation of the density change for the two temperature ranges. However, the separation due to applied stress, as discussed above, is clearly shown for all grades as is the fact that significant density changes do not start to occur until a dose of ~1.1 to 1.4 dpa.

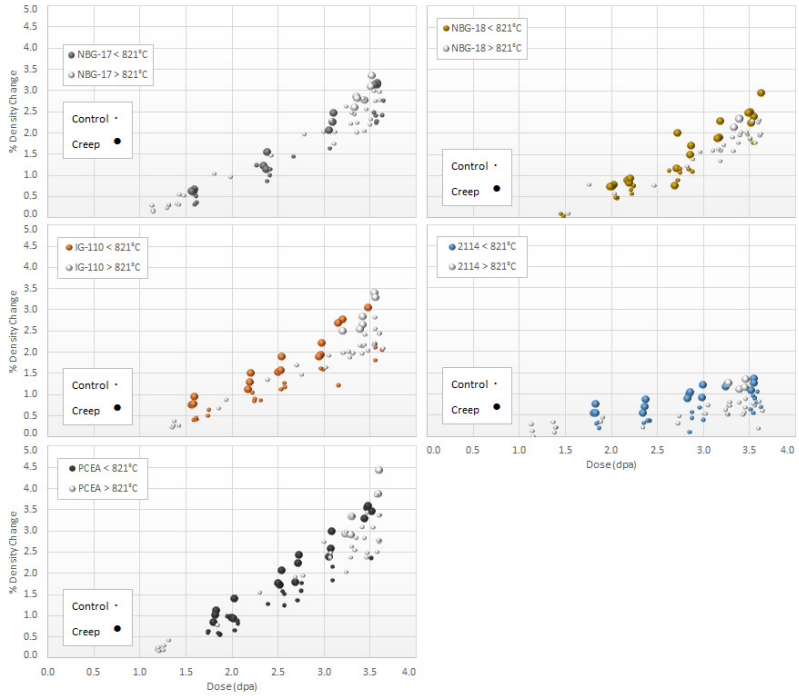

Figure 15. Percent density change versus specimen dose for two temperature ranges, >821°C and <821°C, for different graphite grades.

6.2 Resistivity

Electrical resistivity is used as a rapid, simple means to determine the isotropy, or grain orientation, of manufactured graphite. Changes in electrical resistivity can be used to ascertain irradiation-induced microstructure and crystallinity changes. When used in conjunction with optical microscopy, it can be used to determine the microstructural texture of graphite components with little sample preparation. Resistivity is measured following ASTM C 611-98 (Reapproved 2010). The measurement technique is commonly referred to as a 4-point probe. It consists of passing a known current through the sample and measuring the voltage across the sample at known locations. Based on Ohms Law, the resistance is determined and the resistivity, ρ, is calculated from:

$$\rho = R \cdot A/L \tag{3}$$

where:

ρ = resistivity, Ωm

R = the measured resistance, Ω

A = the cross sectional area, m^2

L = the length over which the voltage is measured, m.

Resistivity measurements were made on the creep and control specimens both before and after irradiation. The overall increase in resistivity was significant for all grades and ranged from 78 to 200% (Figure 16). The average change for all graphite specimens is ~137%. A trend line was plotted (black) along with +/- 1 standard deviation from the trend (dotted lines). The scatter in the data reflects the different variables within the experiment including irradiation temperature, dose, applied stress, graphite grade, and grain orientation.

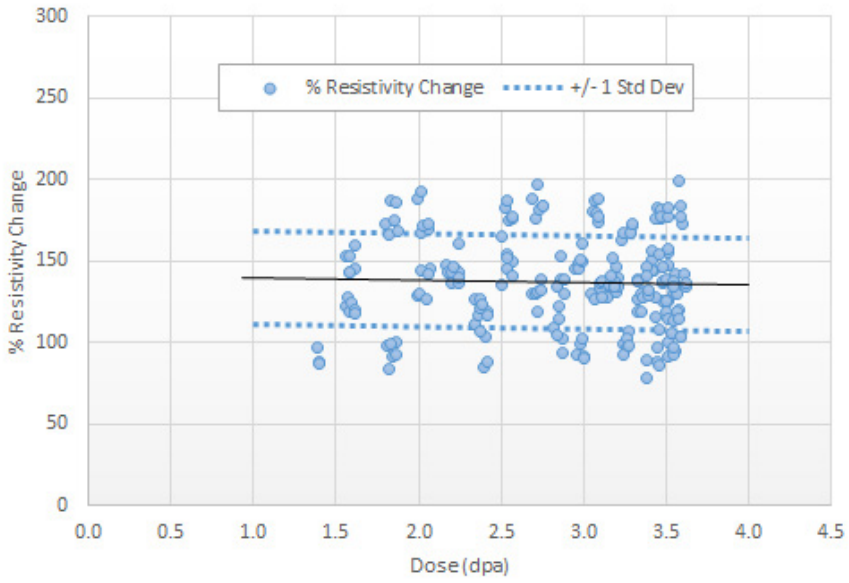

Figure 16. Percent change in resistivity as a function of fast neutron dose for all AGC-3 specimens for which a resistivity measurement was made.

Figure 16 illustrates that while the electrical resistivity changes dramatically after an initial irradiation dose (<1.0 dpa), there is minimal change with increasing dose. This rapid (and large) initial increase in

resistivity change was anticipated and is most likely due to the immediate effects from neutron ballistic damage in the graphite crystal structure leading to point defect populations that disrupt the electrical (and phonon) transfer through the graphitic crystal structures resulting in higher resistivity values. When including all grades, grain sizes, applied stress levels, and grain orientations the resistivity change is generally constant over the entire received dose range of 1.1 – 3.6 dpa. This indicates that electrical resistivity increases rapidly during initial irradiation (<1.0 dpa) but once the maximum change has been reached the resistivity does not continue to change as the dose is increased.

While there are significant similarities between all tested specimens there are some differences between the different graphite grades. Figure 17 illustrates the resistivity effects from irradiation only (no mechanical loaded specimens are considered). Again, all grades exhibit a significant increase in electrical resistivity from irradiation (i.e., percent change in resistivity) by a dose level of less than 1.4 dpa. However, the extruded grade PCEA shows ~175% increase in resistivity while the iso-molded Grade 2114 had a change of only ~90%. As noted in Figure 16, it is interesting that all graphite grades have such a significant rise in resistivity for received dose levels of less than 1.4 dpa followed by near constant resistivity change from a dose of 1.1 to 3.7 dpa. As seen in Figure 17, minimal change occurs for all tested grades for increasing dose levels indicating a constant electrical resistivity with increasing neutron dose.

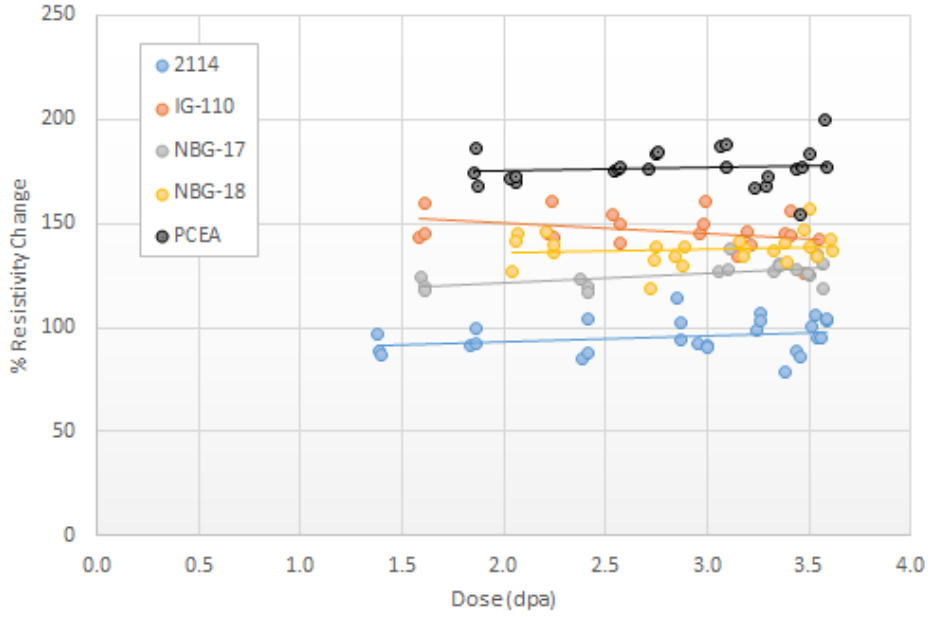

Figure 17. Percent resistivity change versus dose by graphite grade for control specimens.

Figure 18 and Figure 19 demonstrate the effect of stress on the change in resistivity. Figure 18 illustrates the resistivity change for the three stress levels experienced by the different graphite grades. The average percent change in resistivity is indicated by the bar length and the error bars represent ± 1 standard deviation. On average, resistivity changes for all graphite grades remained relatively constant across the increase of applied stress showing minimal affect from applied stress. As noted in Figure 17, the extruded creep specimens demonstrate the largest change in resistivity while Grade 2114 exhibits the least change.

Figure 19, like Figure 17, is a plot of percent change in resistivity versus irradiation dose but with the control (unstressed) and creep (stressed) specimens shown separately. Linear regression lines are

established through the data for each individual grade. There is minimal difference between creep or control specimens for all graphite grades. Any decrease in the resistivity resulting from increasing dose or stress is extremely small and is well within the scatter of the data.

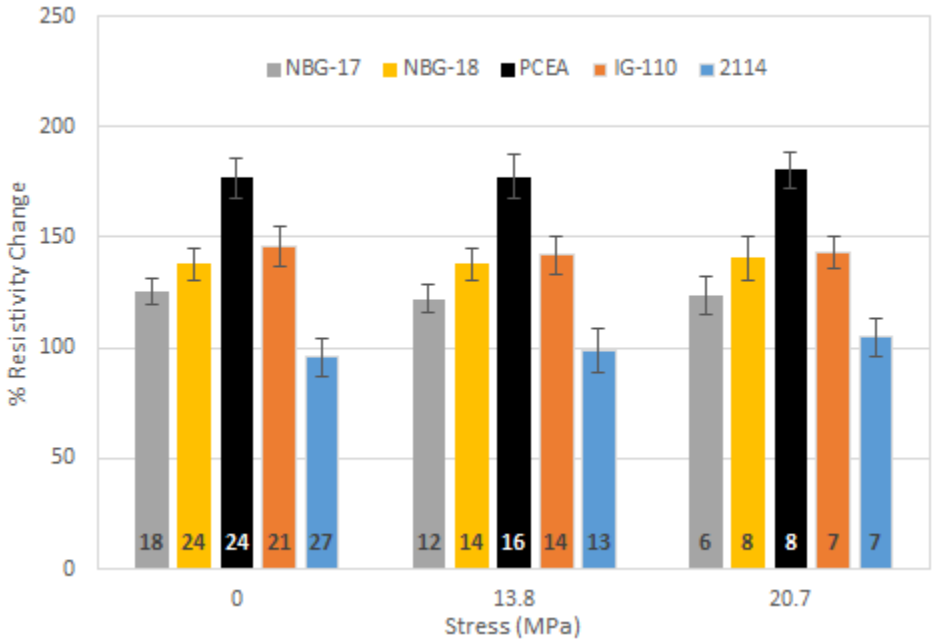

Figure 18. Average percent resistivity change by graphite grade and applied stress. The error bars represent +/- 1 standard deviation from the mean and the numbers in the bars represent the sample size.

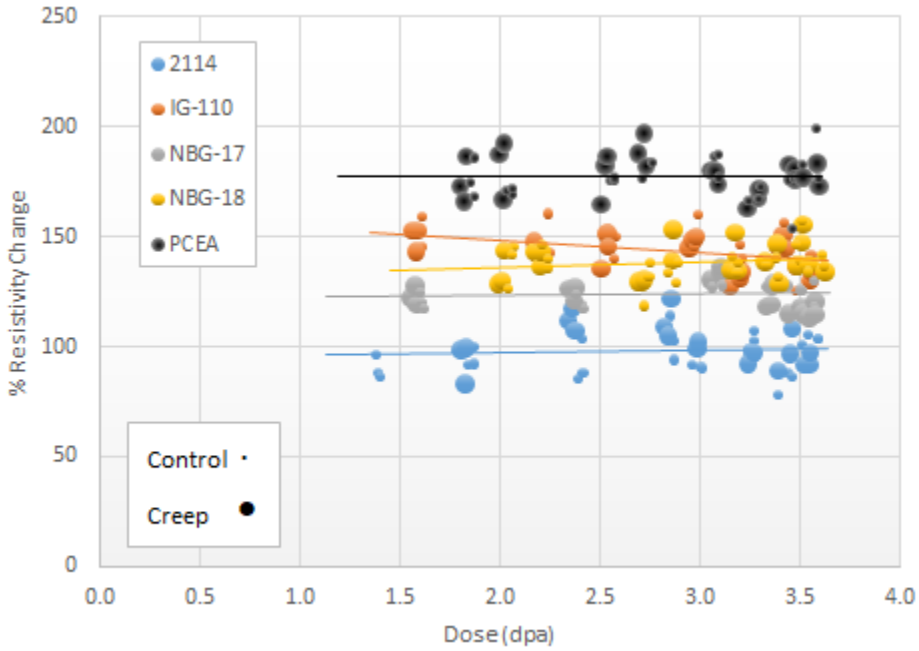

Figure 19. Percent resistivity change versus dose by graphite grade for both control and creep specimens.

Figure 20 shows the effects of irradiation and applied stress for the three separate forming processes. As noted earlier, the extruded grades have the greatest percent increase in resistivity while the iso-molded grades have the lowest. No clear trend in resistivity change exists with respect to dose indicating that the resistivity change for all grades stays generally constant over the AGC-3 dose range regardless of increasing dose.

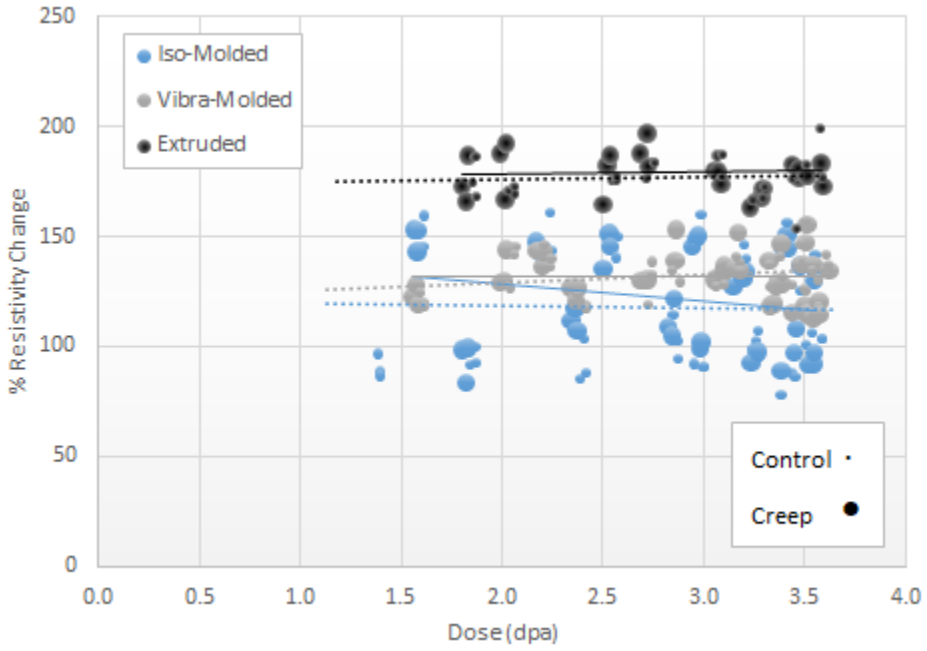

Figure 20. Percent resistivity change versus dose for similar graphite fabrication processes for creep (—) and control (- - -) specimens.

Figure 21 and Figure 22 explore the dependence of grain orientation on the resistivity change for the four major graphite grades that have forming processes which result in distinct grain orientations. Figure 21 examines the effect of grain orientation on electrical resistivity for stressed and unstressed specimens. Minimal differences exist for either orientation or stress on the change in resistivity for the AGC-3 specimens indicating that irradiation and stress affect electrical resistivity similarly for all grain orientations. Figure 22 shows the percent change in resistivity over the irradiation dose range for the two grain orientations (hollow and solid symbols are representative of against- and with-grain, respectively). Similar to the applied stress analysis, the grain orientation appears to have no difference in the percent change in resistivity with respect to irradiation dose.

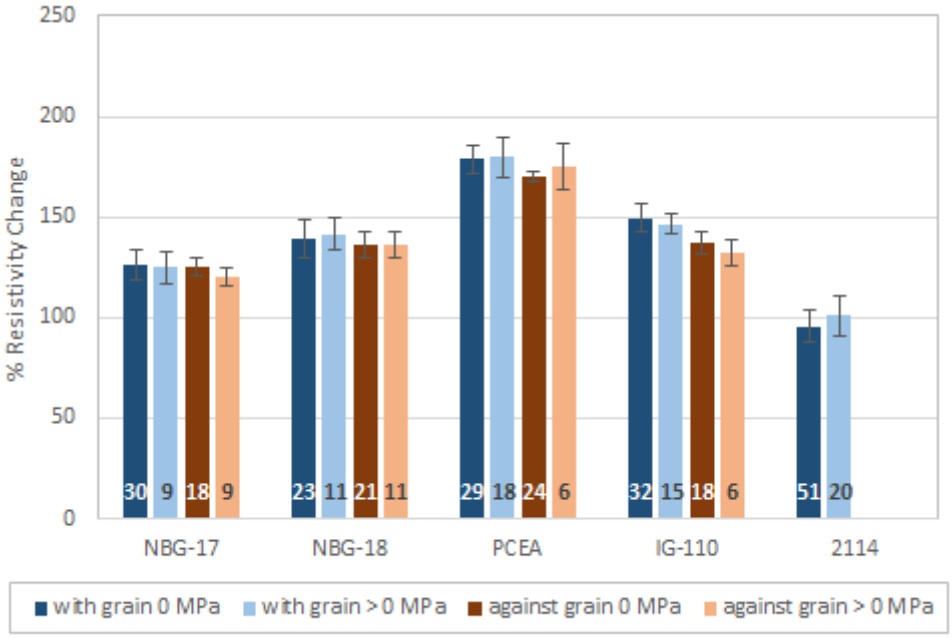

Figure 21. Average percent resistivity change by grain orientation and graphite grade.

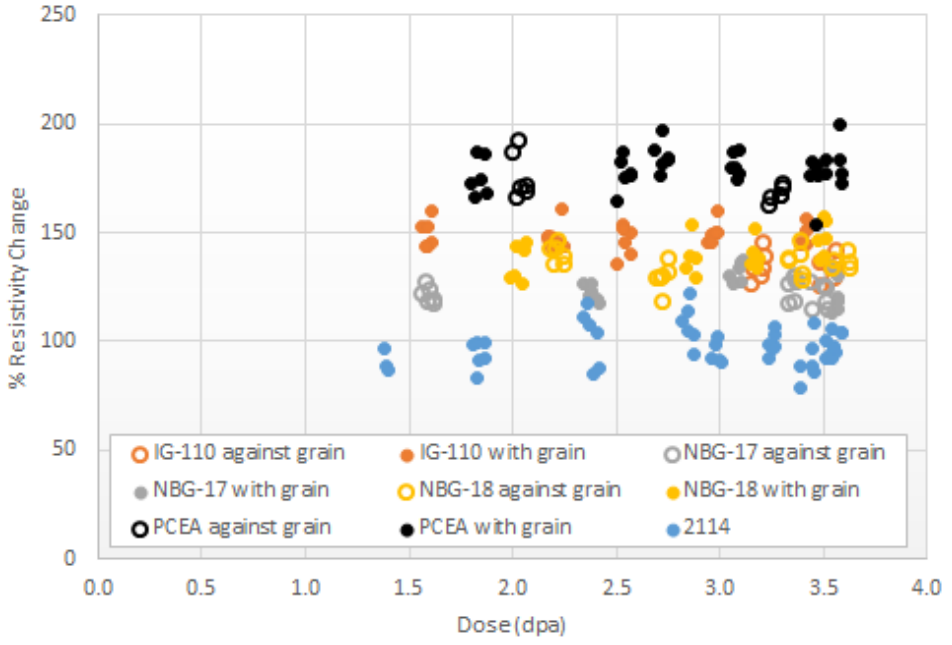

Figure 22. Percent resistivity change versus dose by grade and specimen grain orientation.

Figure 23 illustrates the effects of specimen density (before irradiation) on the change in electrical resistivity after irradiation. Changes in the density of graphite can significantly affect the material property values in all nuclear graphite grades, with lower density resulting in a reduction in mechanical strength, lower thermal diffusivity, and lower modulus values. As seen in Figure 23, there is no clear pattern in the relationship between pre-irradiation density and the change in resistivity due to irradiation.

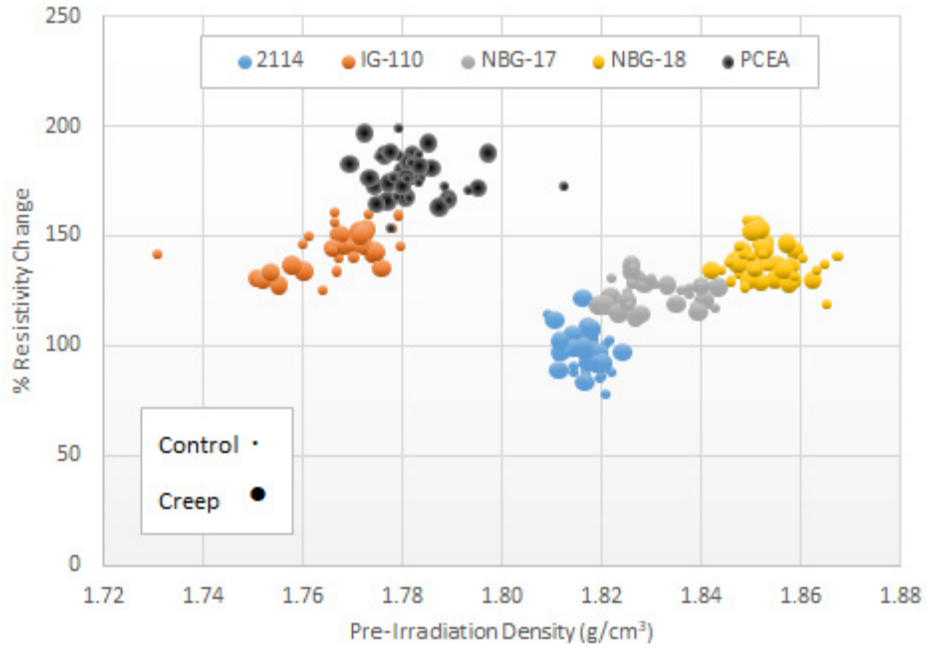

Figure 23. Percent resistivity change versus specimen pre-irradiation density for control and creep specimens.

The affect from irradiation-induced creep strain on electrical resistivity is shown in Figure 24. The data for all grades show a very similar, constant response as strain is increased. An increase in magnitude of strain in the axial direction has no apparent effect on electrical resistivity. As noted previously, the change to resistivity is greatest in the extruded grade PCEA, and lowest in the iso-molded Grade 2114.

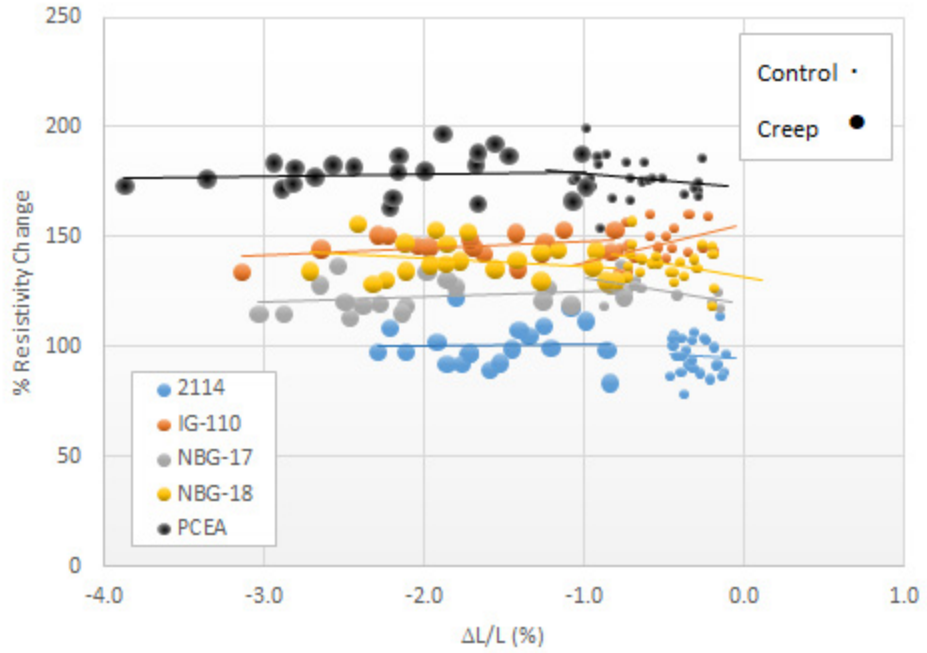

Figure 24. Percent resistivity change versus specimen strain by graphite grade for both control and creep specimens.

Finally, the percent change in resistivity for both stressed and unstressed specimens of the five grades of graphite is plotted separately as a function of dose for two temperature ranges, >821°C and <821°C in Figure 25. By plotting the data in this way, the effect of dose is isolated for two temperature ranges. As expected, no change in resistivity is seen for all graphite grades.

This behavior is somewhat anticipated since resistivity is assumed to be influenced by the atomic damage within the graphite crystal structure (Angstrom length scale defects) and is not expected to be influenced by the bulk microstructure changes (micron length scale defects). Since the crystalline defect population has saturated after initial irradiation (<1.0 dpa) no further change to the electrical resistivity would be expected.

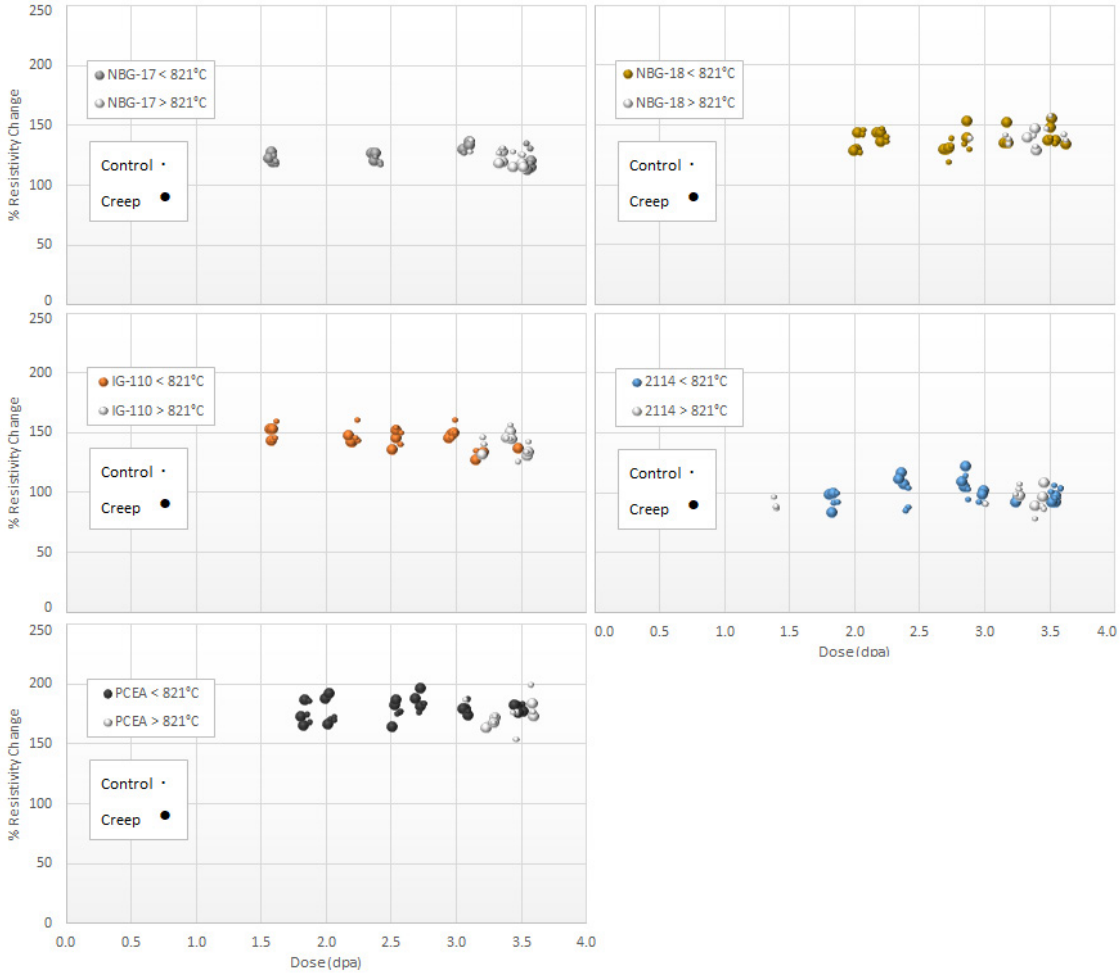

Figure 25. Resistivity change versus specimen dose for two temperature ranges, >821°C and <821°C, for different graphite grades.

6.3 Young's Modulus by Sonic Velocity Method

A material's elastic moduli are a measure of how compliant (or stiff) the material behaves. It is useful for ascertaining a graphite grade's mechanical properties, irradiation creep response, and the structural strength and integrity of graphite components. The measurement of elastic constants by the time of flight or sonic velocity method is carried out in accordance with ASTM C769 98(2005). In this measurement a transmitting piezoelectric transducer sends a sound wave through the sample. At the opposite end of the sample, the acoustic wave is received by another piezoelectric transducer. The sonic velocity of the sound wave through the specimen is the ratio of specimen length to the signal time lapse between transducers. Approximate values for Young's modulus are obtained from the square of the velocity multiplied by the density of the graphite.

$$E = \rho \cdot V^2 \tag{4}$$

Where:

E = Young's modulus, Pascal, N/m^2

ρ = specimen density, kg/m^3

V = sonic velocity, m/s.

Here it is important to note that a later version of Standard C769-98(2005) has been modified to include a term called Poisson's Factor. This term attempts to make an improved estimate of Young's modulus by acknowledging that nuclear graphite is not perfectly isotropic. For more information on this topic refer to ASTM Standard C769-15. For consistency with the previous AGC-3 pre-irradiation examination testing methods, this report continues to estimate the Young's modulus without using Poisson's ratio so that the values calculated can be compared to those in previous ART AGC and Baseline reports.

Also note that C769-98(2005) has been extended to estimate shear modulus by $G = \rho \cdot V_s^2$ where G = shear modulus, ρ = bulk density and V_s = shear velocity as measured per C769-98.

Young's modulus measurements were made on the creep and control specimens both before and after irradiation. The overall trend in Young's modulus for all AGC-3 specimens measured was an immediate increase in modulus for all grades ranging from ~24% to ~94%, Figure 26. This rapid (and significant) initial increase in modulus change was anticipated and is most likely due to the immediate effects from neutron ballistic damage in the graphite crystal structure leading to dislocation pinning which will result in a less compliant and stiffer graphite. A trend line for all graphite specimens is shown as a black line with +/- 1 standard deviation shown as dotted lines. The large scatter in the data reflects the different variables within the experiment including irradiation temperature, dose, applied stress, graphite grade, and grain orientation. The impact of these variables is considered below.

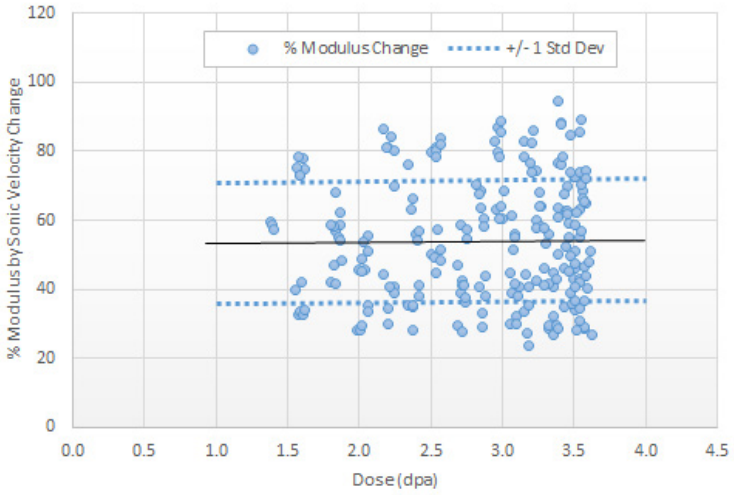

Figure 26. Scatter plot of the percentage of modulus change from all AGC-3 graphite grades, stress conditions and irradiation temperatures.

Figure 27 illustrates the irradiation-induced modulus changes as a function of dose for the five major graphite grades of unstressed specimens. While the initial increase in irradiated modulus is rapid and significant (0–1.5 dpa), further irradiation results in only small increases in modulus for all grades. This behavior was anticipated with the large, low-dose (<2 dpa) increase most likely due to the atomic level irradiation damage to the crystal lattice pinning dislocation movement and increasing the stiffness of the graphite material. The slower modulus increase over the range of ~1.1. to 3.7 dpa is a complex result of many factors. The modulus is obviously affected by the increased densification of the material (as density

increases the modulus, E, will increase as shown in Eq. 4) which would tend to increase the modulus. However, the modulus increase is slowing which indicates competing mechanisms are affecting the stiffness. The reduced modulus increase may indicate that the dislocation pinning mechanism may be saturating (i.e., most dislocations are locked in place) and continuing irradiation damage along with the increased densification only has limited effect. Additionally, other microstructure changes may be contributing to the stiffness change in all graphite grades. Further research in this complex response is required to determine the specific mechanisms responsible for this behavior.

It is interesting to note that the modulus change for the NBG-18 and NBG-17 specimens were nearly identical even though NBG-18 has a grain size two times larger than NBG-17. Clearly, grain size has a limited effect on irradiation-induced modulus changes in graphite. Also of interest, is that the trend line slopes for all grades are very similar over this limited irradiation dose range.

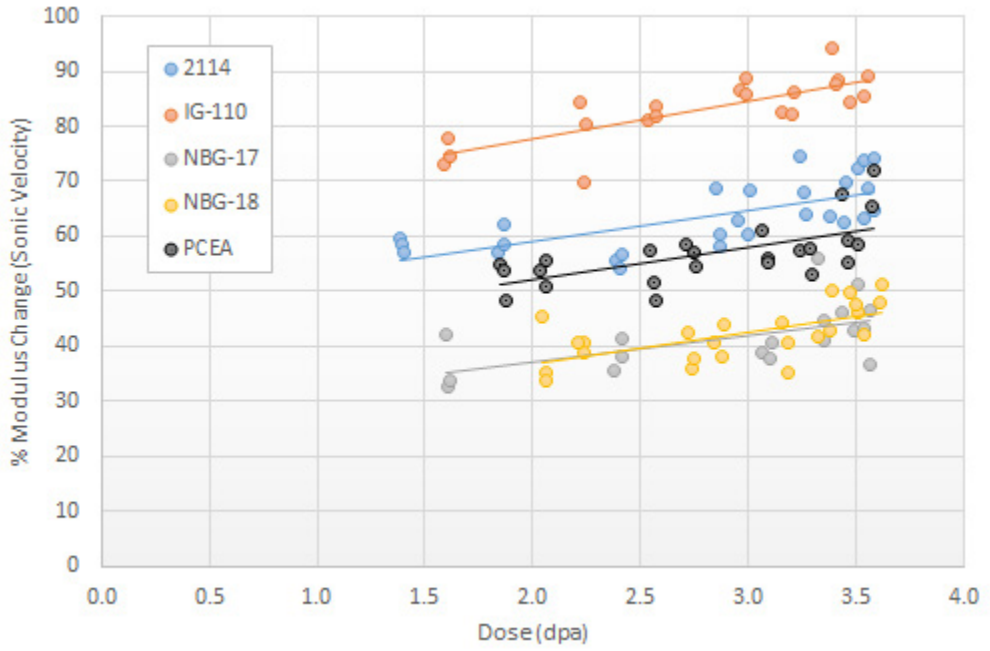

Figure 27. Percent modulus change versus dose by graphite grade for control specimens only.

Figure 28 and Figure 29 investigate the effect of stress on the percent change in modulus. The average changes to the measured modulus resulting from the applied stress levels is shown in Figure 28. The average of the number of specimens indicated in each bar is indicated by the bar length and the error bars represent ± 1 standard deviation. There is a small but definite trend for the percent modulus change in all graphite grades to gradually decrease as the applied stress is increased. IG-110 experienced the largest change in modulus while NBG-17 and NBG-18 exhibit the least.

Figure 29, like Figure 27, is a plot of percent change in modulus versus irradiation dose but now the control (unstressed) and creep (stressed) specimens are shown separately. Linear regression lines are established through the data for each individual grade. Similar to Figure 27, the modulus percentage change increases slowly as the dose increases with only small differences existing between stressed and unstressed specimen behavior. The change in stiffness remains significantly higher for the iso-molded grades than the vibration molded grades and extruded PCEA for all stress levels.

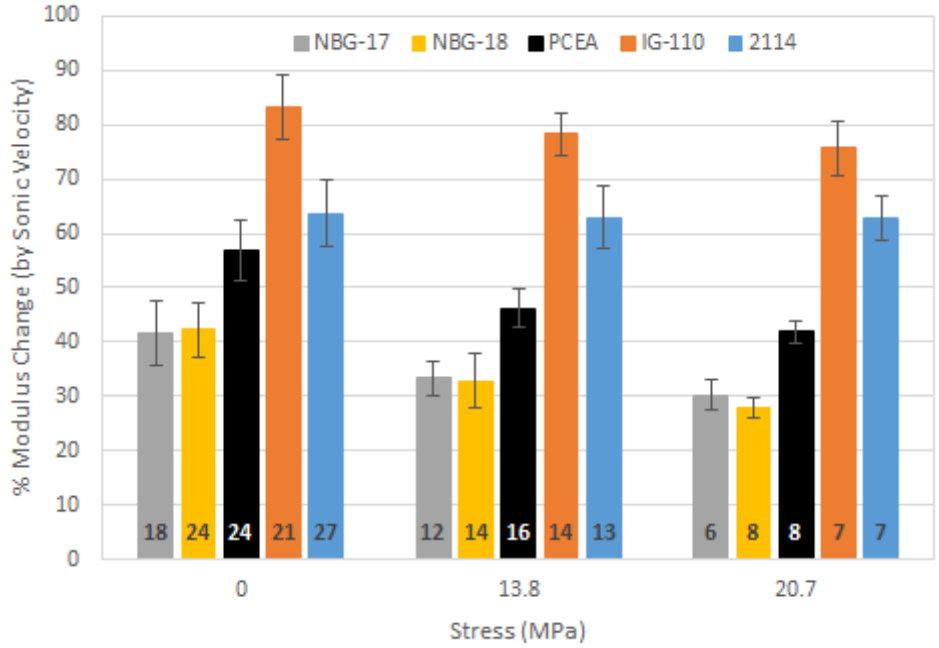

Figure 28. Average percent modulus change by graphite grade and applied stress. The error bars represent +/- 1 standard deviation from the mean and the numbers in the bars represent the sample size.

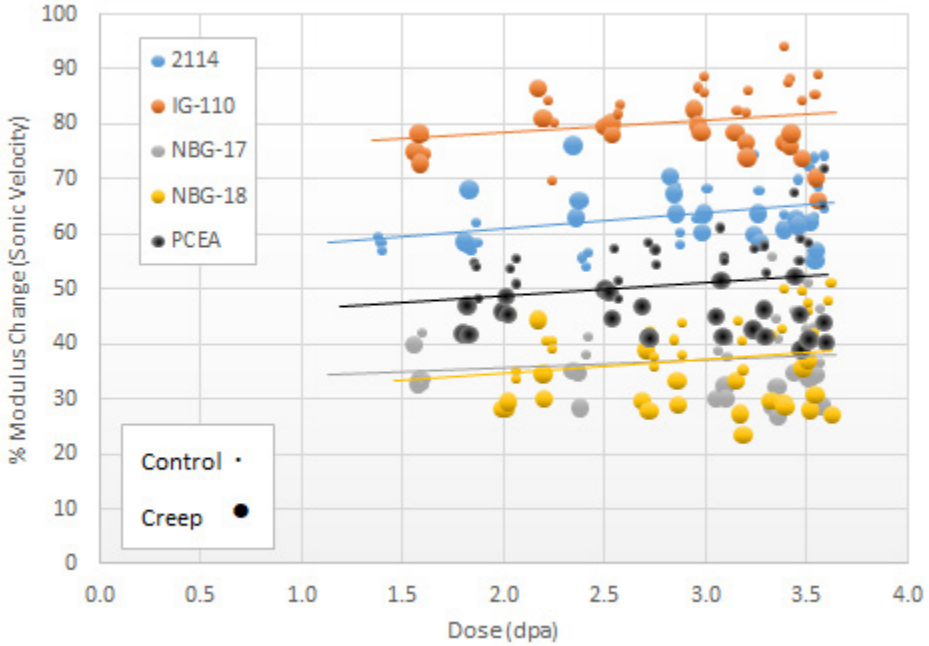

Figure 29. Percent modulus change versus dose by graphite grade for control and creep specimens.

Figure 30 shows the effects of irradiation and applied stress for the three separate forming processes. As noted earlier, the iso-molded graphite exhibits the greatest percent change in modulus and the vibra-molded graphite shows the least change.

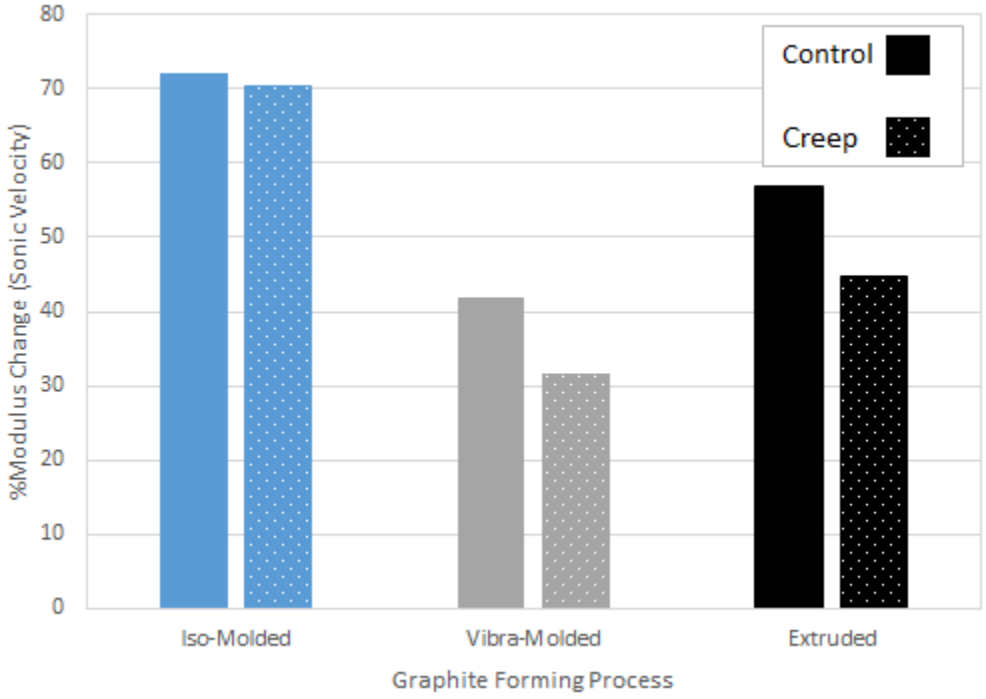

Figure 30. Average percent modulus change versus dose by fabrication process for creep and control specimens.

Figure 31 and Figure 32 investigate the dependence of grain orientation on the change in modulus for the four major graphite grades that have forming processes that result in distinct grain orientations. Figure 31 examines the effect of grain orientation on the change in modulus for stressed and unstressed specimens (error bars represent ± 1 standard deviation of the mean). No significant effect from grain orientation is observed for the unstressed control specimens with only the IG-110 demonstrating a very small change for the stressed creep specimens.

Figure 32 shows the percent change in modulus over the irradiation dose range for the two grain orientations (hollow and solid symbols are representative of against- and with-grain, respectively). Similar to the applied stress analysis, the grain orientation appears to have no significant difference in the percent change in modulus with respect to irradiation dose.

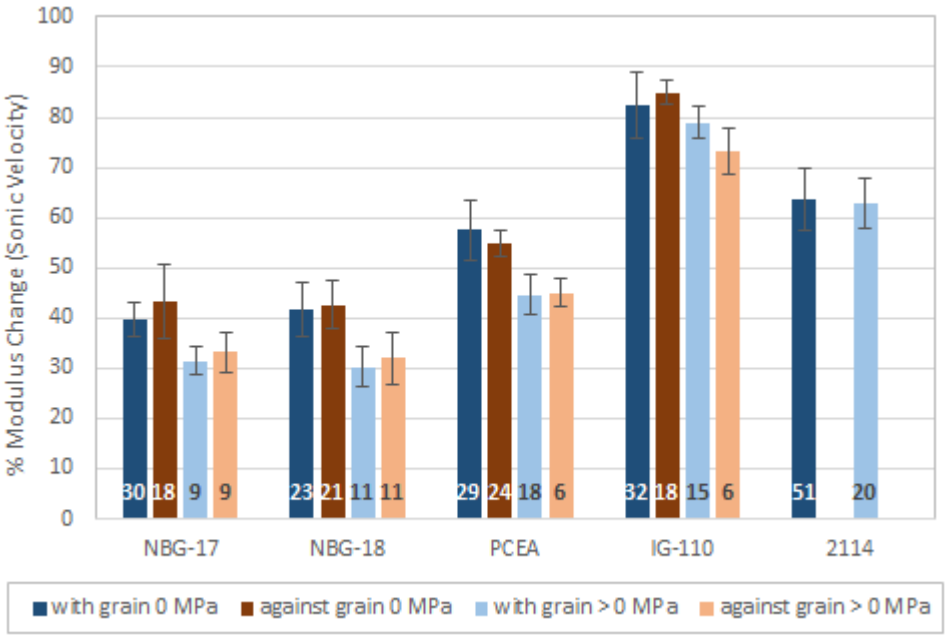

Figure 31. Average percent modulus change by grain orientation and graphite grade.

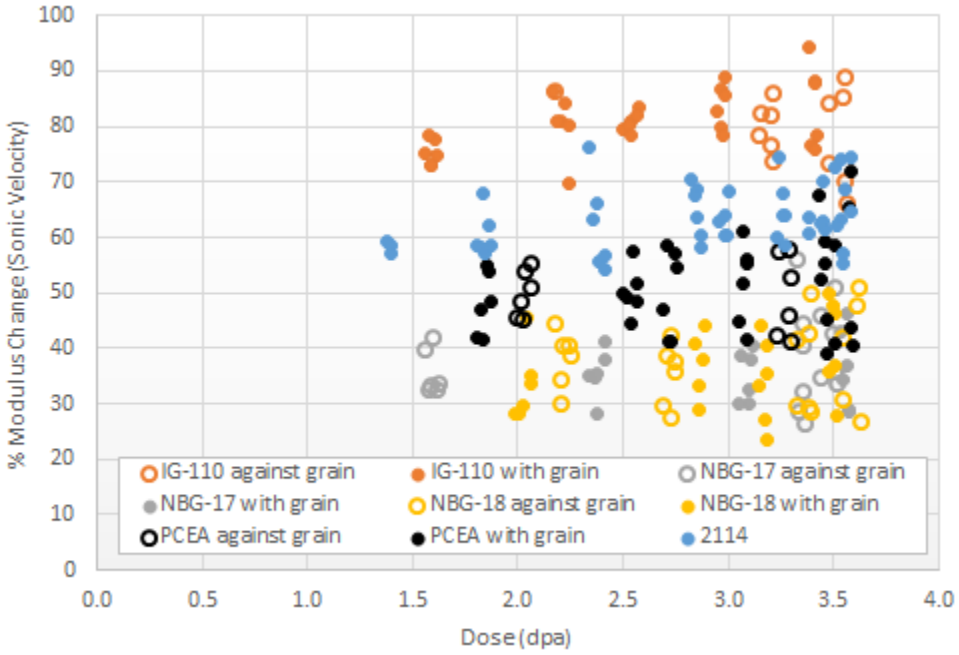

Figure 32. Percent modulus change versus dose by graphite grade and specimen grain orientation.

Figure 33 illustrates the effects of specimen density (before irradiation) on the change in Young's modulus. As noted previously, density has a large effect on the material property values and density related differences may be exacerbated under irradiation. However, the data in Figure 33 shows no clear correlation with unirradiated density values and change in Young's modulus.

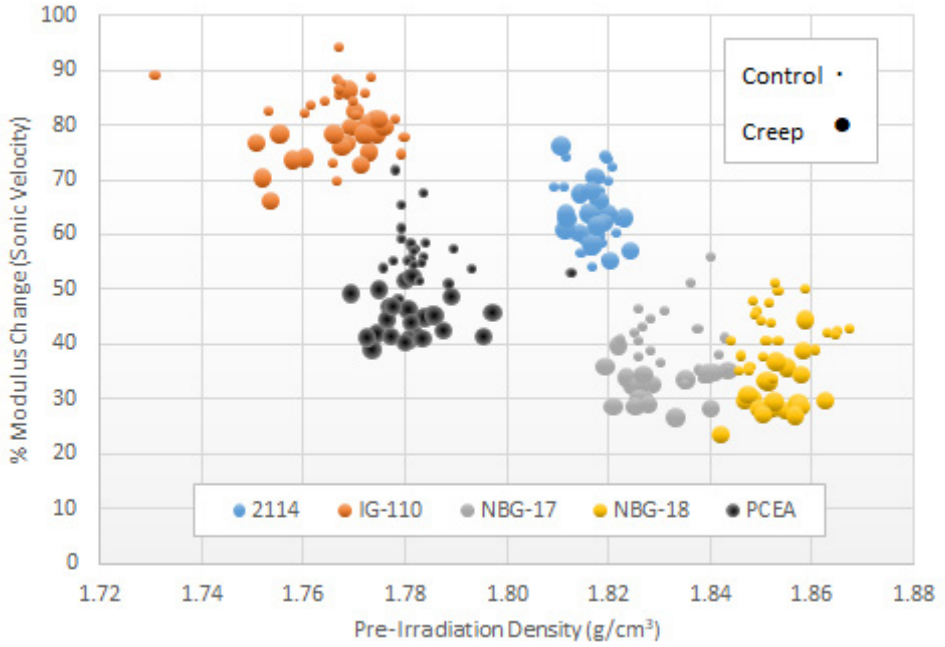

Figure 33. Percent modulus change versus specimen pre-irradiation density by graphite grade for control and creep specimens.

Induced modulus change with respect to irradiation-induced strain is shown in Figure 34. The data are presented as the change in Young's modulus as a function of increasing strain experienced in the specimen axial direction for both mechanically stressed specimens (creep) and unstressed specimens (control) as analyzed in the AGC-3 creep analysis report.[5] The data are separated into control and creep specimens of the major grades of graphite, including all irradiation temperatures and received dose levels. As presented in INL/EXT-19-54725, while all specimens (creep and control) experienced similar neutron irradiation dose and temperatures, the stressed creep specimens showed much larger strains due to the applied mechanical stresses. So that the specimens with the highest experienced strain usually achieved the highest received dose levels. With this understanding, Figure 34 illustrates several interesting trends:

1. High-dose/unstressed samples always have a higher change in modulus than stressed specimens with similar dose levels
2. The modulus change for unstressed specimens has a high positive slope with increasing dose indicating the increased atomic damage within the graphite crystal structure is increasing the stiffness of the material.

   Low stress = atomic damage and smaller microstructure change
3. The modulus change for stressed specimens has a low negative slope with increasing dose (and increased microstructure change) indicating that the effects of atomic damage are being disrupted by the much larger microstructural changes occurring in the stressed samples.

   High stress = atomic damage and much larger microstructure change.

The fact that the stressed and unstressed results have opposite effects on the modulus change is an indication of competing processes. As discussed previously, the rapid initial increase in modulus change is most likely due to neutron damage in the graphite crystal structure leading to dislocation pinning, which will result in a less-compliant and stiffer graphite. For the unstressed control specimens this

increasing modulus change continues for all graphite grades over the relatively small irradiation dose range of the AGC-3 test. However, for the stressed creep specimens, the change is reversed and the modulus begins to demonstrate increased compliance as the strain (and applied stress) is increased. This implies that the microstructural change resulting from the increased strain on the material is competing with irradiation damage, which generally tends to increase the stiffness of graphite. These microstructural changes in the creep specimens may include increased microcracking from the large applied mechanical stresses, pore/grain structure realignment, or pore closure. These results may indicate how the microstructure changes may affect the modulus changes (i.e., it is not just a radiation damage issue). Further fundamental studies will be necessary to assist in the interpretation of these data trends.

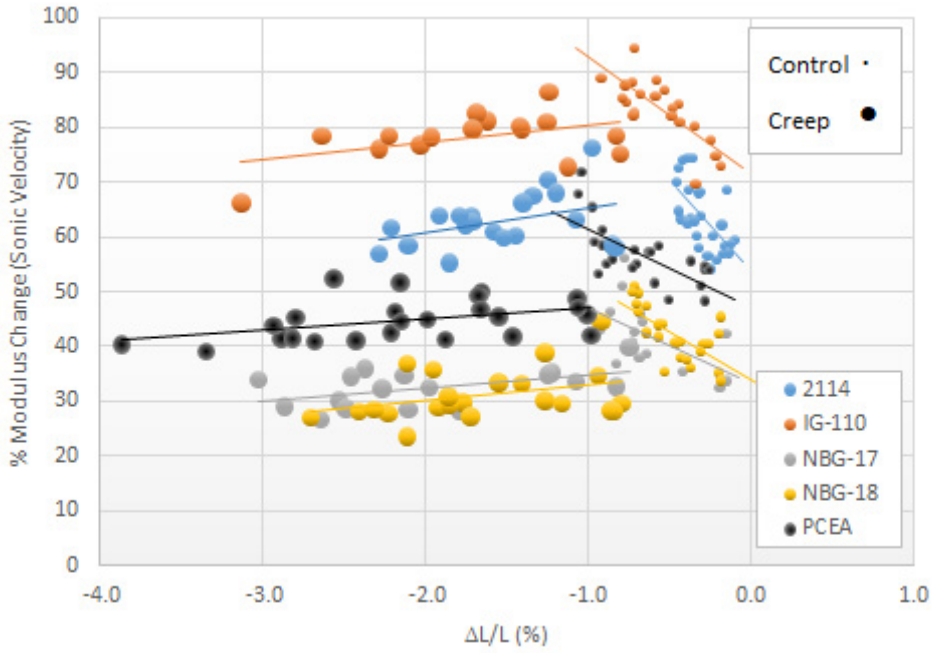

Figure 34. Percent modulus change versus strain experienced for both unstressed control (·) and stressed creep specimens (●) for major graphite grades.

Figure 35 shows the percent change in Young's modulus for both stressed and unstressed specimens of the five grades of graphite separately as a function of dose for two temperature ranges, >821°C and <821°C. By plotting the data in this way, the effect of dose is isolated for two temperature ranges. It should be noted that this is only an initial look at the effects of irradiation temperature over a relatively small range, but it will illustrate the effect of temperature variation on the modulus results. A more complete analysis of the individual effects of both irradiation temperature and dose will be performed when the data of all AGC capsules is combined. Figure 35 demonstrates that for this limited dose range case all grades of graphite show no real separation in the magnitude of the change in Young's modulus for the two temperature ranges This implies that temperature variation within the AGC-3 capsule has no significant effect on these material property values.

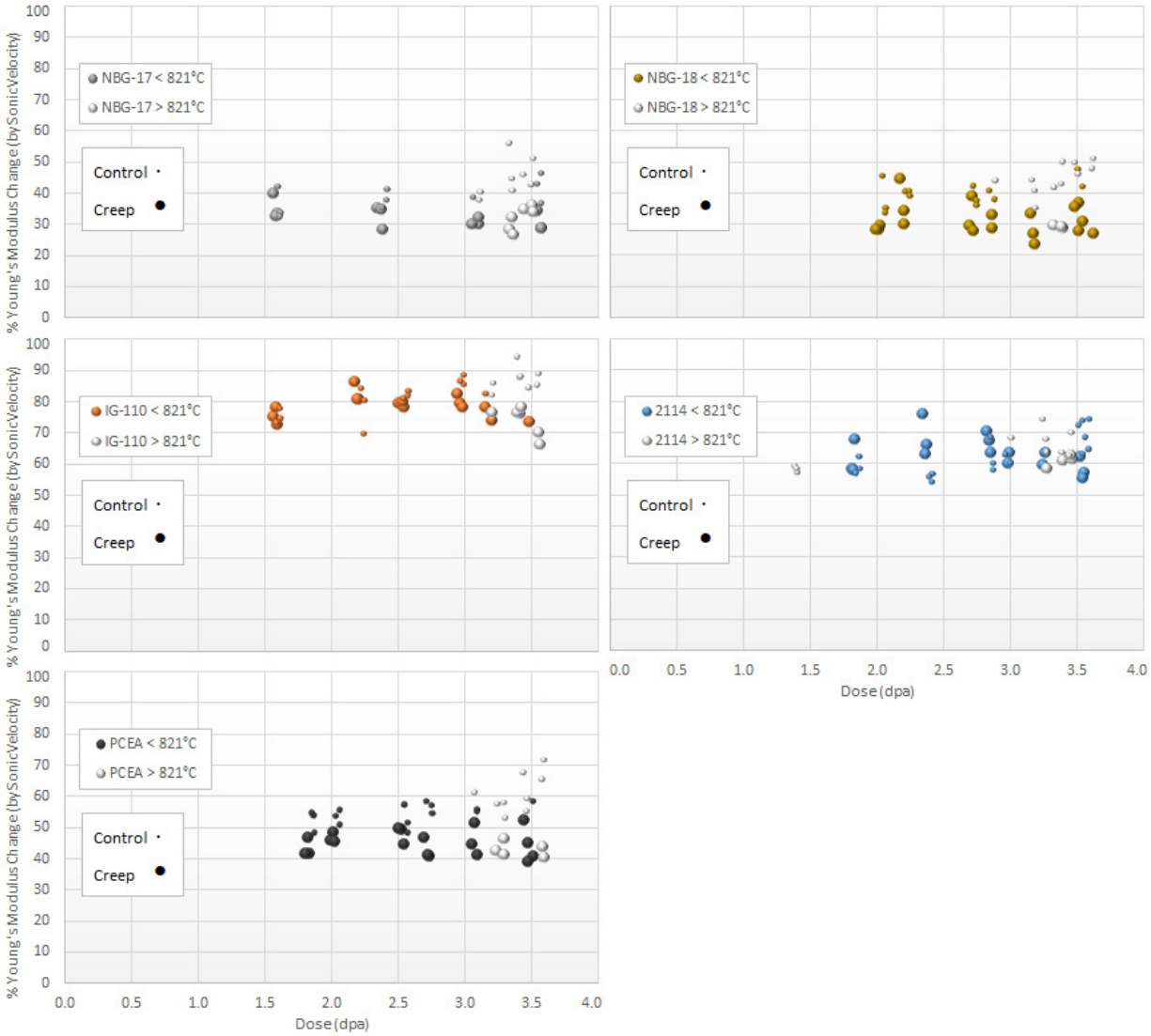

Figure 35. Percent Young's modulus change versus specimen dose for two temperature ranges, >821°C and <821°C, for different graphite grades.

6.4 Young's Modulus by Sonic Resonance Method

Measurements of Young's modulus were also made using a different testing methodology, the sonic resonance method. This test method measures the fundamental resonant frequency of test specimens of suitable geometry by exciting them mechanically with a singular elastic strike. Specimen supports, impulse locations, and signal pick-up points are selected to induce and measure specific modes of the transient vibration of the specimen. The transient signals are analyzed, and the fundamental resonant frequency is isolated by a signal analyzer. The measured fundamental resonant frequency, specimen dimensions, and mass are used to calculate Young's modulus using ASTM C747-16. For the fundamental flexural frequency of a rod of circular cross section:

$$E = 1.6067\left(\frac{L^3}{D^4}\right)\left(mf_f^2\right)T_1' \tag{5}$$

where:

E = Young's modulus, Pa

m = mass of the bar, kg

L = length of the bar, m

μ = Poisson's Ratio,

f_f = fundamental resonant frequency of bar in flexure, Hz, s^{-1}

D = diameter of rod, m

T'_1 = correction factor for fundamental flexural mode to account for finite thickness of bar, Poisson's ratio, etc.

Similar to the Young's modulus measurements made from the sonic velocity technique, measurements were made on creep and control specimens both before and after irradiation. The percent change of the calculated Young's modulus and analysis were, unsurprisingly, very similar to the results of the modulus measurements made with the sonic velocity technique. As demonstrated previously, there is an immediate and significant increase in modulus for all specimens at relatively low dose levels (less than 2.0 dpa). With this technique, the average percent change increase was 59% and ranged from ~35% to ~90% increase. There is a slight increasing trend as shown by the linear fit line (black line) in Figure 36.

As expected, the Young's modulus results from sonic resonance and sonic velocity are extremely similar. Due to these similarities, the analysis and conclusions are the same and no further analysis for the sonic resonance results will be presented in the main report. Specific data results of the sonic resonance data may be found in Appendix A.

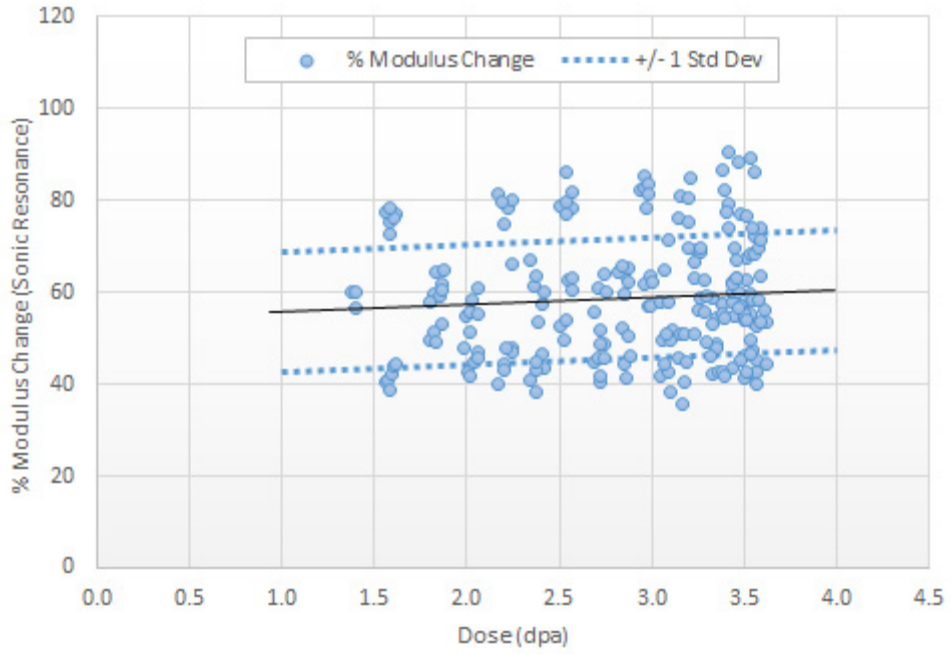

Figure 36. Scatter plot of the percentage of Young's modulus change by Sonic Resonance Method for all graphite grades, irradiation temperatures and stresses.

6.5 Shear Modulus

A material's shear modulus (Modulus of Rigidity) are a measure of how compliant (or stiff) the material behaves when shearing or torsion forces are applied. Shear modulus is part of a material's elastic moduli and has similar uses to the Young's modulus. The determination of shear modulus using the sonic velocity method was also carried out in accordance with ASTM C769 98(2005). Much like determining Young's modulus, a transmitting piezoelectric transducer sends a *transverse shear* wave through the sample. At the opposite end of the sample, the wave is received by a second piezoelectric transducer. The sonic velocity of the shear wave through the specimen is the ratio of specimen length to the signal time lapse between transducers. Approximate values of the shear modulus are obtained from the square of the velocity multiplied by the density of the graphite.

$$G = \rho \cdot V^2 \tag{6}$$

Where:

G = shear modulus, Pa

ρ = specimen density, kg/m^3

V = sonic velocity, m/sec.

Shear modulus measurements were made on the creep and control specimens both before and after irradiation. Similar to the Young's modulus results, the shear modulus percent changes were immediate and significant with an average of 58% increase for all grades and ranging between 34% and 93%, Figure 37. The scatter in the data is not as broad as Young's modulus measurements using the same ASTM method.[28] This shear data covers all irradiation temperatures between 748°C and 937°C, for all grades, all stress levels, and all grain orientations.

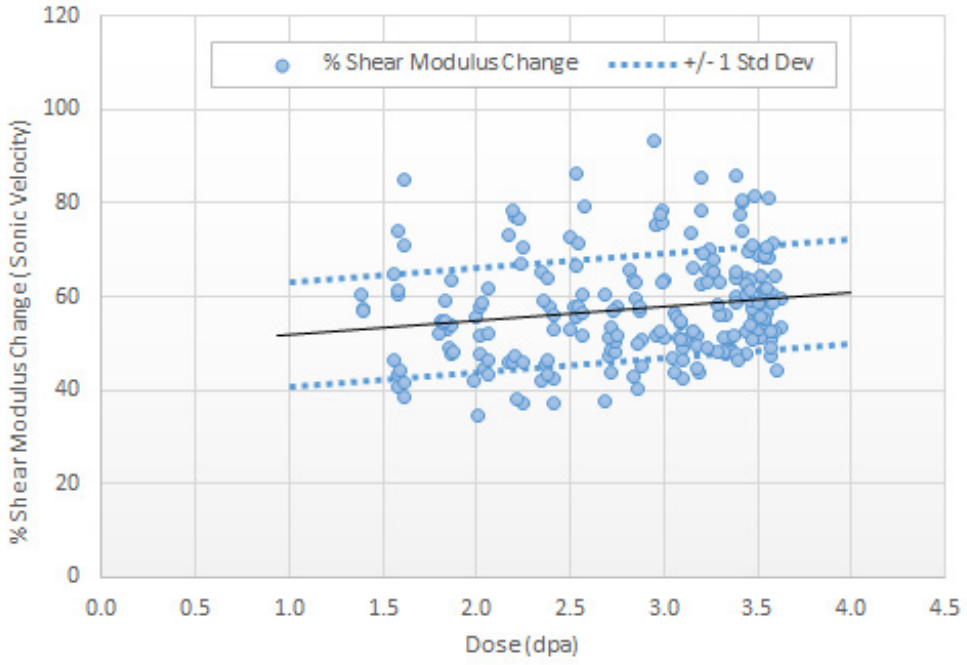

Figure 37. Scatter plot of the percentage of irradiated shear modulus change from all graphite grades.

Similar to the results for Young's modulus, Figure 37 demonstrates remarkable similarity in irradiation modulus values for all AGC-3 specimens regardless of nuclear grade, grain size, stressed/unstressed condition, or grain orientation. As before, the initial increase in modulus is significant for all specimens and reaches a maximum at relatively low dose levels (less than 2.0 dpa). There is only a slight rise in the shear modulus change as the dose increases over its range of ~1.1 to 3.7 dpa.

Figure 38 illustrates the irradiation-induced shear modulus changes between the five major graphite grades from irradiation for unstressed specimens only. Overall, the change in shear modulus is significant with IG-110 exhibiting the greatest overall change (60%–85% increase) and NBG-18 the least change (37%–60%). The linear regressions, for each grade of graphite, show only a slight increase in the percent change of the shear modulus as a function of the AGC-3 dose range. As described in Section 6.3, the large (immediate) increase at low dose levels is most likely due to the atomic level irradiation damage to the crystal lattice pinning dislocation movement and increasing the stiffness of the graphite material. Similar to the Young's modulus behavior, the smaller modulus increase over the range of 1.1. to 3.7 dpa is a complex combination of densification, irradiation damage, dislocation pinning, and microstructural changes which requires additional research to ascertain the interrelationship between these mechanisms.

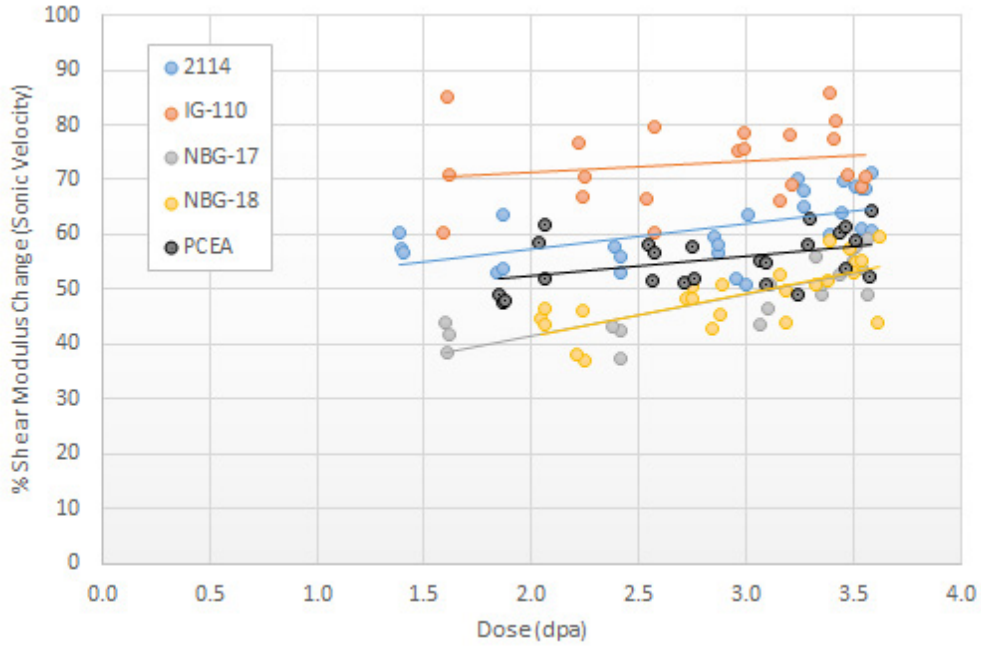

Figure 38. Percent shear modulus change versus irradiation dose by graphite grade for control specimens only.

The changes to the measured shear modulus resulting from the three applied stress levels is shown in Figure 39. Error bars represent +/- 1 standard deviation from the mean and the numbers in the bars represent the sample size. The size of the standard deviation and the small differences in averages combine to make it difficult to identify any clear trend in the percent change in shear modulus with the level of axial stress.

Figure 40 is a plot of percent change in modulus versus irradiation dose where the control (unstressed) and creep (stressed) specimens are shown separately. Linear regression lines are established through the data for each individual grade. Similar to Figure 39, there is only a weak correlation of shear modulus increase to received dose for either creep or control specimens.

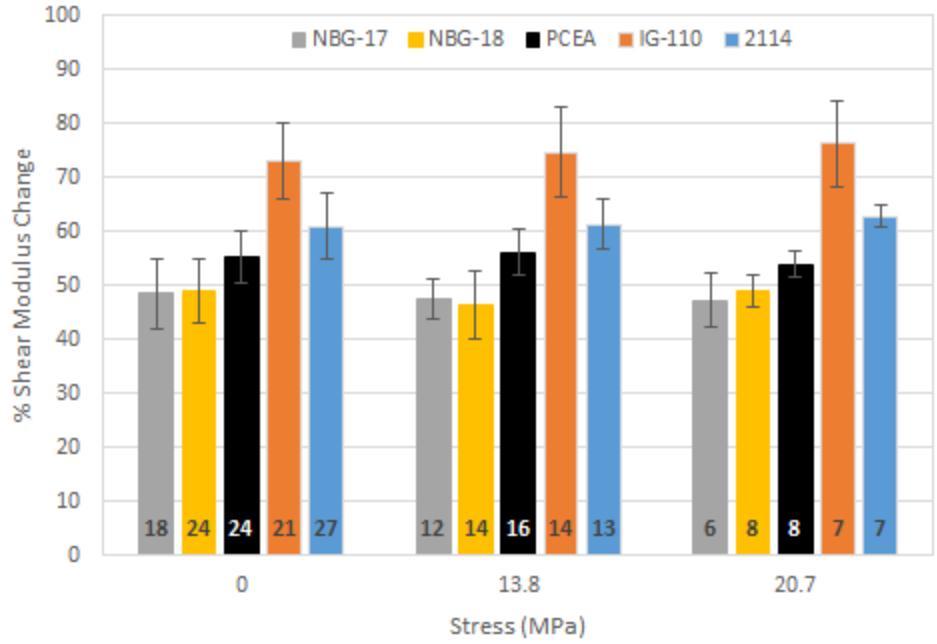

Figure 39. Average percent irradiated shear modulus change by graphite grade and applied load. The error bars represent +/- 1 standard deviation from the mean and the numbers in the bars represent the sample size.

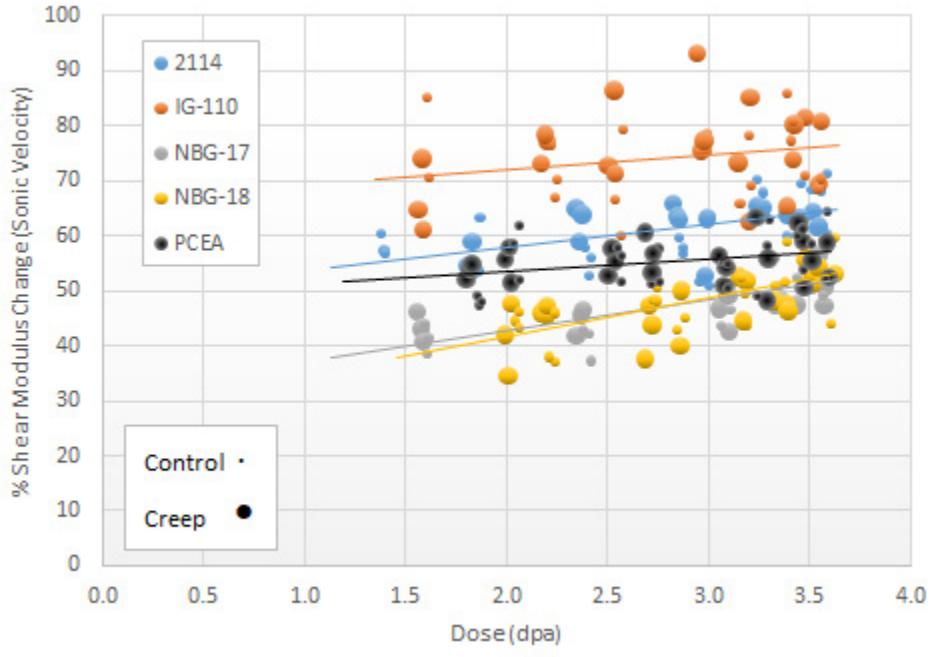

Figure 40. Percent shear modulus change versus irradiation dose by graphite grade for control and creep specimens.

Figure 41 adds together the effects of irradiation and applied stress for the three separate forming processes. The percent change in shear modulus shows the percentage modulus change for both stressed creep (—) and unstressed control and piggyback (···) specimens over the entire AGC-3 irradiation dose range. Similar to what has been observed previously, the iso-molded graphite experiences the largest percent change in shear modulus and the vibra-molded graphite grades experiencing less change.

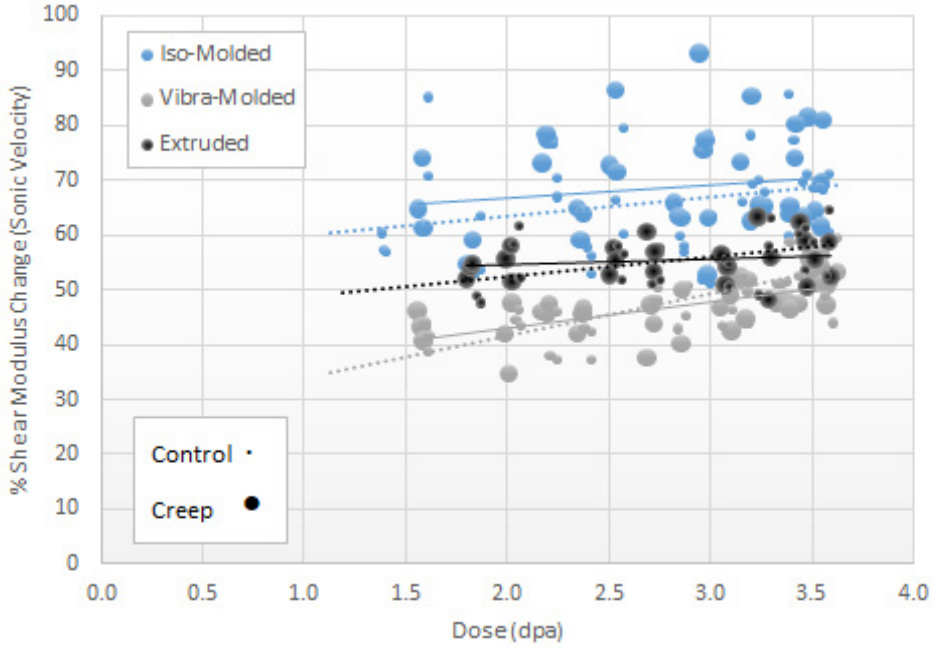

Figure 41. Percent shear modulus change versus irradiation dose by graphite fabrication process for control and creep specimens.

Figure 42 and Figure 43 investigate the dependence of grain orientation on the change in shear modulus for the three major graphite grades that have forming processes which result in distinct grain orientations. Figure 42 examines the effect of grain orientation on the percentage change in shear modulus for stressed and unstressed specimens (error bars represent ±1 standard deviation in the data). The percent change in shear modulus is nearly equal between the two grain orientations for all grades and average stress conditions indicating no significant effect from grain orientation. Figure 43 also demonstrates no significant difference in percent shear modulus change from grain orientation as a function of irradiation dose.

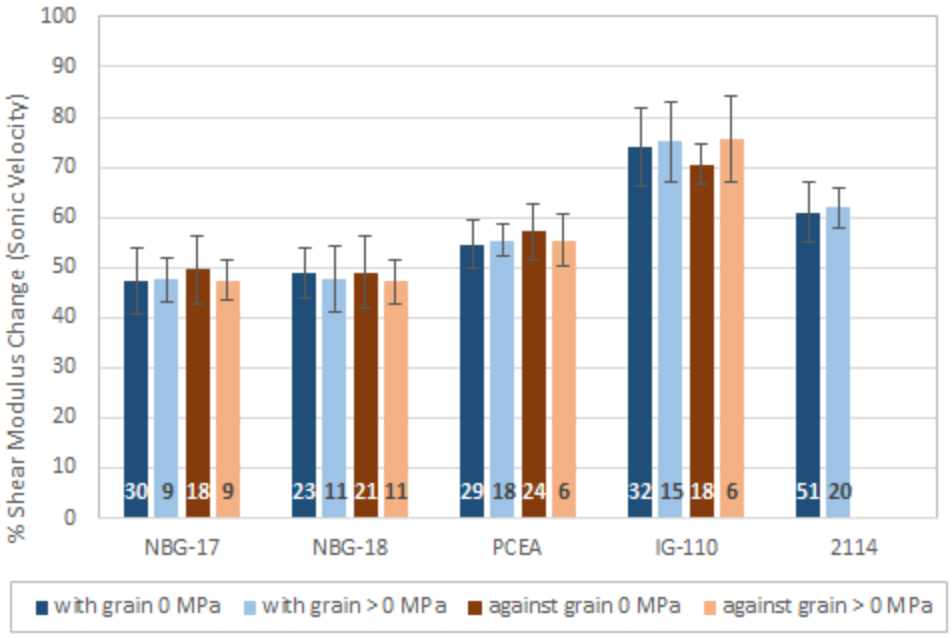

Figure 42. Average percent shear modulus change by grain orientation, stress, and graphite grade.

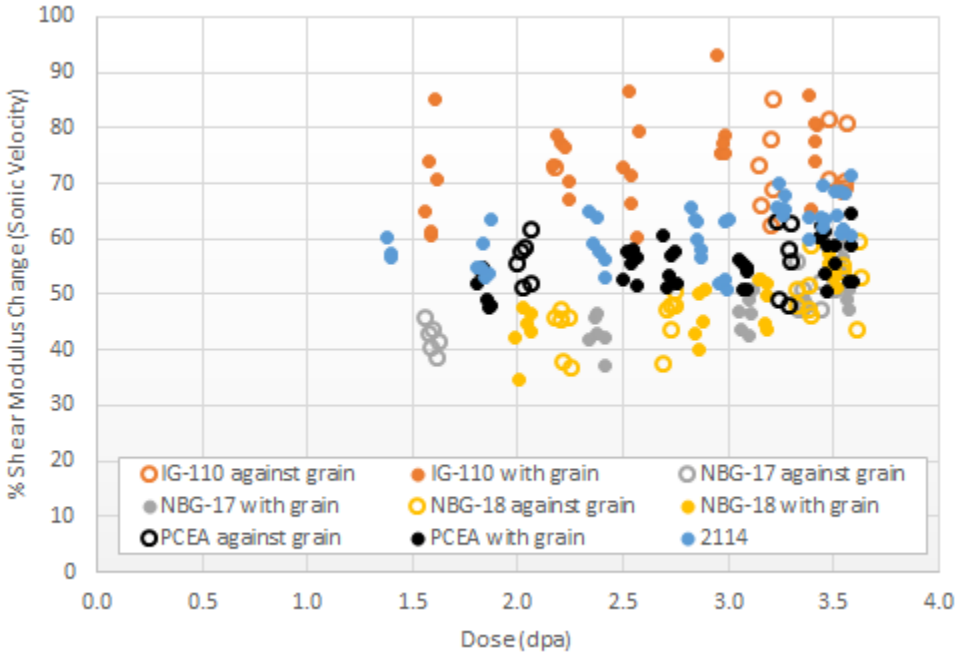

Figure 43. Percent shear modulus change versus dose by graphite grade and specimen orientation.

Figure 44 illustrates the effects of specimen density (before irradiation) on the change in shear modulus. As noted previously, density has a large effect on the material property values and density related differences may be exacerbated under irradiation. The data in Figure 44 shows only a slight correlation with the percent change in shear modulus decreasing with increased pre-irradiation density

(excluding grade PCEA). It is interesting that the most established nuclear graphite grade, IG-110, demonstrates the highest level of density variation and the greatest range of modulus change for all tested grades.

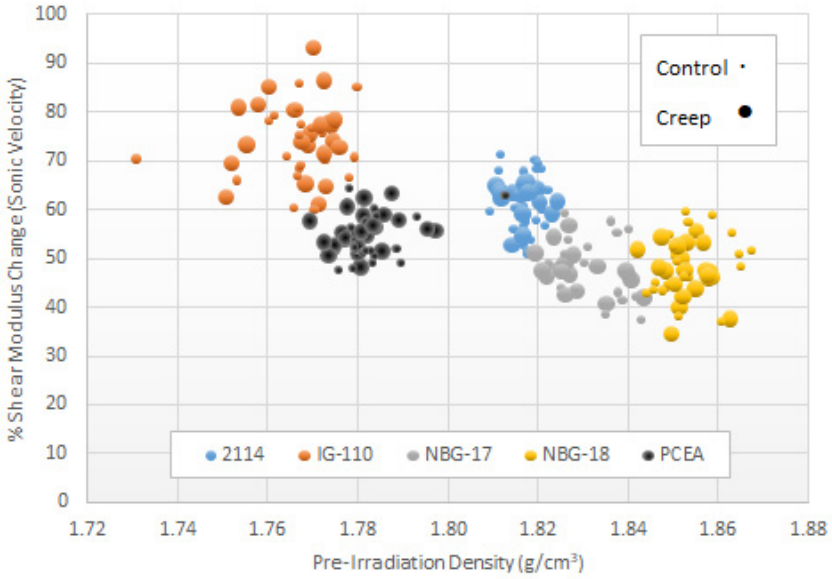

Figure 44. Percent shear modulus change versus specimen pre-irradiation density by graphite grade for control and creep specimens.

The effect of irradiation-induced strain on shear modulus is shown in Figure 45. This figure shows the changes in shear modulus as a function of the strain in the specimen axial direction. The data are separated into control and creep specimens of the major grades of graphite, including all irradiation temperatures and received dose levels.

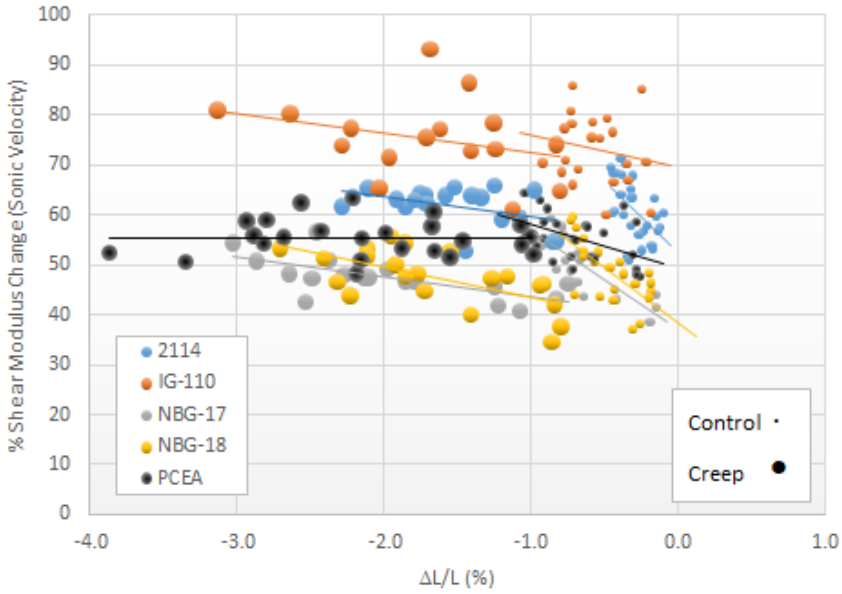

Figure 45. Percent shear modulus change versus specimen strain by graphite grade for unstressed control and stressed creep specimens.

Unlike the results for Young's modulus, Figure 45 does not show as clear a difference between the unstressed (control) and the stressed (creep) shear modulus changes. While the unstressed control data clearly shows an increase in shear modulus with increasing dose and strain the change is not as dramatic or consistent as the Young's modulus change in Sections 6.3 and 6.4. In addition, the shear modulus change for the stressed (creep) specimens are mixed with PCEA (extruded grade) showing no change and the other grades demonstrating small *increases* in shear modulus change as the bulk strain increases. However, all grades demonstrate the similar trend of unstressed specimens exhibiting higher shear modulus changes for the specimens with higher dose levels. Additionally, the change in shear modulus is clearly slower for the stressed specimens indicating that microstructural changes, while not as dramatic as for Young's modulus changes, do have an effect on the shear response of the irradiated graphite.

Figure 46 shows the percent change in shear modulus for both stressed and unstressed specimens of the five grades of graphite separately as a function of dose for two temperature ranges: >821°C and <821°C. By plotting the data in this way, the effect of dose is isolated for two temperature ranges and the effects from different irradiation temperatures can be determined. All grades of graphite show no real separation in the magnitude of the change in shear modulus between the two temperature ranges, indicating that temperature effects are minimal for these material property values. The effects of irradiation temperature over a much larger range will be analyzed when the data of all AGC capsules are combined.

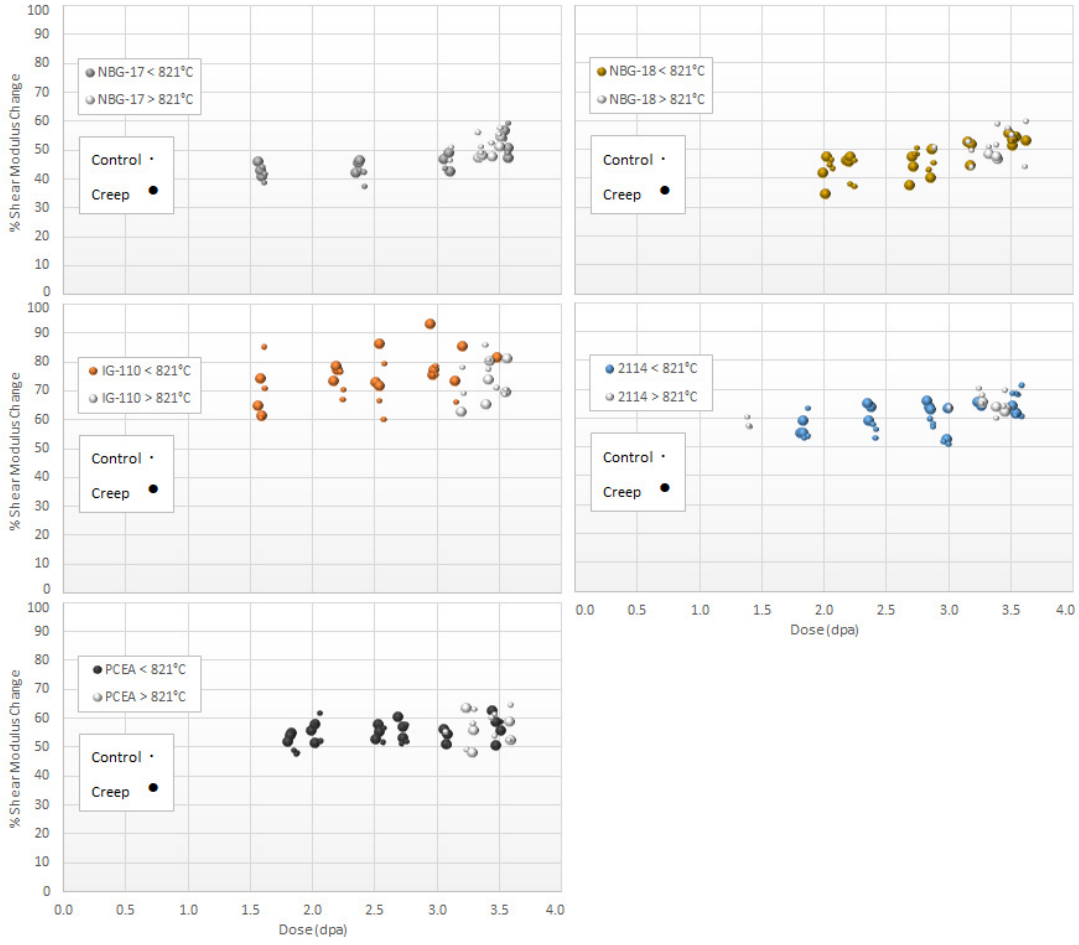

Figure 46. Shear modulus change versus specimen dose for two temperature ranges, >821°C and <821°C, for different graphite grades.

6.6 Coefficient of Thermal Expansion

The coefficient of thermal expansion (CTE) describes how the physical size of an object changes with temperature. Specifically, it measures the fractional change in size per degree change in temperature at a constant pressure. The CTE is a key parameter for determining thermally induced stress states within graphite components, volumetric changes, and irradiation creep rates. These stresses occur from thermally induced dimensional changes and can combine with other mechanical (internal or external) stresses induced from differential dimensional changes, as well as external stresses resulting from interlocked graphite core components.

The CTE is measured in accordance with ASTM E228-06. This test method uses a push-rod dilatometer to determine the change in length of a graphite specimen relative to that of the holder as a function of increasing/decreasing temperature. The temperature is varied over the desired range at a slow constant heating or cooling rate. Using a calibration to subtract the growth of instrument fixtures, the change in length of the specimen is recorded as a function of temperature. The mean coefficient of thermal expansion is calculated from the slope of a line drawn from the reference temperature, typically 20°C, and a specified temperature using Equation (7). This is performed for specific temperatures covered by the growth curve to produce mean thermal expansion coefficient values.

$$\alpha = \frac{\Delta L}{L_O} \cdot \frac{1}{\Delta T} \tag{7}$$

where:

α = coefficient of thermal expansion, K^{-1}

ΔL= change in length, m

ΔT= change in temperature, K

L_0 = initial length at 20°C, m.

Mean CTE measurements were made on the creep and control specimens both before and after irradiation up to temperatures of 650°C (just below the minimum sample irradiation temperature to forestall any irradiation damage annealing). The initial CTE increase (<1.1 dpa) was smaller than all other irradiated material property changes in the graphite but were still significant with an average increase of ~15–20% (Figure 47). It should be noted that Figure 47 incorporates CTE results at five different test temperatures for each specimen. This data plot is different from the density, elastic modulus, and resistivity measurements, which are tested only at room temperature. This adds an additional variable to the data scatter in addition to the irradiation temperature, dose, applied stress, graphite grade, and grain orientation and is addressed in the data analysis after Figure 47.

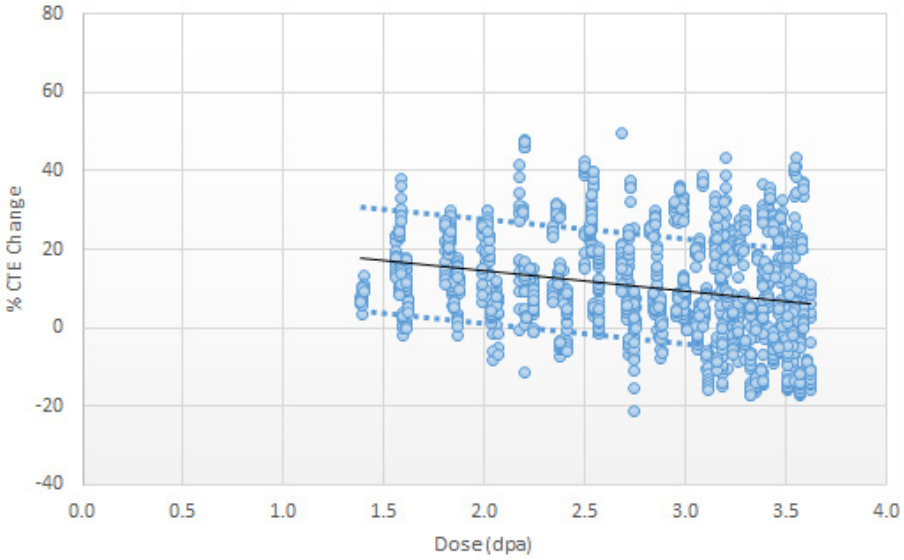

Figure 47. Percent change of CTE for all graphite specimens at all test temperatures (100°C, 200°C, 300°C, 400°C, 500°C, 600°C, and 650°C).

To allow the CTE data to be analyzed similarly to the previous material properties, the CTE results for a single measurement temperature of 500°C are analyzed against the dose only (Figure 48). For these single test temperature results, the CTE is observed to have the rapid increase for low dose (<1.4 dpa) ~20% with a standard deviation of ~13%. This rapid increase is followed by a slow decrease for the AGC-3 dose range of 1.4 to 3.7 dpa. As discussed previously, the scatter in the data reflects the different variables within the experiment including irradiation temperature, dose, load, graphite grade, and grain orientation.

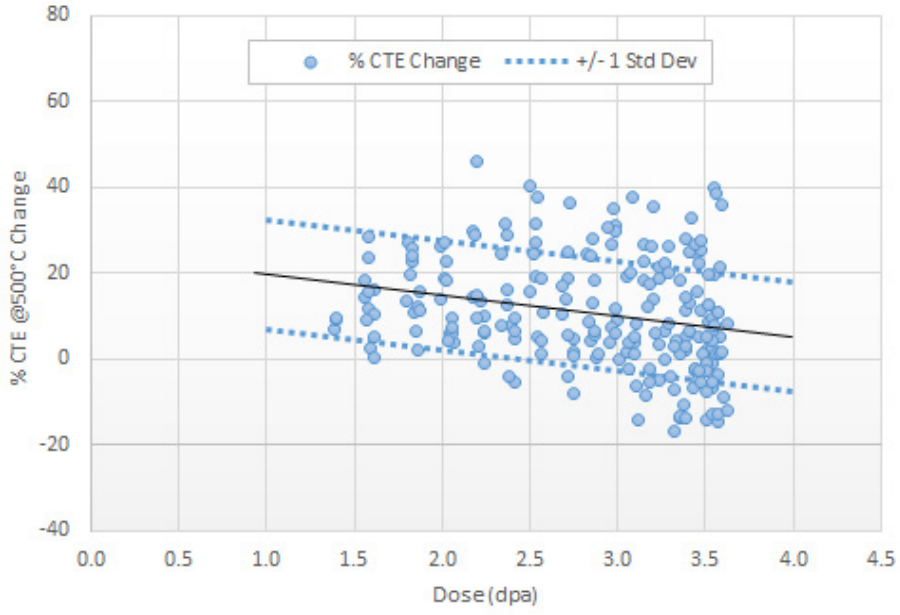

Figure 48. Percentage change of CTE at a single measurement temperature of 500°C for all tested specimens.

While Figure 48 demonstrates a similar CTE response for all AGC-3 specimens (regardless of nuclear grade, grain size, stressed/unstressed condition, or grain orientation) the scatter in the data is considerable. The percent change in CTE at 500°C has a large range from -17% to greater than 46%, which is most likely a result of differences in grade and applied stress (irradiation-induced strain) as we show in Figure 49 and Figure 50. Further analysis of the data isolating irradiation dose, applied stress, grade, and grain orientation is needed to determine these effects on CTE.

Figure 49 illustrates the irradiation-induced CTE changes between the five major graphite grades from irradiation only (no mechanical loaded specimens are considered). For all graphite grades, the percent change in CTE decreases over the AGC-3 neutron dose range (1.4–3.7 dpa) after the initial increase. In general, iso-molded grades demonstrated the largest overall CTE increase while NBG-17 had the lowest percent change and eventually demonstrated a negative CTE change. All grades, except for IG-110, had tested specimens that exhibited a negative change to CTE at the higher dose levels.

This behavior was expected. Generally, irradiated graphite has been demonstrated to experience an immediate rise in CTE due to initial irradiation damage and the closure of nanocracks within the graphite crystal structure. After this initial rise, the CTE peaks before turnaround dose and then *before* volume turnaround the CTE will begin to decrease. This decrease in CTE values are generally understood to result from initial formation of nanocracks within the crystal structure followed by more extensive crack formation throughout the graphite microstructure. These nano and microstructure cracks are dependent upon the temperature of irradiation, with crack formation initiating at lower dose levels for higher temperatures and cracks initiating at higher dose levels for low irradiation temperatures. This is why large negative CTE changes are not seen for the 600°C irradiated AGC-1 and AGC-2 results..[29, 30]

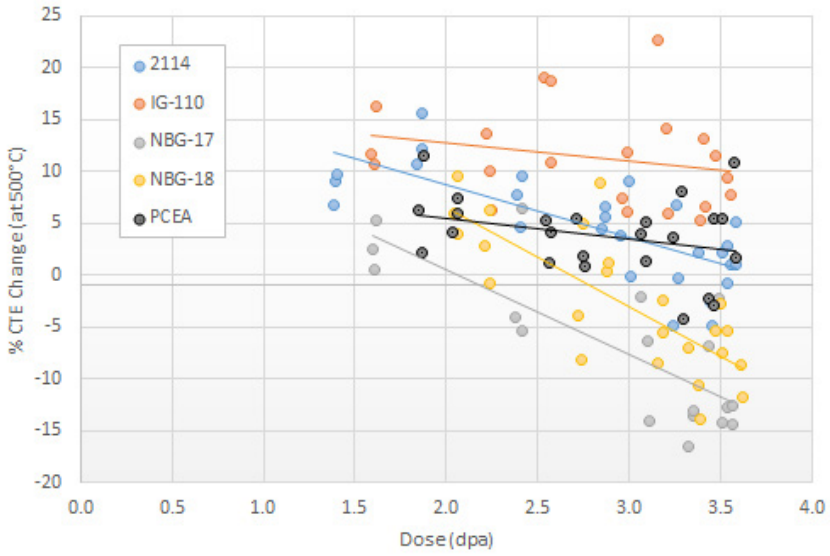

Figure 49. Percent change in mean CTE at 500°C versus dose by graphite grade for unstressed control specimens only.

Since CTE is measured over a range of temperatures, Figure 50 presents the average percent CTE change by graphite grade at measurement temperatures of 100°C through 650°C for both creep and control specimens. Error bars represent +/- 1 standard deviation from the mean. The large CTE difference between stressed and unstressed specimens is immediately observed with some stressed specimens demonstrating differences of more than a factor of 6 (PCEA at 650°C). The change in CTE within all grades is observed to be similar over all CTE test measurement temperatures.

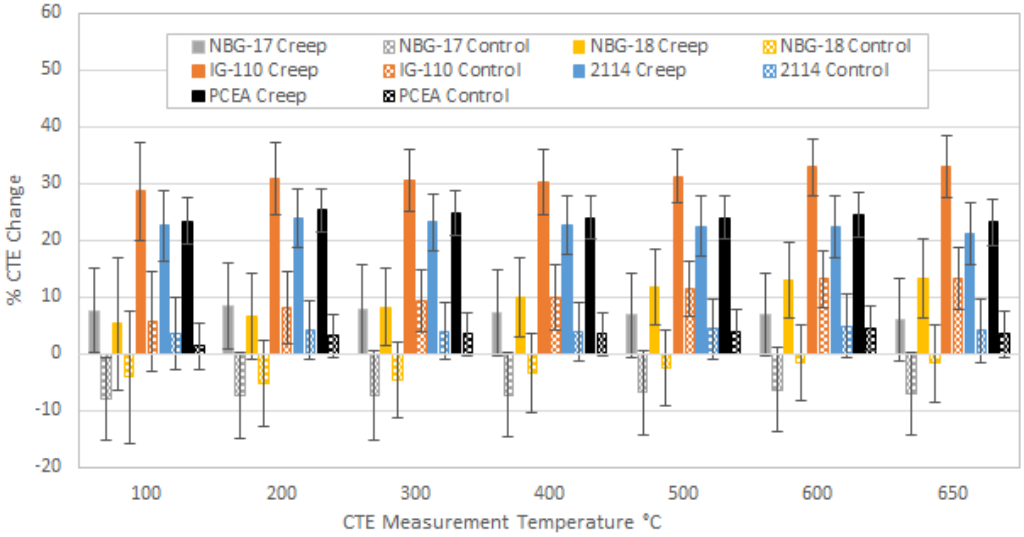

Figure 50. Average percent CTE change by graphite grade and applied stress for measurement temperatures 100°C–650°C.

To assess the effects from the different applied stress levels in the creep specimens, the changes to the measured CTE at a single test temperature (500°C) for the three applied stress levels is shown in Figure 51. Error bars represent +/- 1 standard deviation from the mean and the numbers in the bars represent the sample size. There is a clear trend to greater positive change in CTE (i.e., CTE increases) with increased axial stress in the specimens. This is explained by the increased densification of the microstructure during irradiation creep, which closes nano and microcracks within the graphite microstructure. Crack closure creates a denser material that will result in a higher thermal expansion behavior for the same material with more cracks within the microstructure.

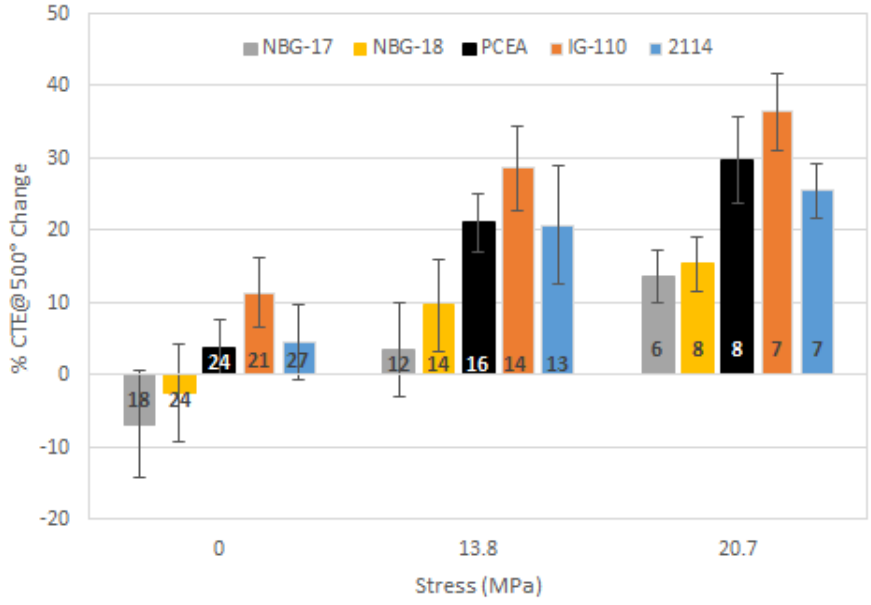

Figure 51. Average percent CTE change by graphite grade and applied stress. The error bars represent +/- 1 standard deviation from the mean and the numbers in the bars represent the sample size.

Figure 52, as in Figure 51, is a plot of percent change in CTE at 500°C versus irradiation dose but now the control (unstressed) and creep (stressed) specimens are shown separately. Linear regression lines are established for some individual grades to aid in clarity. To more accurately determine the effects from applied stress (and subsequent induced strain), the four stress levels are represented for each grade. The significant difference between stressed and unstressed specimens is apparent, but it becomes clear that the CTE generally increases with increasing applied stress indicating that CTE is sensitive to changes in the microstructure occurring from the induced strain.

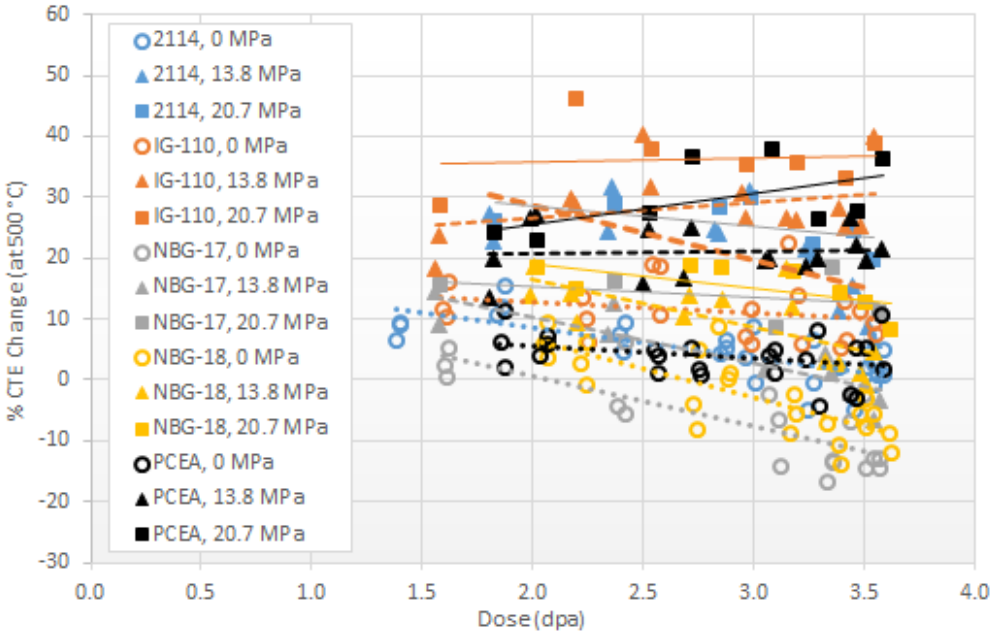

Figure 52. Percent CTE change at 500°C by graphite grade for stress levels of 0, 13.8, 17.2, and 20.7 MPa.

Figure 53 adds together the effects of irradiation and applied stress on the CTE at 500°C for the three separate forming processes. Only data from the 500°C testing temperature is used, and linear regression lines are established for both creep (—) and control (- - -) specimens. From this data the large difference in CTE behavior between the creep and control specimens is demonstrated along with the overall trend for each forming process. The scatter within the data is extensive over the relatively short dose range shown indicating fabrication processes have only a weak influence on the CTE behavior. Stronger influences from test parameters other than fabrication processes (e.g., grains size, coke source, orientation) may have a larger effect.

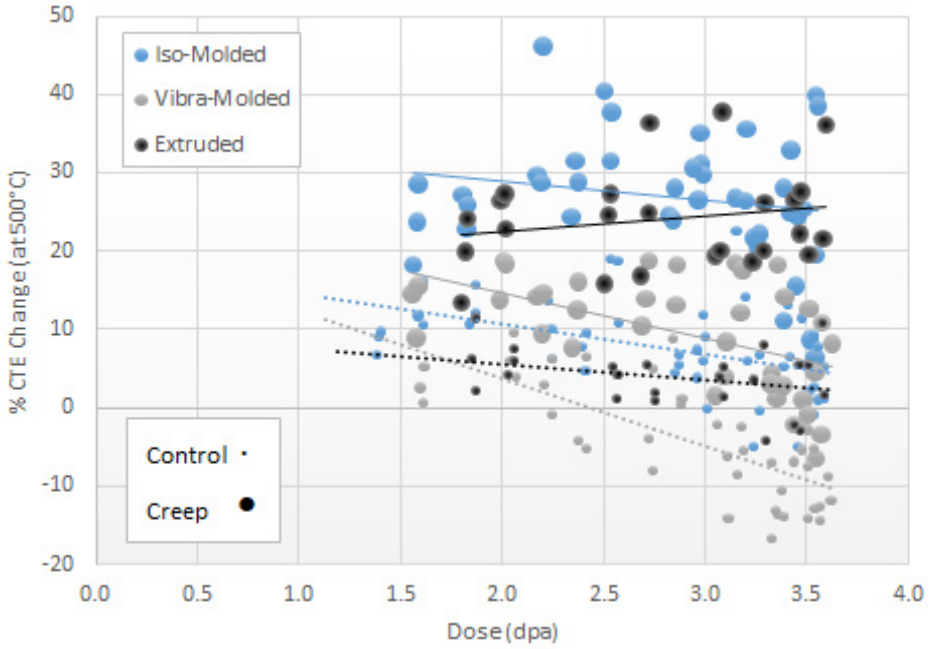

Figure 53. Percent change CTE at 500°C versus dose by fabrication process for creep (—) and control (- - -) specimens.

Figure 54 and Figure 55 investigate the dependence of grain orientation on the change of CTE at 500°C for the three major graphite grades that have forming processes which result in distinct grain orientations. Note that because of the strong influence of applied stress on the CTE behavior, the data must be analyzed separately for the stressed and unstressed specimens. Unstressed WG and AG results (□ and □) must be analyzed together as well as the stressed WG and AG results (□ and □). As observed, the percent change in CTE is nearly equal between the two grain orientations for all grades and average stress conditions (the exception being the NBG-18 unstressed specimens). The scatter within the data is significant so clear conclusions are not possible.

Figure 55 examines the percent change in CTE at 500°C over the irradiation dose range for the two grain orientations (hollow and solid symbols are representative of AG and WG, respectively). Similar to the applied stress analysis, no distinctive differences in percent CTE change are observed for grain orientation as a function of irradiation dose.

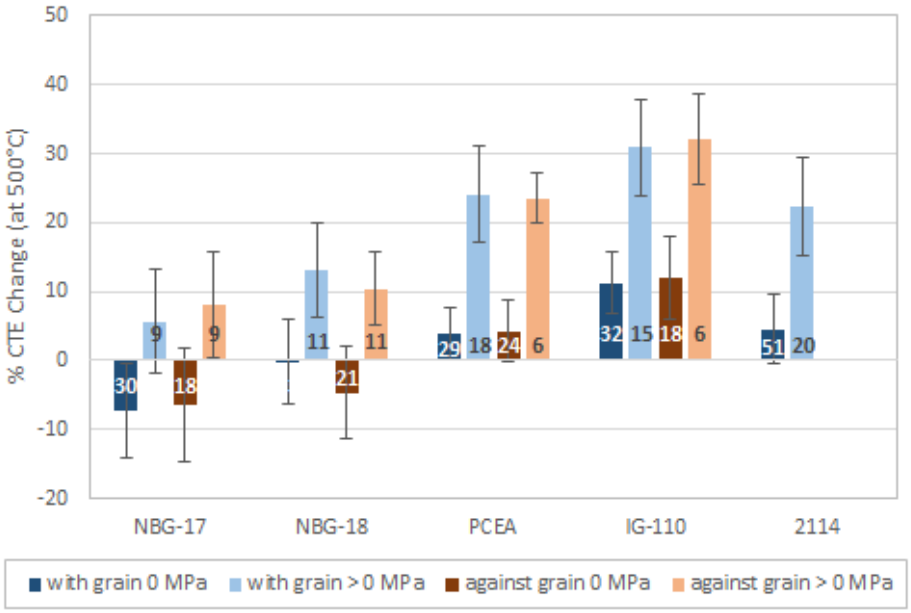

Figure 54. Average percent change CTE at 500°C by graphite grade, applied stress, and grain orientation for measurement temperatures at 500°C.

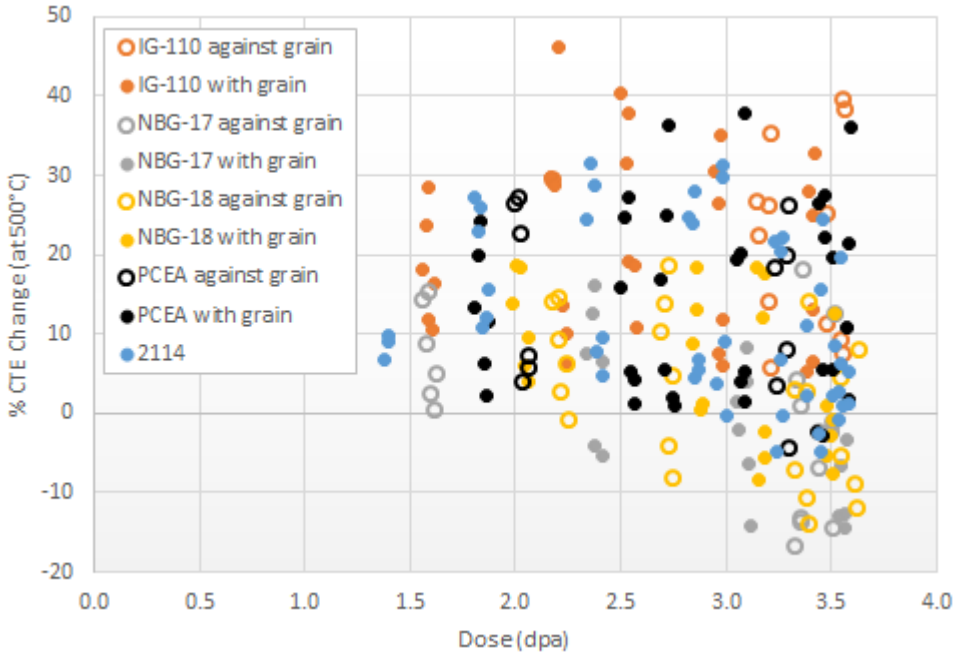

Figure 55. Percent change CTE at 500°C versus dose by graphite grade and specimen orientation.

Figure 56 illustrates the effects of specimen density (before irradiation) on the change in CTE at 500°C. As noted previously, density has a large effect on the material property values and density related differences may be exacerbated under irradiation. A general trend is observed when all the CTE data are considered (not distinguishing between the different grades). Changes to the CTE are observed to

decreases with increased pre-irradiation density for all specimens of all grades. So, in general, grades with higher initial (unirradiated) densities exhibited less CTE change over the limited irradiation dose experienced in AGC-3. For the case of the high-density vibrationally molded grades the control specimens CTE actually resulted in a negative change after a dose <4 dpa.

When analyzing the behavior of individual grades, no clear trends are apparent other than the differences between stressed and unstressed specimen which has been discussed previously.

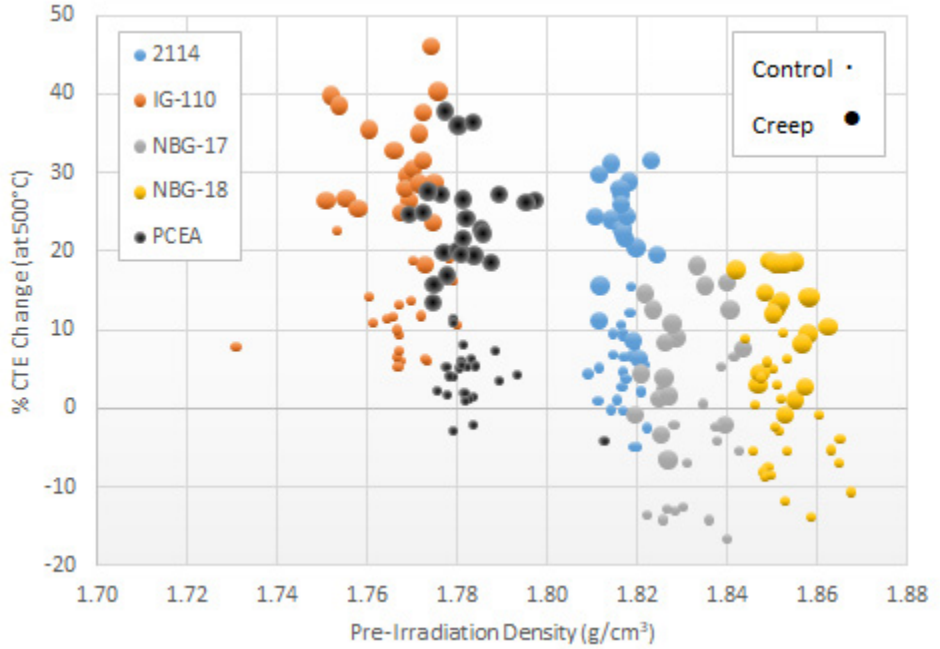

Figure 56. Percent CTE at 500°C change versus specimen pre-irradiation density by graphite grade for control and creep specimens.

The affect from irradiation-induced strain on CTE at 500°C is shown in Figure 57. The data are presented as the change in CTE at 500°C as a function of increasing strain experienced in the specimen axial direction as analyzed in the AGC-3 creep analysis report.[5] The data are separated into control and creep specimens, including all irradiation temperatures and received dose levels, with linear regression lines established for each individual grade.

As demonstrated previously, no clear trend emerges from this relatively short strain response other than the major difference between stressed and unstressed specimens. One interesting point observed from this data is that the stressed creep specimens from graphite grades with low unirradiated density (IG-110 and PCEA) had continuously increasing CTE changes, while creep specimens from the higher density grades (2114, NBG-17, NBG-18) show a slow decrease after the initial (<1.4 dpa) CTE increase. This trend is not observed within the unstressed control specimens; however, the rate of CTE decrease for the low density grades is significantly lower than for the high density grades (Figure 57).

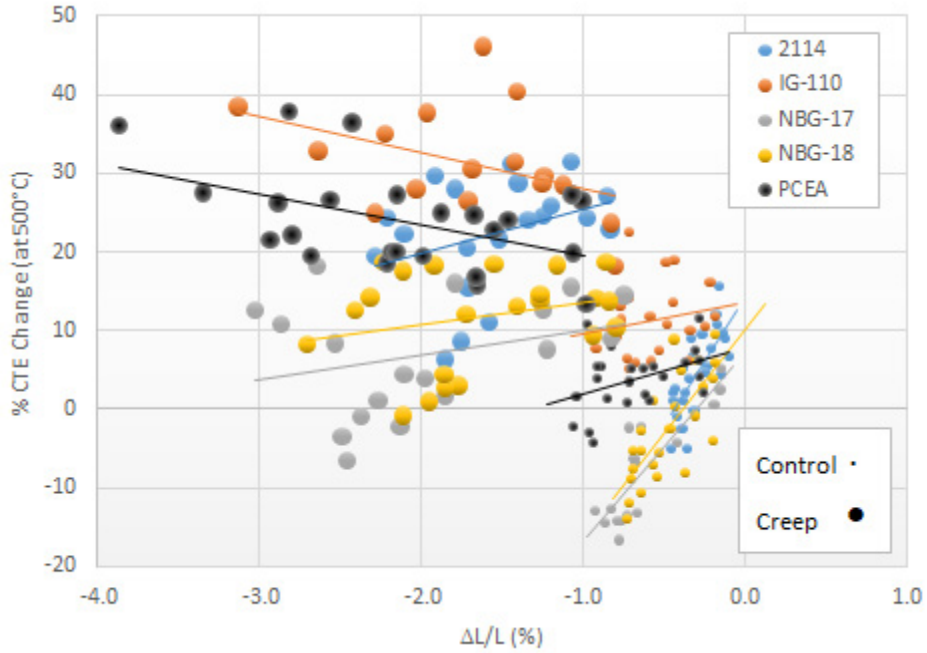

Figure 57. Percent CTE change at 500°C versus specimen strain by graphite grade for control and creep specimens.

Figure 58 shows the percent change in CTE for both stressed and unstressed specimens of the five grades of graphite separately as a function of dose for two temperature ranges, >821°C and <821°C. By plotting the data in this way, the effect of dose is isolated for two temperature ranges. For this dataset, all grades of graphite show no real separation in the magnitude of the change in CTE for the two temperature ranges. It is interesting to note that specimens irradiated at higher temperatures generally show lower CTE changes than the specimens irradiated at slightly lower temperatures. However, the changes are well within the data scatter and there is only a slight difference. Again, this is only an initial look at the effects of irradiation dose for narrow temperature ranges. More complete analysis of the individual effects of both irradiation temperature and dose will be performed when the data of all AGC capsules is combined.

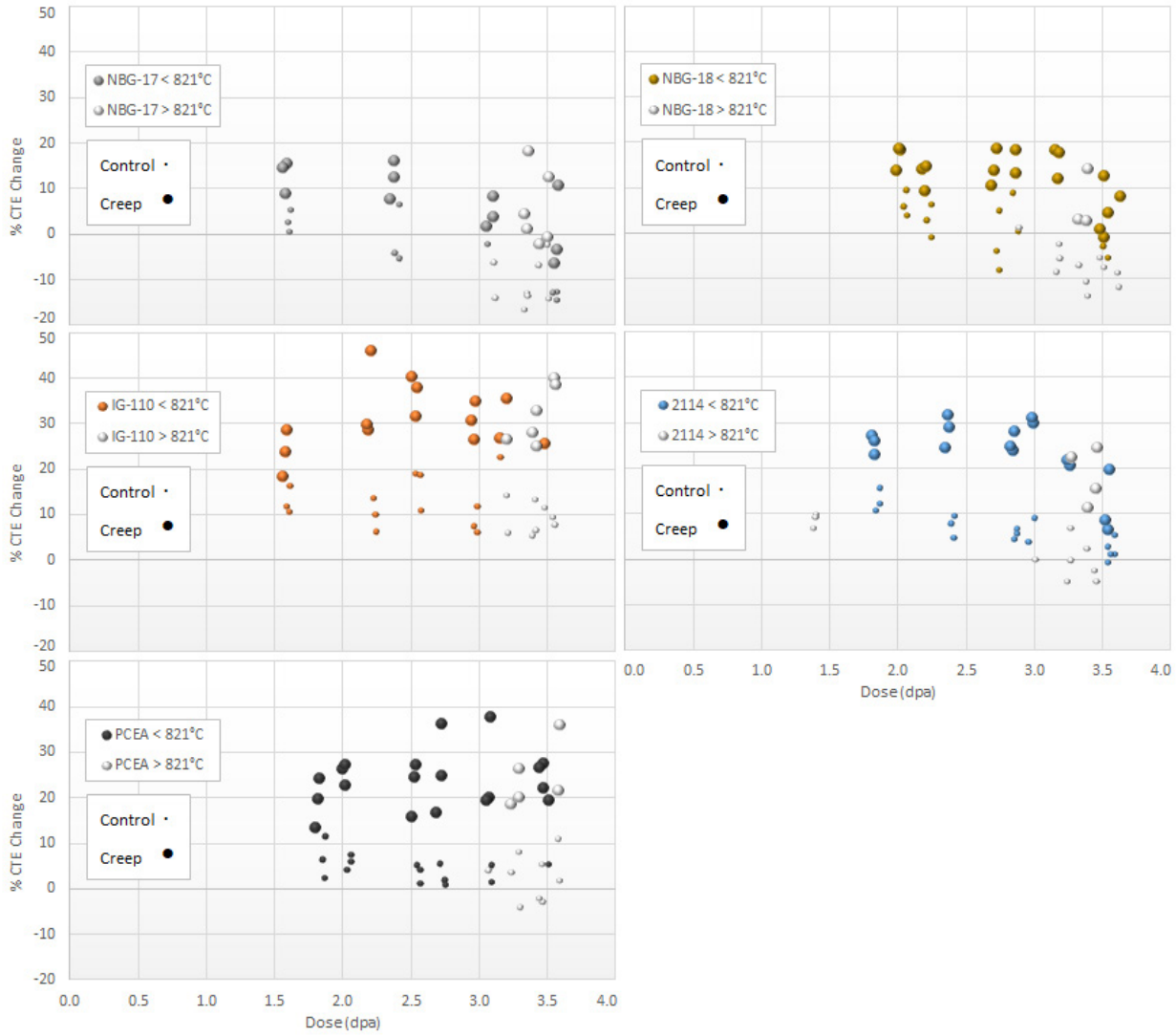

Figure 58. Percent CTE change versus specimen dose for two temperature ranges, >821°C and <821°C, for different graphite grades.

6.7 Thermal Diffusivity

Thermal conductivity and diffusivity are the most important thermophysical material parameters for the description of the heat transport properties of a graphite component. Thermal diffusivity measures the rate of heat transfer in a material (i.e., how fast heat is transferred from the hot side to the cold side of a material). It is useful for ascertaining heat conduction through the graphite core for passive decay heat removal, calculations of stress due to differential thermal expansion, and modeling core physics in a graphite moderated design.

The AGC-3 thermal diffusivity measurements were carried out in accordance with ASTM E1461-13. The measurement is performed on small, thin, disk-shaped specimens. A pulsed laser is used to subject one surface of the specimen to a high-intensity, short-duration energy pulse. The energy of this pulse is absorbed on the front surface of the specimen and the resulting rise in rear-face temperature is recorded.

The thermal diffusivity is calculated from the specimen thickness and the time required for the rear-face temperature to reach 50% of its maximum value.

$$\alpha = 0.13879 \cdot \left({}^{L^2}\!/_{t_{1/2}} \right) \tag{8}$$

where:

α = thermal diffusivity, mm^2/sec

L = specimen thickness, mm

$t_{1/2}$ = half rise time of the detector signal, sec.

The more familiar thermal conductivity is derived from diffusivity values by multiplying thermal diffusivity by the material density and specific heat capacity.

$$K = \alpha \cdot \rho \cdot C_p \tag{9}$$

where:

K = thermal conductivity, $Wm^{-1} \cdot K^{-1}$

α = thermal diffusivity, mm^2 /sec

ρ = density, g/cm^2

C_p = specific heat, $J \cdot g^{-1} \cdot K^{-1}$

Thermal diffusivity is a strong function of the tested graphite temperature; therefore, it is measured as a function of temperature here. Due to the physical limitations necessary to conduct diffusivity measurements (i.e., a relatively thin specimen), the measurements were performed on the unstressed piggyback specimens only. The piggyback specimens included all five different graphite grades analyzed in AGC-3. Pre-irradiation diffusivity measurements were performed starting at 25°C and then successively in 100° increments to 1000°C. Post-irradiation diffusivity was measured at 25°C and then at successive 100°C increments over the temperature range 100–600°C (and also at 650°C). Thus, percent change calculations were made up to only 600°C. Due to size and AGC-3 design limitations, none of the piggyback specimens were subjected to an applied mechanical stress during irradiation and accelerated creep was not attempted for these specimens.

Figure 59 shows the average pre and post-irradiation diffusivity for all graphite grades and irradiation conditions as a function of measurement temperature. As with the other material property measurements, the percent change in thermal diffusivity was substantial experiencing a maximum reduction of 80% at a measurement temperature of 25°C and a minimum reduction of 39% at 500°C (average diffusivity values are shown as a dashed line with +/- 1 standard deviation shown as solid lines). The full range of the data at each measurement temperature is depicted by arrows. This range is a result of the different variables within the experiment including irradiation temperature, dose, applied stress, graphite grade, and grain orientation.

It should be noted that graphite thermal diffusivity is normally expected to gradually reduce as the testing temperatures increase due to grain boundary and phonon-phonon (Umklapp scattering) scattering effects.[31, 32] Grain boundary phonon scattering dominates the thermal resistance at low temperatures but becomes insignificant above a few hundred degrees Celsius while the Umklapp scattering dominates at higher temperatures and defines the upper limit to the thermal conductivity for a “perfect” graphite. This gradual reduction due to temperature scattering effects are observed in both pre- and post-irradiation data, Figure 59.

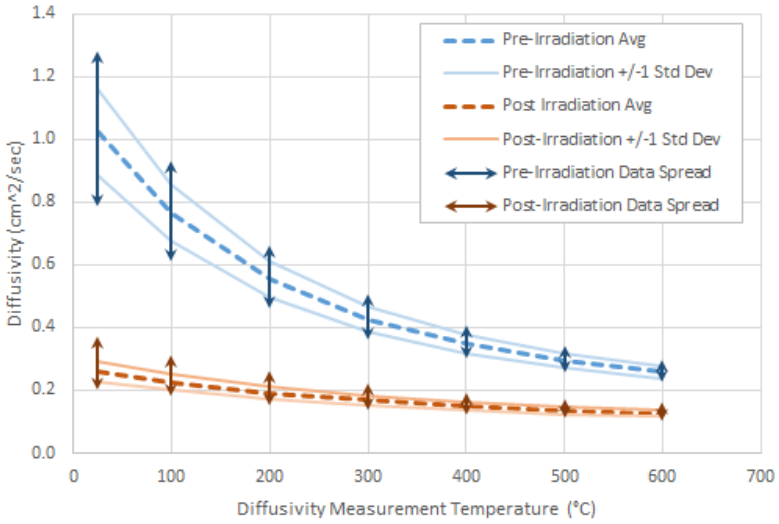

Figure 59. Specimen diffusivity versus measurement temperature for all AGC-3 piggyback specimens.

As seen in Figure 59, the thermal diffusivity data are remarkable in that all specimens including different grades, different grain sizes, with different grain orientations all respond similarly over the relatively small irradiation dose range of AGC-3. In fact, the scatter in measurement data actually decreases after irradiation despite the wide variations in the different graphite grades.

Figure 60 shows the average percent change for all specimens tested at the seven measurement temperatures. The similarity between the various grades is consistent over all measurement temperatures with all grades displaying a consistent behavior (i.e., IG-110 has the highest change in diffusivity measured values while Grade 2114 remains the lowest throughout all measurement temperatures). The standard deviations for all grades (shown as error bars in Figure 60) are extremely small and consistent between grades across the entire measurement temperature range. This is different from what has been observed for the other irradiated material properties, which show large and variable data scatter within and between the different grades.

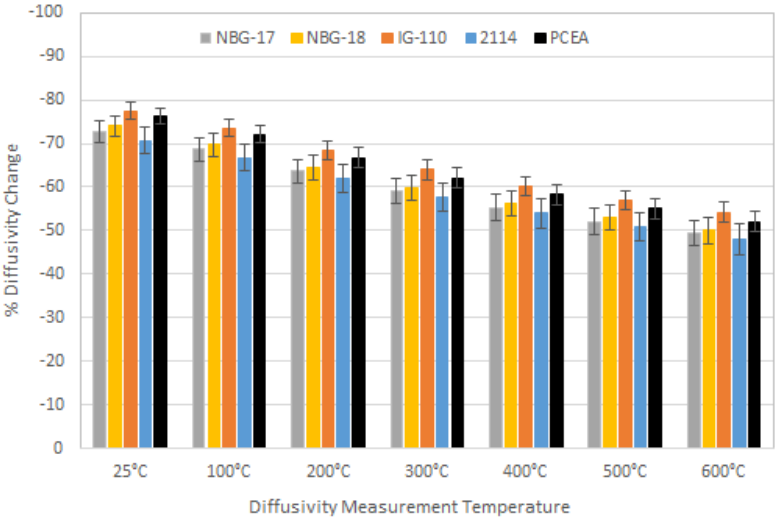

Figure 60. Average percent diffusivity change by graphite grade for measurement temperatures 25-600°C. Note that the Y-axis is inverted.

Since piggyback specimens did not receive applied stresses, there is no data comparing the effects of different stress levels (and induced accelerated strains). Only the effects from irradiation, fabrication processes, and irradiation-induced dimensional change strain on the different tested grades are compared in this analysis.

Figure 61 illustrates the thermal diffusivity behavior at 500°C from irradiation only. After the initial large (~80% drop) in diffusivity, the change in diffusivity resulting from increased irradiation dose continues to decrease with increasing irradiation dose. This implies that irradiation damage or the effects resulting from irradiation damage continues to affect the thermal diffusivity over the relatively short irradiation dose range in AGC-3. IG-110 exhibited the largest reduction in thermal diffusivity but one of the smallest change over the measured dose range (1.1–3.7 dpa) while Grade 2114 showed the least amount of change in diffusivity but the highest percentage change (~ 8%) over the measured dose range.

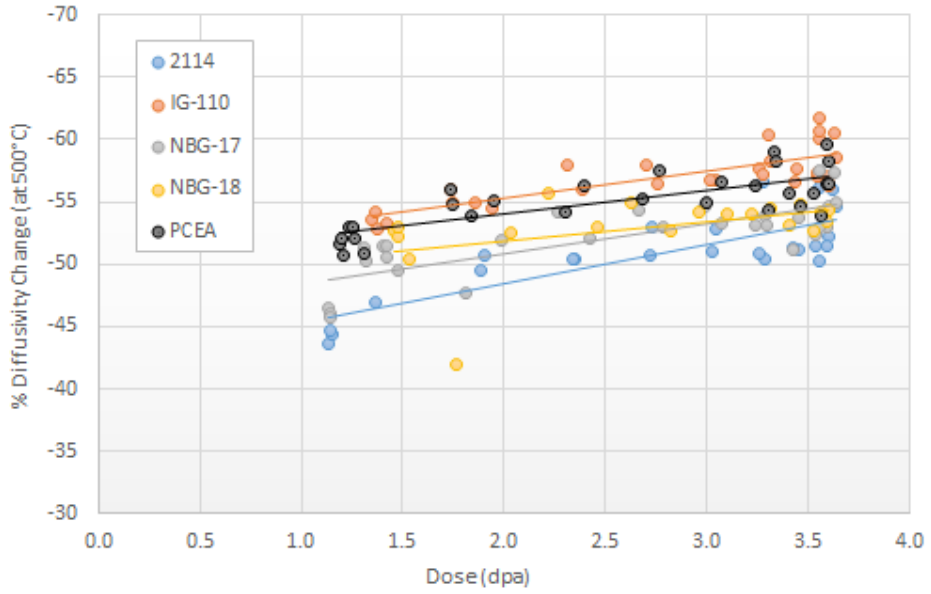

Figure 61. Percent change in diffusivity at 500°C as a function of irradiation dose. Note that the Y-axis is inverted.

Figure 62 investigates the dependence of grain orientation on the diffusivity change for the four major graphite grades that have forming processes, which result in distinct grain orientations. The average percent change in thermal diffusivity for measurement temperatures of 100°C and 500°C are shown with the error bars indicating ±1 standard deviation. As observed, minimal differences exist for either orientation at either measurement temperature indicating that irradiation affects thermal diffusivity similarly for all specimen orientations.

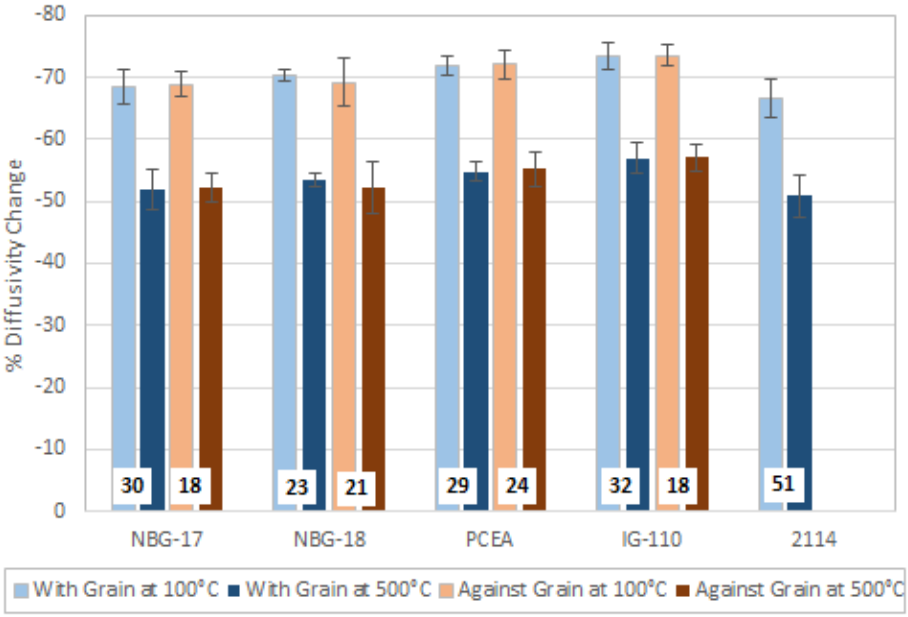

Figure 62. Average percent diffusivity change by graphite grade and grain orientation. Note the Y-axis is inverted.

Figure 63 illustrates the effects of specimen density (before irradiation) on the change in thermal diffusivity. As noted previously, density has a large effect on the material property values and density related differences may be exacerbated under irradiation. However, the data in Figure 62 shows no obvious changes to the irradiation thermal diffusivity percentage change as a function of pre-irradiated density for either between or within the various grades.

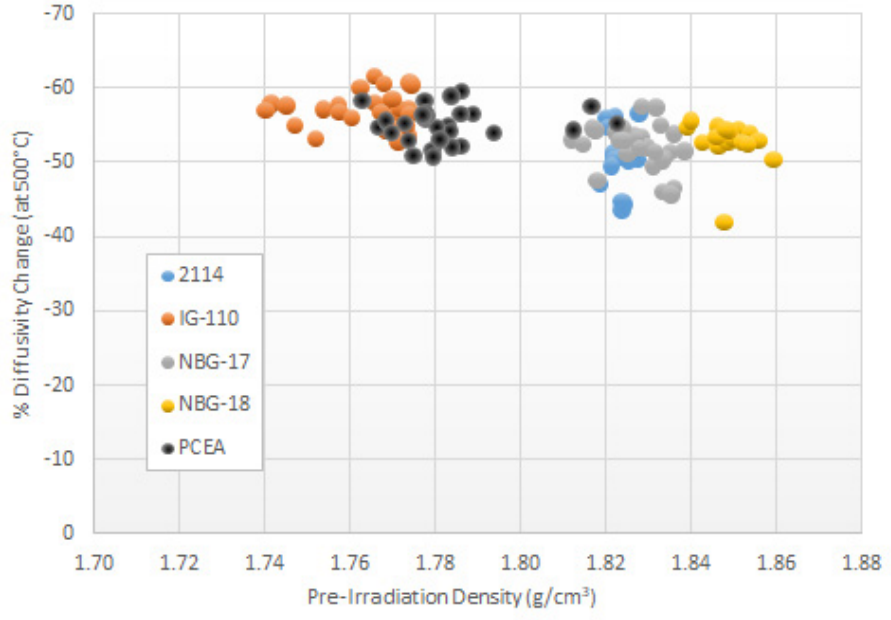

Figure 63. Percent diffusivity change versus specimen pre-irradiation density by graphite grade. Note that the Y-axis is inverted.

Figure 64 demonstrates the effect of irradiation-induced strain at 500°C on the thermal diffusivity response for the five major grades of graphite. Note that there are no stressed creep specimens to provide mechanically enhanced irradiation-induced strain. This data only represent the behavior of unstressed dimensionally changed specimens with limited irradiation-induced strain values. As seen, there is a large initial reduction in the diffusivity noted for all grades, but the diffusivity continues to decrease much more slowly as the irradiation-induced strain increases for these unstressed control specimens. However, this change is most likely resulting strictly from increasing neutron dose since the trends closely match the change noted in Figure 61. Since there is no accelerated strain response data from applied stresses, any conclusions other than the thermal diffusivity continues to decrease with increasing strain and dose cannot be made at this time.

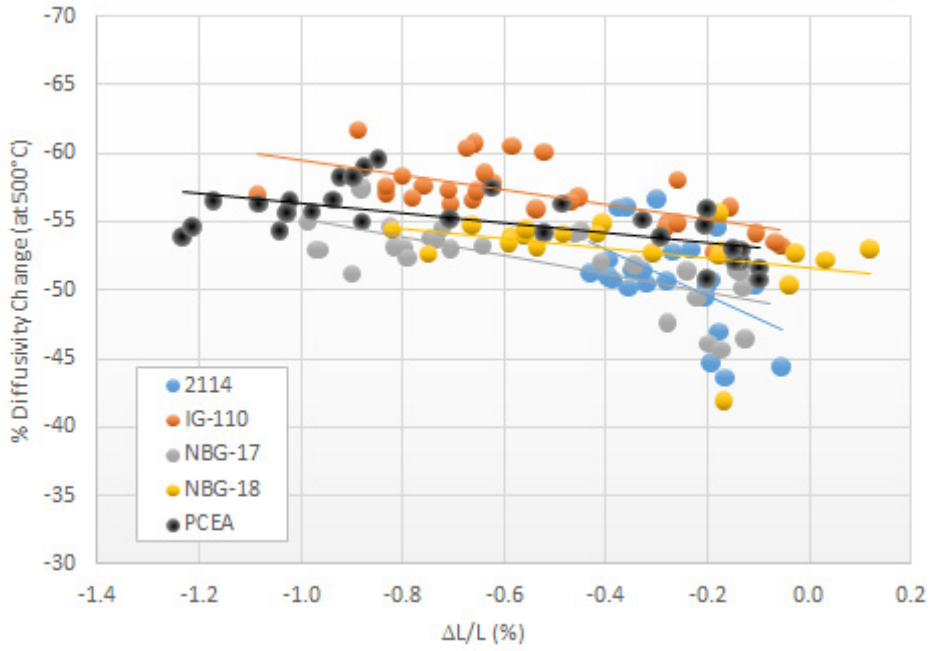

Figure 64. Percent diffusivity change at 500°C versus specimen strain for the unstressed control specimens (no accelerated irradiation-induced creep) for all major graphite grades. Note that the Y-axis is inverted.

Figure 65 shows the percent change in thermal diffusivity for the five grades of graphite separately as a function of dose for two temperature ranges, >821°C and <821°C. By plotting the data in this way, the effect of dose is isolated for two temperature ranges. The number of data points for the upper temperature range is sparse. However, for the data available, all grades of graphite show no real separation in the magnitude of change in thermal diffusivity between the two temperature ranges. The effects of irradiation temperature over a much larger range will be analyzed when the data of all AGC capsules is combined.

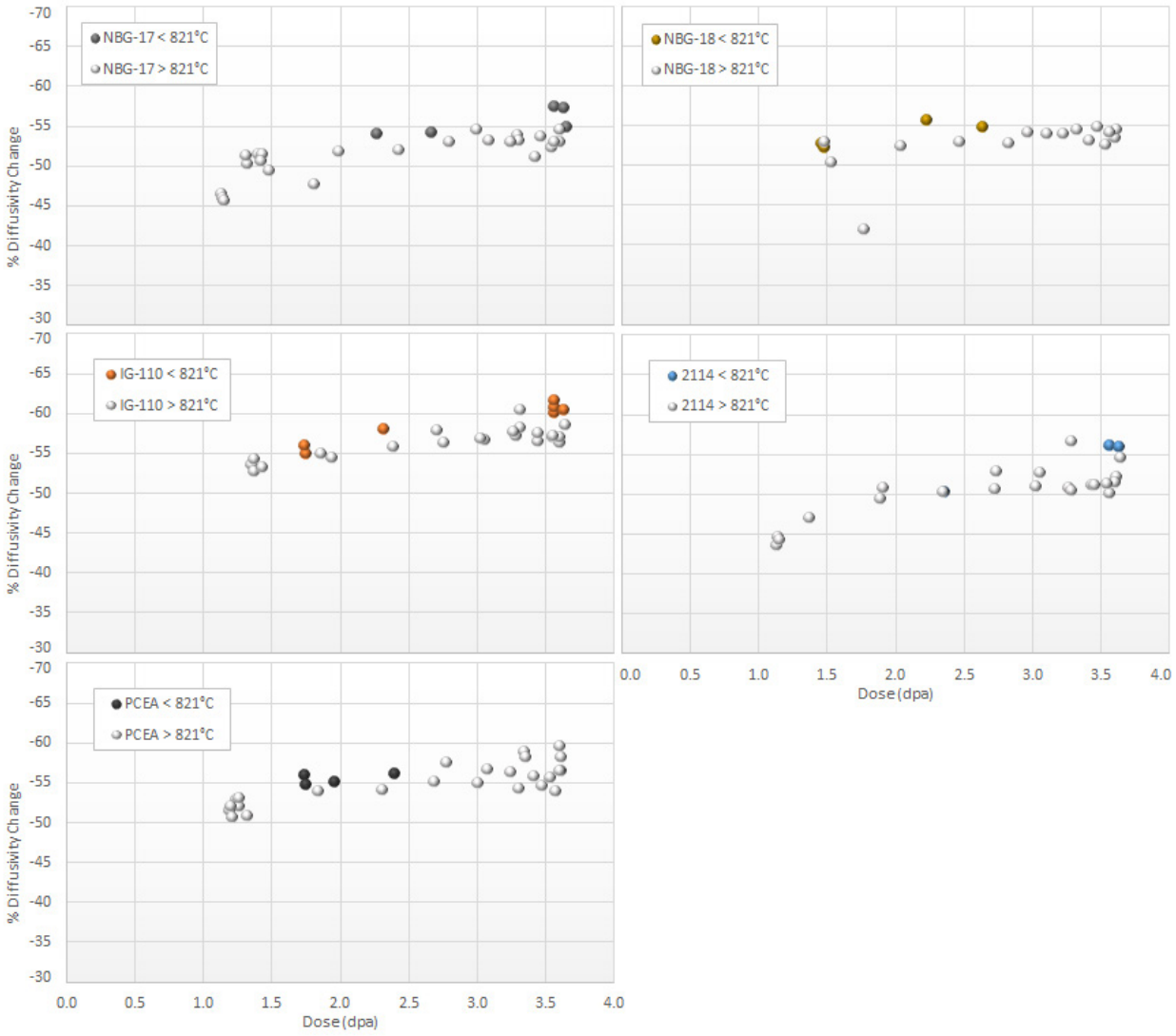

Figure 65. Percent thermal diffusivity change (at a measurement temperature of 500°C) versus specimen dose for two temperature ranges, >821°C and <821°C, for different graphite grades. Note that the Y-axis is inverted.

7. CONCLUSIONS

This report documents the analysis of the irradiated material property data from the graphite specimens irradiated within the AGC-3 capsule. The AGC-3 capsule was the first of two planned (now three planned, as of 2018) capsules irradiated at 800°C. The AGC-3 irradiation temperature range was 748–937°C (average 821°C, 30°C standard deviation). AGC-3 was irradiated for the shortest time and had the lowest expected dose range of 1.0 to 3.7 dpa. AGC-4 capsule will be irradiated immediately after AGC-3 at 800°C but to an anticipated dose range of 2.5 to 7.5 dpa. The new HDG-2 capsule will complete the 800°C irradiations and bring the dose range of the graphite specimens to a range of ~7 to 15 dpa.

Material property data on specimen resistivity, Young's modulus (both by sonic resonance method and sonic velocity method), shear modulus, coefficient of thermal expansion, and thermal diffusivity were

analyzed. Behavior trends from the data were discussed with respect to the experimental variables of irradiation dose, temperature, stress, and graphite grade affecting these property changes. Comments from this analysis are summarized as general observations (Section 7.1) common to all analyses and specific observations (Section 7.2) discussing interpretations for each individual material property analysis.

7.1 General Observations

1. The AGC-3 irradiation dose range is relatively small and short (1.0–3.7 dpa). This is a small fraction of the anticipated 1.0–15.0 dpa dose range for the 600°C graphite irradiations. Thus, the trends and behavior over this short dose range must be considered preliminary and incomplete. They are but a part of the larger irradiation behavior to be analyzed over the complete dose range (1–15 dpa).
2. Except for density change, which is related to the linear dimensional change behavior, all material properties experience a significant and rapid change after irradiation.
3. The irradiation-induced changes within each material property were remarkably similar for all tested specimens over this short dose range regardless of nuclear grade, grain size, stressed/unstressed condition, or grain orientation.
4. Strong evidence exists that many of the changes are a result of both irradiation damage mechanisms as well as microstructural changes, such as internal strain from dimensional change or irradiation-induced creep.
5. Only very small differences (if any) occurred in material property changes due to grain orientation. The percentage change was very similar for with-grain and against-grain orientation for all irradiated material properties.

Except for density changes, irradiation appeared to produce significant changes to all material properties analyzed. In nearly all cases, the majority of the change appeared to occur at relatively low dose levels (<1.0 dpa) well before any significant bulk microstructural changes should begin to affect the changes. This implies that irradiation damage to the atomic crystal structure is likely responsible for these initial rapid and significant changes to the material properties. Density was the notable exception to this behavior.

In general, the initial irradiation-induced increase for the 800°C AGC-3 results were slightly lower than the results from the 600°C AGC-2 irradiated results. This difference is not large but is still significant and most likely results from the higher irradiation temperature, which would cause higher Frenkel pair recombination. A higher recombination rate would produce a slight reduction in the point defect population within the crystal structures and may explain the slightly lower irradiation-induced initial increases in material property. However, since these observed trends are weak, this difference may just be a result of differences between the AGC-2 and AGC-3 specimens that were machined from different billets of the same grade. These trends will need to be explored for the higher dose irradiations of AGC-1, AGC-4, and HDG-2.

Once this sudden irradiation-induced change to the material property was achieved, the measured material properties (other than density changes) with increasing dose showed a mixed reaction with some increasing, some showing no change, and some actually showing a decrease from the initial peak increase. This was different from the 600°C AGC-2 irradiated results, which appeared to remain nearly constant over a similar small irradiation dose range (1.3 to 4.7 dpa). Since AGC-3 was irradiated at the higher 800°C, this implies that the irradiation temperature may be accelerating the irradiation-induced behavior over the 600°C irradiations. This is expected as higher irradiation temperature can accelerate microstructural changes and is a major factor in changing the turnaround dose in irradiated graphite. Thus, the higher irradiation temperature appears to be changing the material property behavior of the AGC-3 specimens, as expected.

While the general irradiation response for all grades was fairly similar, the magnitude of the irradiation-induced property change was significantly affected by grade type, fabrication method, and applied stress/strain levels in the tested specimens. Other than irradiation dose, the applied stress, which induced accelerated strain within the specimens, was the largest parameter to affect material property changes. In many cases the data showed that continued changes in the graphite properties, after the initial irradiation-induced change, could be attributed to the stress-induced strain. These two mechanisms, irradiation-induced atomic damage and stress-induced dimensional change or irradiation creep, appeared to be responsible for nearly all material property changes.

Historically, it has been proposed that these competing mechanisms (irradiation damage and microstructural strains) are responsible for the changes in graphite properties due to irradiation. Notably, the changes the CTE of graphite have traditionally been attributed to an irradiation damage component and physical graphite crystalline change (strain) component. The significance for both irradiation damage and irradiation-induced strain are aptly demonstrated here in this AGC-3 CTE analysis.

It was surprising that grain orientation and density variations had only minimal impact on the irradiation-induced changes. The differences in unirradiated material property values between with-grain and against-grain measurements can be significant, especially for the extruded grades. However, as was demonstrated for all analyses, the radiation-induced changes were nearly equivalent for both with and against-grain orientations. Similarly, density has an outsized influence on graphite material properties with even small changes to the density affecting the elastic moduli, strength, and thermal properties. The density variations within individual graphite grades was very small (~1%) and no correlation to property changes were observed.

7.2 Specific Comments

Specific comments are provided for each of the analyses noting material property specific trends for dose, strain, and graphite grade differences.

7.2.1 Density

Similar to previous irradiation analysis in AGC-1 and AGC-2, density changes did not initiate until ~1.1 dpa and rose gradually and linearly in correlation with the irradiation-induced dimensional change (i.e., internal strain) that has a linear dependence upon the received neutron dose. Since density change occurs from microstructural densification, this is logical as any irradiation damage-induced density change would have been largely masked by Mrozowski volume accommodation mechanisms.

Nearly all material properties experience a significant and rapid change after irradiation. Density was the primary exception to this behavior rising gradually and linearly as a function of dose. This behavior is expected since density change occurs from microstructural densification, and any initial irradiation damage-induced density change would have been largely masked by Mrozowski volume accommodation mechanisms. Thus, macroscopic density changes will closely follow the microstructural strain.

Figure 10 clearly illustrates this strong dependency of density change to the observed strain for both the stressed and unstressed specimens. This is an example of how a single direct measurement of the change in density may be used to predict an intrinsic property value, such as internal strain (and stress). It is conceivable that real-time measurements of density could be made for reactor core blocks or sections of blocks, which could indicate the irradiation or thermally induced internal stress levels of components. These stress values could then be used as property value input to a probabilistic fracture model of the reactor core components.

7.2.2 Electrical Resistivity

The rapid (<1.0 dpa) irradiation-induced changes in electrical resistivity were the largest of any material property change at a maximum of ~200% increase. Once the initial change had occurred, little change in resistivity could be seen over the relatively small dose range (~1.1 to ~3.7 dpa) of this experiment and no change in resistivity was observed relative to the irradiation-induced strain. This indicates that changes to the electrical resistivity of graphite over small dose ranges (~1.1 to ~3.7 dpa) is purely dependent upon irradiation damage mechanisms within the graphitic crystallites, and microstructural changes have minimal effect on the changes in resistivity.

It should be noted that the resistivity response was mixed for the various grades. The extruded grade PCEA with 800 μm grain size had the highest resistivity change while the small grain size (~30 μm) isostatic Grade 2114 had the smallest resistivity changes. However, the isostatic, small grained (~30 μm) IG-110 grade had the second highest resistivity change while the largest grain sized grade (NBG-18, 1800 μm) had changes lower than the PCEA and IG-110. It appears grain size, fabrication processes, and initial density had little to do with the change in resistivity, but both IG-110 and PCEA are produced with petroleum coke while NBG grades use pitch coke sources.

7.2.3 Elastic Modulus

After the initial irradiation-induced modulus increase (<1 dpa) the modulus behavior appears to be much more sensitive to graphite grade than for any other material property change. Figure 27 and Figure 29 illustrate the modulus behavior differences between individual grades and fabrication processes where the fine-grain, iso-molded grades show the largest change and the vibrationally molded grades demonstrate the lowest change. Of note, is the similarity between NBG-17 and NBG-18 response even though NBG-18 grain size is twice the size of NBG-17.

The initial change in modulus (<1.0 dpa) is large signifying that irradiation induced dislocation pinning mechanisms within the graphite crystal structures have increased the stiffness of the material. However, this rate of elastic modulus increase over the relatively short AGC-3 dose range is much smaller and indicates that competing mechanisms are affecting the graphite behavior. This behavior is a complex interrelationship between several competing mechanisms including irradiation induced densification, irradiation damage, dislocation pinning/movement, and microcrack behavior within the microstructure.

As discussed previously, this behavior is expected from past studies: modulus changes as a function of dose follow the pattern of a sudden increase in modulus, a slower rise to the peak increase, followed by a decrease in stiffness once turnaround begins to be dominant and microcracks begin to form. For the relatively short AGC-3 dose range, the sudden and gradual increases of the modulus would be expected even for these specimens irradiated at a higher temperature (800°C).

Figure 34 illustrates the effect of microstructural change (i.e., strain) on the bulk modulus behavior. As demonstrated, the modulus change is strongly positive for unstressed specimens, which clearly shows the dislocation pinning mechanisms speculated as the primary cause for this increase. However, the stressed specimens actually show a small decrease in modulus change over the AGC-3 dose range signifying that microstructural changes, as represented by the accumulating bulk strain, has an effect on the modulus changes as well. These two competing mechanisms combine to produce the overall bulk elastic stiffness response of the graphite with the initial sudden increase controlled by atomic ballistic damage and the decrease in stiffness controlled by the gradual accumulation of microstructural change.

7.2.4 Shear Modulus

The observed shear modulus behavior was very similar to the Young's modulus behavior with a large initial increase in modulus (<1.0 dpa) and only a small increase over the AGC-3 received dose range. While the initial change in shear modulus was not as large as the Young's modulus change, Figure 37 and Figure 39 show the initial response and gradual increase in shear modulus. Again, the NBG-17 and NBG-18 responses are nearly identical despite the grain size differences.

Reviewing Figure 40 and Figure 45 it is obvious that the shear modulus response is not as sensitive to the microstructural changes (as represented by the accumulating mechanical strain). This indicates the shear modulus is only weakly sensitive to induced microstructural change with both unstressed and stressed specimens showing small increases over the AGC-3 dose range. This behavior is somewhat unexpected as similar to Young's modulus the shear modulus is sensitive to dislocation movement in the crystal structure (compliance), and is also expected to be sensitive to changes in the microstructure (e.g., pore sizes, grain orientation, and connected cracks), which is not detected in the shear data. Further fundamental studies will be necessary to assist in the interpretation of these data trends.

7.2.5 CTE

Similar to the other material properties, there was an initial increase in CTE (for <1.0 dpa), but the increase was modest, especially for the vibrationally molded grades (NBG-17 and NBG-18). Almost immediately the average CTE change (combining both stressed and unstressed results) started to decrease (Figure 48). However, it became very apparent (Figure 53) that CTE is extremely sensitive to microstructural change with a clear difference between stressed and unstressed specimen behavior. It is clear that with increasing stress (and by definition, strain) the CTE change continues to increase with increasing dose. The opposite is occurring for unstressed specimen with the CTE change gradually decreasing with increasing dose levels.

This behavior is somewhat expected where the CTE initially increases, peaks at a dose level smaller than turnaround dose, and then decreases into a negative CTE change as the dose continues to increase. This behavior is understood to be a combination of initial irradiation damage and gradual accumulation of microstructure defects. The initial CTE increase within the graphite crystal structure occurs with an increase in the density of the crystal structure through closure of the nanocracks within the crystals. The decrease occurs from the gradual accumulation of microstructure defects (e.g., new Mrozowski crack formation, pores, microstructure cracks) gradually decreasing the graphitic unit density and decreasing the thermal expansion coefficient. The current behavior is somewhat difficult to interpret since the neutron dose range is so small that only the initial rise and the gradual increase of CTE is expected. However, clearly some of the graphite grades are experiencing a shortening of the CTE increase and the negative CTE change is occurring faster.

This is most likely due to the higher irradiation temperature (800°C), which is known to affect when the CTE changes occur within an irradiated graphite. At the higher temperatures, the nanocracks within the crystals begin to close faster. Thus, irradiation-induced microstructural defects produced by crystal changes begin at lower neutron dose levels. This is similar to what happens to the turnaround dose at higher temperatures, the required dose to achieve turnaround becomes smaller at higher temperatures. However, the current data are not enough to form firm conclusions on how microstructure strain and irradiation damage directly affects changes to the CTE. These trends will be re-analyzed for the higher dose irradiation capsules (AGC-4 and HDG-2) to more clearly determine the effect of temperature and dose on the CTE. Additionally, further fundamental studies will be required to assist in the interpretation of these data trends.

7.2.6 Thermal Diffusivity

Thermal diffusivity was the only material property that did not include a measurement of the effects from applied stress and irradiation-induced accelerated strain. Only irradiation effects from crystallographic damage and the resulting small dimensional changes were measured. Additionally, the diffusivity was the only material property that demonstrated a strong initial (<1 dpa) decrease from unirradiated values (Figure 59). Diffusivity continues to decrease with increasing neutron dose, albeit at considerable reduced rate. This observation may show that simple defects, such as Frenkel pair dislocations, occur at very low doses but more complex atomic defects, which continue to disrupt phonon transport, may occur at higher neutron dose levels >1 dpa.

Of importance was the remarkable similarity in response for all tested grades. In fact, the measured error within and between the different grades actually decreased with increasing dose (Figure 59 and Figure 60). This implies that a mechanism common to all grades was the primary factor responsible for the diffusivity changes. Since there was minimal microstructure change (i.e., creep strain) the irradiation damage to the graphitic crystal structure through neutron ballistic interaction creating Frenkel pair point defects is the most likely mechanism for thermal diffusivity changes. It is generally understood that point defects within the graphitic crystals can affect the phonon transport and may decrease the thermal diffusivity of neutron irradiated graphite. Other effects, such as new nanocrack formation, crystallite reorientation, and increased microcracking, may also continue the decrease and may be responsible for the further (slow) decrease in the thermal diffusivity behavior. Further fundamental studies will be required to assist in the interpretation of these data trends.

8. REFERENCES

1. T. Burchell, R. Bratton, and W. Windes, *NGNP Graphite Selection and Acquisition Strategy*, ORNL/TM-2007/153, Oak Ridge National Laboratory, September 2007.

2. R. L. Bratton and T. D. Burchell, 2005, *NGNP Graphite Testing and Qualification Specimen Selection Strategy*, INL/EXT-05-00269, Idaho National Laboratory, May 2005.

3. PLN-2497, "Graphite Technology Development Plan," Revision 1, Idaho National Laboratory, October 2010.

4. W. E. Windes, T. D. Burchell, M. Davenport, "The Advanced Reactor Technologies (ART) Graphite R&D Program," *Nuclear Engineering Design*, Vol. 362, 2020, NED_110586, ISSN 0029-5493.

5. W. E. Windes, D. T. Rohrbaugh, W. D. Swank, *AGC-3 Irradiation Creep Strain Data Analysis*, INL/EXT-19-54725, July 2019.

6. W. E. Windes, D. T. Rohrbaugh, W. D. Swank, and D. L. Cottle, *AGC-3 Specimen Post-Irradiation Examination Data Package Report*, INL/EXT 17-43823, Idaho National Laboratory, December 2017

7. T. Burchell and R. Bratton, 2005, *Graphite Irradiation Creep Capsule AGC 1 Experimental Plan*, ORNL/TM 2005/505, Oak Ridge National Laboratory, May 2005.

8. TFR-791, "Technical and Functional Requirements for NGNP Advanced Graphite Capsule AGC-3 Experiment Test Train," Rev 1, June 2012.

9. W. Windes, D. Swank, D. Rohrbaugh, and J. Lord, *AGC-3 Graphite Preirradiation Data Analysis Report*, INL/EXT-13-30297, Idaho National Laboratory, September 2013.

10. INL Drawing 601501 Rev. 4, “ATR Advanced Graphite Capsule (AGC) AGC-3 Graphite Specimen Cutout Diagrams,” July 09, 2012.
11. INL Drawing 603523, Rev. 1, “ATR Advanced Graphite Capsule Miscellaneous Graphite Component Assembly and Details,” May 24, 2012.
12. INL Drawing 600001, “ATR TMIST-1 Oxidation Experiment In-Vessel Installation,” Rev. 2, Idaho National Laboratory, March 2009.
13. T. Burchell and R. Bratton, *Graphite Irradiation Creep Capsule AGC-1 Experimental Plan*, ORNL/TM-2005/505, Oak Ridge National Laboratory, May 2005.
14. ECAR-1842, “Thermal Evaluations for the AGC-3 Experiment Irradiated in the ATR East Flux Trap,” Rev. 0, April 26, 2012.
15. ECAR-1788, “Reactor Physics Projections for the AGC-3 Experiment irradiated in the ATR East Flux Trap,” J.R. Parry, Rev 0, April 19, 2012.
16. TFR-510, “Advanced Graphite Capsule Compressive Load Control Gas System,” M. Davenport, Rev. 3, June 18, 2013.
17. TFR-509, “Advanced Graphite Capsule Temperature Control System,” Rev 2, Idaho National Laboratory, December 2011.
18. TFR-645, “Technical and Functional Requirements Advanced Graphite Capsule AGC-2 Experiment Test Train,” Rev. 1, April 28, 2016.
19. INL Drawing 603520, “ATR Advanced Graphite Capsule (AGC-3) Test Train Facility Assembly,” Rev. 0, June 25, 2012.
20. INL Drawing 603540, “ATR Advanced Graphite Capsule (AGC-3) Test Train Installation,” Rev. 1, July 26, 2012.
21. INL Drawing 603524, “ATR Advanced Graphite Capsule 3 (AGC-3) Specimen Stack-Up Arrangements,” Rev. 0, May 17, 2012.
22. WO 15970401, “Engineering Work Instructions for Assembling the AGC-3 Experiment,” June 4, 2012.
23. W. Windes, P. Winston, and W. D. Swank, *AGC-3 Disassembly Report*, INL/EXT-15-34675, Idaho National Laboratory, May 2015.
24. L. Hull, 2014, *AGC-3 Experiment Irradiation Monitoring Data Qualification Final Report*, INL/EXT-14-32425, Rev. 1, Idaho National Laboratory, October 2014.
25. ECAR-3386, “As-Run Thermal Analysis of the AGC-3 Experiment,” P. E. Murray, Rev. 0, Idaho National Laboratory, September 2016.
26. ECAR-4430, “AGC-3 Specimen Position Calculations by Stack,” INL/MIS-19-53379, D. Rohrbaugh, Rev. 0, June 11, 2019
27. PLN-3858, “AGC-3 Graphite Specimen Pre-Irradiation Characterization Plan,” June 16, 2011.
28. PLN-4888, Rev. 0, “AGC-3 Graphite Specimen Post-irradiation Characterization Plan,” May 08, 2015.
29. Tim Burchell, *AGC-1 Irradiation Induced Property Changes Analysis Report: Dynamic Elastic Modulus*, ORNL/SR-2015/378, March 2016.

30. W. E. Windes D. T. Rohrbaugh W. D. Swank, *AGC-2 Irradiated Material Properties Analysis*, INL/EXT-17-41165, May 2017.

31. L. L. Snead and T. D. Burchell, "Thermal conductivity degradation of graphites due to neutron irradiation at low temperature," *Journal of Nuclear Materials*, Vol. 224, 1995, pp. 222–229.

32. B. Kelly, *Physics of Graphite*, Applied Science Publishers Ltd, London and New Jersey, 1981.

Appendix A

Data Plots for Dynamic Young's Modulus Measured by the Sonic Resonance Technique

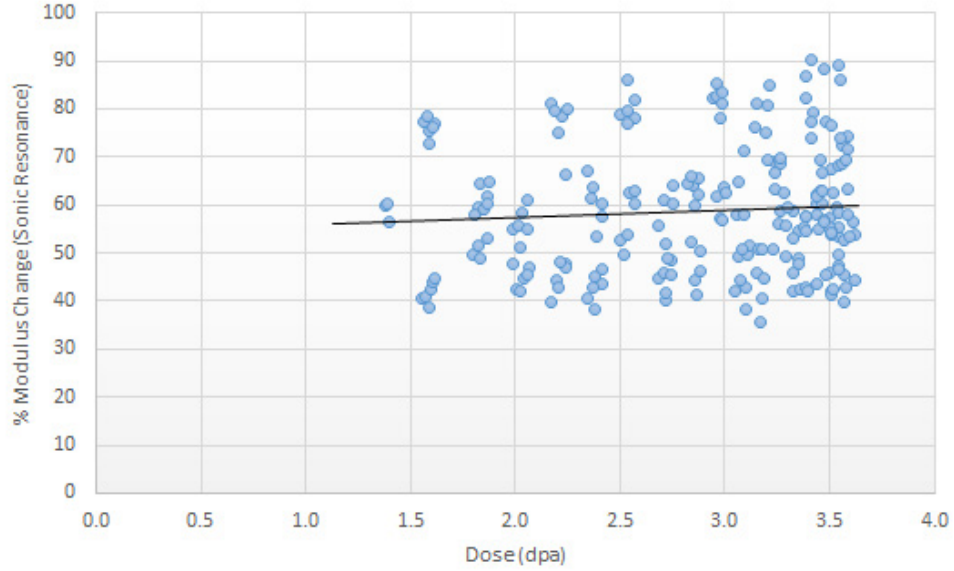

Figure A-1. Percent change in modulus as a function of fast neutron dose for all AGC-3 specimens for which the measurement was made.

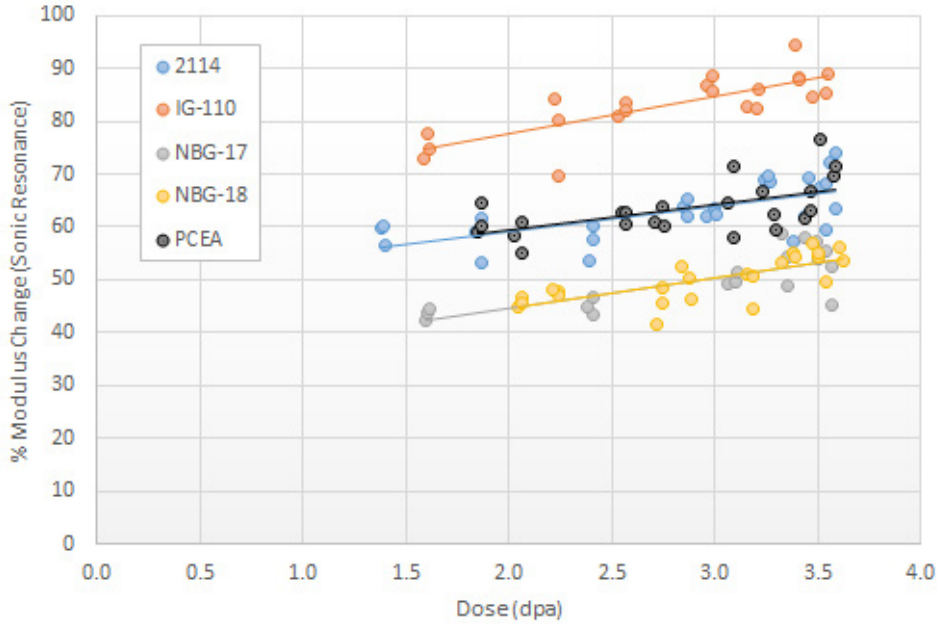

Figure A-2. Percent modulus change versus dose by graphite grade for control specimens.

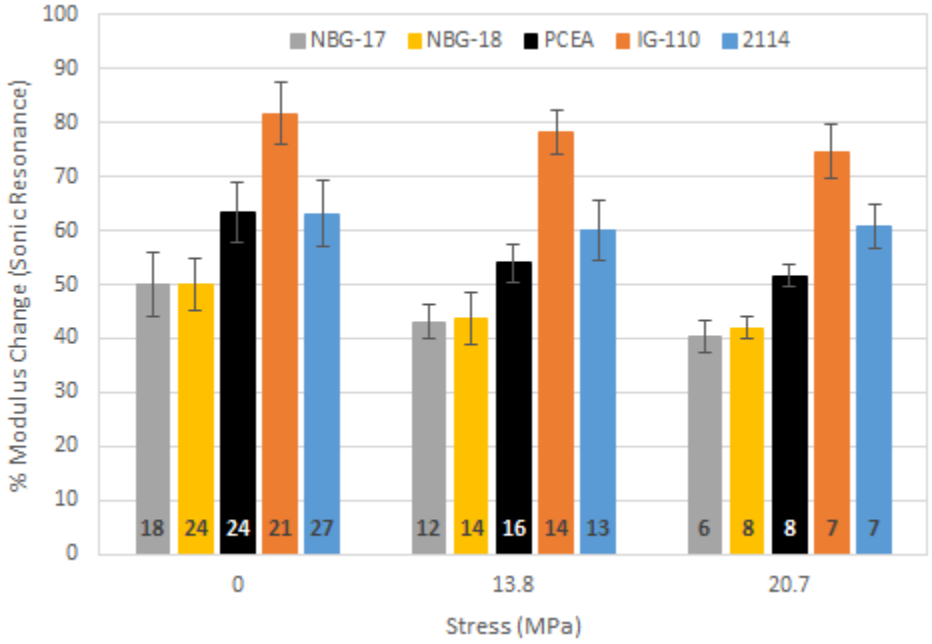

Figure A-3. Average percent modulus change by graphite grade and applied stress. The error bars represent +/- 1 standard deviation from the mean and the numbers in the bars represent the sample size.

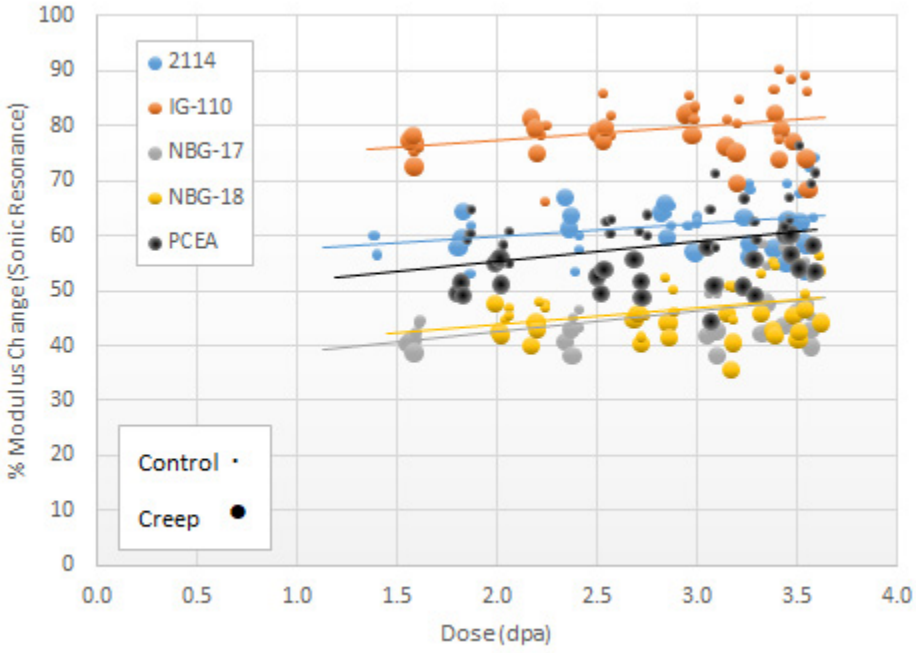

Figure A-4. Percent modulus change versus dose by graphite grade for both control and creep specimens.

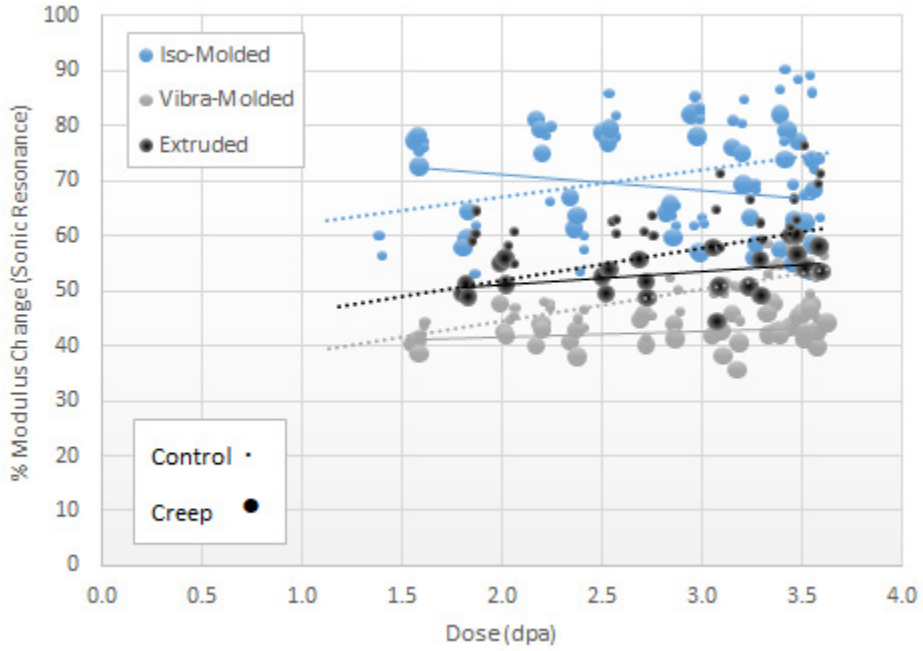

Figure A-5. Percent modulus change versus dose for similar graphite fabrication processes for creep (—) and control (- - -) specimens.

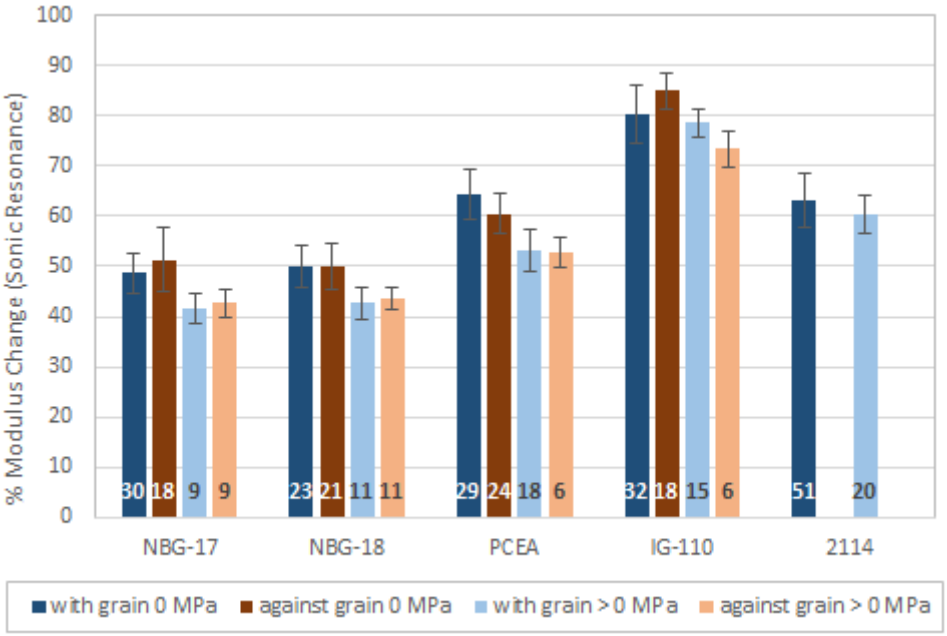

Figure A-6. Average percent modulus change by grain orientation and graphite grade.

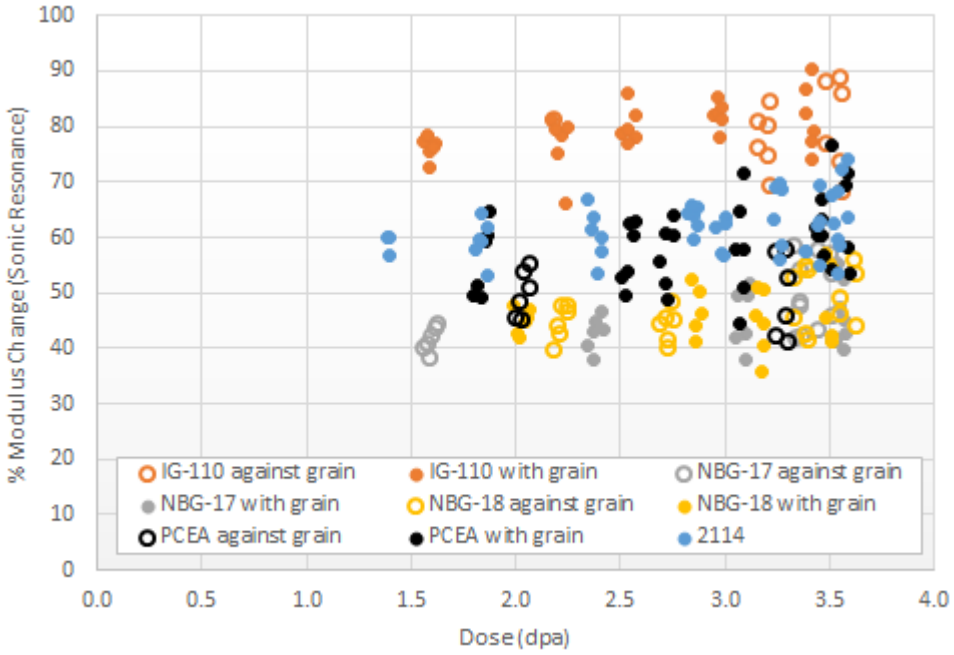

Figure A-7. Percent modulus change versus dose by grade and specimen grain orientation.

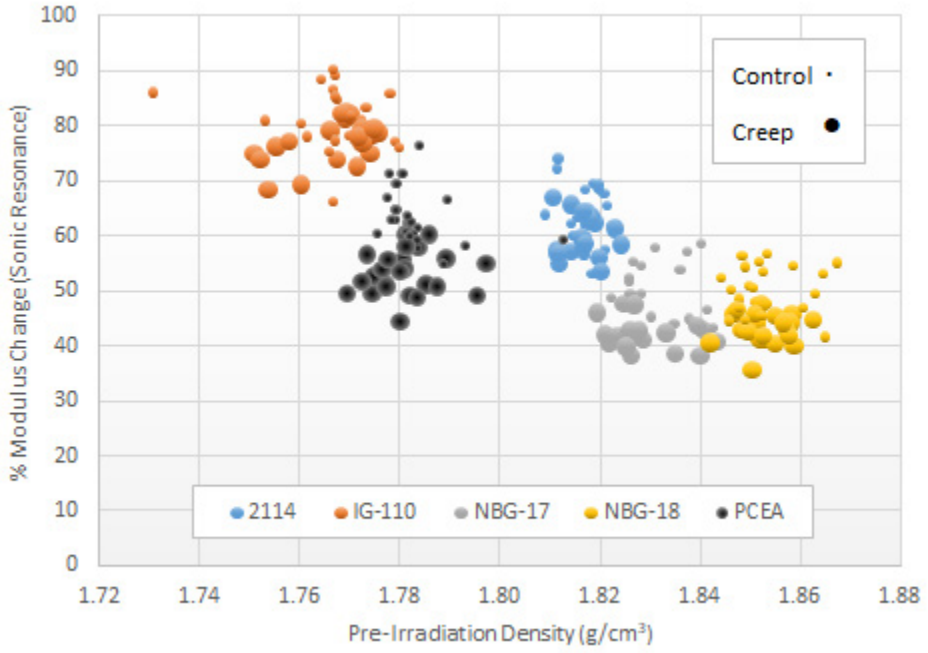

Figure A-8. Percent modulus change versus specimen pre-irradiation density for control and creep specimens.

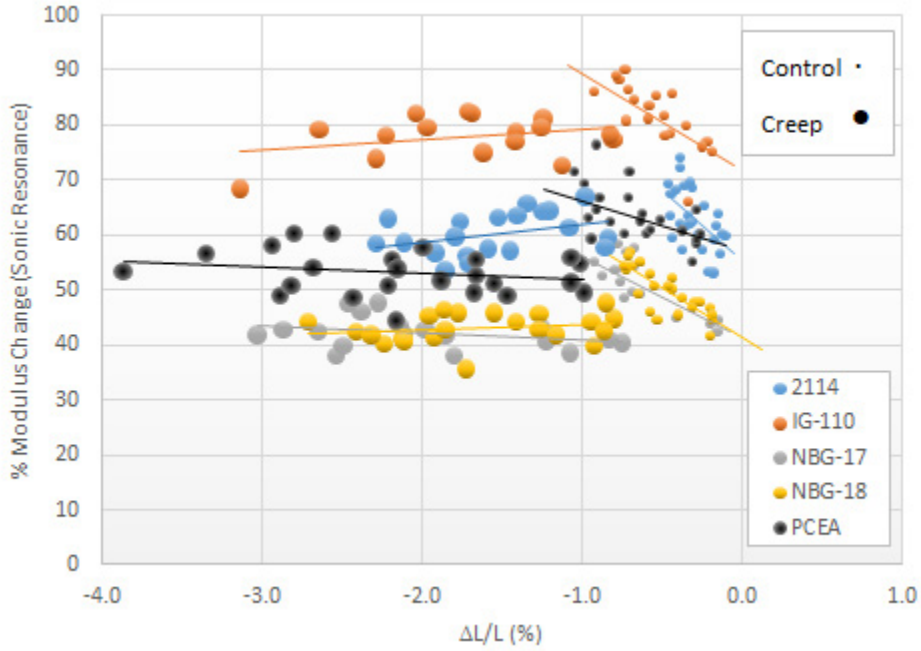

Figure A-9. Percent modulus change versus specimen strain by graphite grade for both control and creep specimens.

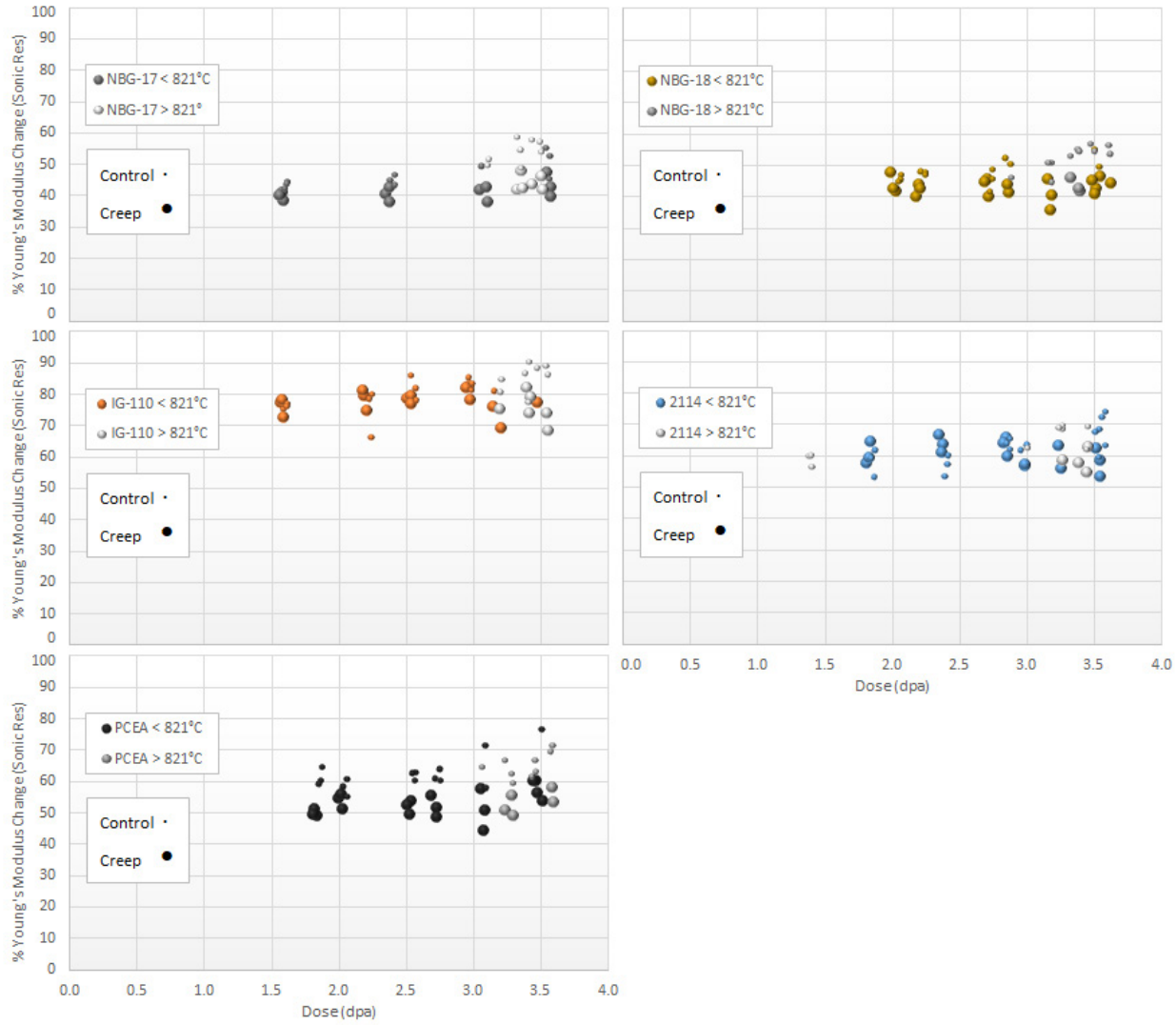

Figure A-10. Modulus change versus specimen dose for two temperature ranges, >821°C and <821°C, for different graphite grades.